UNITED STATES
DEPARTMENT OF THE INTERIOR
GEOLOGICAL SURVEY

SEISMIC-REFRACTION STUDIES OF THE IMPERIAL VALLEY REGION, CALIFORNIA-- PROFILE MODELS, A TRAVELTIME CONTOUR MAP, AND A GRAVITY MODEL

by

G.S. Fuis, W.D. Mooney, J.H. Healy, G.A. McMechan,

and W.J. Lutter

Open-File Report 81- 270

Contents

Illustrations
(Plate in pocket)

Tables

ABSTRACT

The Imperial Valley region is of tectonic and geothermal importance. An extensive seismic refraction survey was conducted to determine the crustal structure in more detail, over a wider area, and to greater depth than was accomplished by earlier studies. A combination of new instrumentation and improved methods of analysis expedited this project.

This paper describes in detail a) models for 4 seismic refraction profiles, b) a traveltime contour map, and c) a gravity model. A model for a fifth refraction profile is presented in Mooney and McMechan (in press). For a discussion of the petrologic and tectonic implications of the models, the reader is referred to Fuis and others (in press).

Forty shots, ranging in yield from 1000 to 2000 pounds, were fired at 7 shotpoints. Each shot was recorded by 100 portable seismic instruments arranged in profiles and arrays with typical instrument spacing of 0.5 to 1 km. More than 1300 recording locations were occupied and more than 3000 usable seismograms obtained.

Analysis of the data from this survey was accomplished primarily through a standard ray-tracing program newly adapted for interactive computing. This program enables rapid testing of models for traveltime consistency with the data and for qualitatively correct amplitude behavior.

All profile models have in common a sedimentary section (modeled in one to three parts), a transition zone, a basement, and subbasement.

Sediment velocity increases with depth without discontinuities but, in many cases, with changes in gradient. In the central valley, velocity increases from 1.8 km/s at the surface to about 5 km/s at the base of the sediments. Along the axis of the trough, sediment thickness ranges from about 4.8 km at the U.S.-Mexico border to 3.7 km along the southwest shore of the Salton Sea.

In the central Imperial Valley the sediment/basement transition zone is generally 1 km thick and velocity increases from 5 km/s at the base of the sediments to 5.65 km/s, in most places, at the top of the basement. On West Mesa and in other places where the sediments are thinner than 2.5 km, a prominent velocity discontinuity is present at the top of this zone, and the zone is less than 1 km thick.

Upper basement has a velocity of 5.65 km/s in most places in the Imperial Valley, but on West Mesa, its velocity is about 6 km/s.

Several structures are seen which affect basement, transition zone, and deeper sediments. They are a) a scarp along the Imperial fault, decreasing in height from 1 km southeast of El Centro to 0 km southwest of Brawley, b) a structure in deeper sediments along the Brawley seismic zone north of Brawley, and c) a scarp passing under shotpoint 1, ranging in height from 1 to 3.5 km. The latter scarp probably correlates with the Superstition Mountain fault northwest of shotpoint 1 and with a roughly north-south trending basement bench south of shotpoint 1 which has no surface expression.

A subbasement, with a velocity of 7.2 km/s near its top, is present at depths ranging from 10 km at the U.S.-Mexico border to 16 km at the south end of the Salton Sea.

A contour map of reduced traveltime constructed for our most widely recorded shotpoint is qualitatively analogous to a sediment isopach map. Steep scarps are seen on this map along some major mapped faults and along some structures not seen at the surface. Subtle patches of early arrivals among the otherwise late arrivals in the central Imperial Valley correlate uniquely with known geothermal resource areas having reservoir temperatures of more than 150°C. The shapes of these patches are roughly linear with lengths of the order of 15 km and a northeast trend.

Using the new velocity structure for the Imperial Valley region to constrain a gravity model, we discover that a) gravitational compensation for the sediments is accomplished largely by the subbasement, with a model density of 3.1 g/cc, b) the relatively flat gravity profile across the Salton Trough requires that the upper surface of this subbasement largely mirror the contact between sediments and basement, and c) the negative gravity anomalies over the Peninsular Ranges and Chocolate Mountains require that the subbasement deepen and pinch out in those directions.

INTRODUCTION

The Imperial Valley region of southeastern California is of tectonic and geothermal importance. During a 3-month period in 1979, we conducted a detailed seismic refraction survey of the region primarily to determine the crustal structure in more detail, over a wider area, and to greater depth than was accomplished in previous surveys by Kovach and others (1962) and Biehler and others (1964). A combination of new instrumentation and improved methods of analysis expedited this survey.

In this paper, we describe in detail the models for three reversed refraction profiles and one unreversed profile crossing the Imperial Valley region at different azimuths. These profiles are 6NW-1SE-1NW, 1E-2W, 10SE-2NW, and 1ESE (fig. 1)[1/]. In a paper by Mooney and McMechan (in press) a fourth reversed profile, 6NNW-13SSE (fig. 1), is described. We present a contour map of reduced traveltime from our most widely recorded shotpoint. In addition, we present a model for an existing gravity profile across the Imperial Valley region based on our refraction models. This paper is intended to be a presentation of data and a detailed discussion of modeling. For an expanded discussion of the background for this experiment and for a discussion of the petrologic and tectonic implications of the models developed here, the reader is referred to Fuis and others (in press).

1/ Seismic lines constituting a profile are given names such as 6NW and 1SE. These names derive from the shotpoints from which the lines originate and the azimuths of the lines, NW--northwest, SE--southeast, and so forth.

DATA COLLECTION

The refraction survey was conducted primarily during the period January through March 1979. Following the October 1979 earthquake, one profile, 1E-2W was reshot and another profile, 1ESE, was recorded from 0 to 25 km at 50-100 m spacing.

During the primary survey, forty shots ranging in yield from 1000 to 2000 pounds of high explosives were fired at 7 shotpoints (fig. 1, table 1). The shotpoints were located for obtaining reversed profiles in key areas, but gaps in the pattern can be seen, most notably in the Brawley-El Centro area, where culture precluded a shotpoint, and in the area east of the Salton Sea where time, money, and logistics of obtaining a shot hole penetrating the water table prevented a good location from being obtained. The explosives for each shot were in most instances loaded into a single hole 15 cm (6 inches) in diameter and about 50 meters (over 160 feet) deep. Most of the shot holes had to be cased, as the material penetrated at all shotpoints was Quaternary lake deposits consisting of sand, silt, and clay. The water table was apparently penetrated at most shotpoints, promoting relatively high efficiency in converting explosive energy into seismic energy.

The seismic recorders in this experiment are of new design (Blank and others, 1979). Each instrument consists of a single vertical-component seismometer, with a free period of 1 second, a programmable clock, a calibrator, an amplifier with three adjustable gain levels, a tape-speed-compensation tone generator, and a cassette tape recorder. About half the instruments also have a WWVB radio receiver backup. The instruments can be programmed to turn on for as many as 10 shots with 3 minutes of recording time per shot, of which about one minute is used for recording of the calibration sequence.

Each shot was recorded by 100 of these seismic instruments arranged in lines and arrays with typical instrument spacing of 0.5 km to 1 km (fig. 1). On a typical night, shots were fired at 3 different shotpoints and recorded by these patterns of instruments. More than 1300 recording locations were occupied (plate 1, table 2) and more than 3000 usable seismograms were recorded. At a temporary field office in Brawley, data from each instrument was dubbed onto master library tapes and digitized. Using a portable computer and plotter, digital record sections from all shots were produced; these record sections were frequently completed within 3 or 4 days of a shot, so that the survey could be monitored and changed during its course.

DATA ANALYSIS

A ray tracing method described by Červený and others (1977) and coded by I. Pšenčík and V. Červený was adapted for interactive computing by R.L. Nowack. This program made possible rapid testing of models for traveltime consistency with the data. In addition, it enabled us to use amplitudes in a qualitative (and, after modification, in a semi-quantitative way--see Mooney and McMechan, in press) to further constrain the data. Traveltimes and the amplitude behavior of both first arrivals and multiple refractions were fitted. The extra time constraints provided by multiple refractions plus the sensitivity of these arrivals to lateral velocity changes made them very useful in constraining the model.

Analysis of the five profiles reported here was split up among various combinations of the authors of this paper. Except for agreeing on the starting model at mutual shotpoints the analyses were carried out more or less independently, although the models were largely patterned after that of Mooney and McMechan (in press) for profile 6NNW-13SSE (fig. 1), where the structure is simple and where use is made of amplitude ratios. The models are largely consistent with one another in places where they cross one another or where they are near one another. For example, where reversed profiles 6NNW-13SSE and 1E-2W cross, velocity contours and structural boundaries in the models agree in depth to within a few tenths of a kilometer down to a depth of over 5 km, but deeper contours and boundaries diverge by as much as 1 km (compare fig. 4c with fig. 4a of Mooney and McMechan, in press). The area of this intersection represents our best control on structure anywhere in the Imperial Valley region. Note that agreement between models near mutual shotpoints is not necessarily expected due to the fact that these regions are unreversed, if sampled at all.

Some features of the model may relate to the specific capability of the computer program used to calculate ray paths through the models. A brief description of the pertinent features of this program is needed here. The program permits the construction of two-dimensional models consisting of layers separated by boundaries which can vary laterally in velocity and depth. The analyst may assign linear, vertical velocity gradients within each layer along arbitrary numbers of vertical grid lines. The reader will note that if velocity gradients are assigned to a layer with an irregular variation horizontally the boundaries between layers cannot be lines of constant velocity; rather, they are lines at which the gradient changes. In the models presented (figs. 2c, 4c, 5c, 6b), the heavy lines indicate the boundaries between layers and the dashed lines are contours of constant velocity. One can envision changing these models by a trade-off between velocity gradient and the position of the layer boundaries. We believe that it is not a serious ambiguity, but it certainly introduces some degree of nonuniqueness.

Further possible uncertainties on the complex structure may result from the fact that the ray theory involved in the program used to interpret the data does not calculate the diffracted waves. This could present a problem in the determination of velocity gradients in the deeper horizons where the ray theory approach demands a velocity increase with depth to bend the ray and return it to the surface, whereas a more complete wave theory might explain some of the arrivals as diffracted energy without requiring a velocity increase with depth. With these exceptions, it is our belief that the main features of the models are approximately correct and will not be dramatically changed by further work. Traveltimes generated by all models generally agree with the data to within 0.05 s, and in the worst case the agreement is 0.15 s. Both the first arrivals and the secondary phases are fitted by the models presented.

In the following discussion of profile modeling, the modeling procedures and model limits are discussed at length for the first profile 6NW-1SE-1NW, and more briefly for the remaining three. It should be noted that the major features of the model described for 6NW-1SE-1NW, including a sedimentary section with a continuous velocity increase, a transition zone, a basement, and a subbasement, are seen in all the models.

PROFILE MODELS

Profile 6NW-1SE-1NW

Data

Explosions at shotpoints 6 and 1 were recorded along refraction lines 6NW, 1SE, and 1NW. These lines cross the southwest part of the Imperial Valley and also West Mesa (fig. 1). Shotpoint 6 is located on the U.S.-Mexico border approximately 30 km southeast of El Centro. It is approximately on the geometric axis of the Salton Trough[1/], but about 30 km east of the topographic center of the Imperial Valley, on the edge of East Mesa. Geologically, it is on the east shoreline of ancient Lake Cahuilla and penetrates basin sediments. Shotpoint 1 is 22 km northwest of El Centro, on the opposite side of the Imperial Valley, on the edge of West Mesa. Geologically, it is on the west shoreline of Lake Cahuilla and also penetrates basin sediments. It is 3 km southwest of the Superstition Mountain fault, an branch of the San Jacinto fault zone in the Imperial Valley. Superstition Mountain, 9 km northwest, is a block of Mesozoic granodiorite uplifted along this fault.

The parts of the refraction lines between shotpoints 6 and 1 cross the Imperial fault obliquely and are parallel to and southwest of the Superstition Mountain fault. The parts of the lines that lie northwest of shotpoint 1 are also parallel to, and southwest of, the Superstition Mountain fault, but cross and recross the Coyote Creek fault, its apparent continuation to the northwest.

Line 6NW is 98 km long, extending 45 km beyond shotpoint 1. It contains 64 seismic traces of which 51 are shown (fig. 2a). Line 1SE is 54 km long, extending to shotpoint 6. It contains 41 traces of which 39 are shown (fig. 2b). Line 1NW is 45 km long and contains about 40 traces of which 16 are shown (fig. 2b).

1/ In this report, we define the "axis of the Salton Trough" to be line that bisects the Salton Sea and projects southeastward with the same trend, passing a few kilometers east of shotpoint 6 (fig. 1). Note that the topographic axis of the Imperial Valley diverges from the trough axis to the south; at the U.S.-Mexico border, it lies approximately 30 km west. In this report, we use the phrases "Imperial Valley", "central Imperial Valley", and "central valley" to denote the cultivated lowlands south of the Salton Sea within the confines of the Lake Cahuilla shorelines. The phrase "Imperial Valley region" includes Imperial Valley, Salton Sea, East and West Mesas and flanking mountains.

Between shotpoints 6 and 1, all arrivals define smooth traveltime curves with little scatter. Northwest of shotpoint 1, however, the first arrivals define a bumpy travel-time curve (figs. 2a and 2b). This observation is seen even more dramatically where only traveltime picks are plotted (fig. 3). On this plot, arrivals between shotpoints 1 and 6 define smooth curves except in the vicinity of the Imperial fault where an offset of about 0.18 s is conspicuous, with earlier arrivals northwest of the fault. The irregularity beyond shotpoint 1 on 6NW and 1NW is striking in contrast but is similar on both profiles. The picks appear to "track" each other, with differing overall apparent velocities. The time difference between late and early arrivals is greater on 6NW (1.05 s) than on 1NW (0.70 s).

Between 0 and 17 km on 6NW and between 0 and 10 km on 1SE, the travel-time curve has strong curvature, and apparent velocities range progressively from 1.6 km/s to 4.85 km/s (fig. 3). These velocities correspond to sediments (see discussion in Fuis and others, in press). In contrast, the travel-time curve between 17 and 27 km on 6NW and between 10 and 40 km on 1SE is flat, with apparent velocities of 5.80 km/s and 5.67 km/s, respectively. These velocities correspond to "basement" (see discussion in Fuis and others, in press). Note the prominent gap in clear first arrivals on 6NW between 27 and 53 km, although two weak arrivals at 42 and 45 km can be seen which may define a higher velocity of 6.9 km/s for this portion of the traveltime curve (figs. 2a and 3). A prominent gap in clear first arrivals is also seen on 1SE between 16 and 34 km, within the 5.67 km/s branch (figs. 2b and 3). Indeed, arrivals between 10 and 16 km on this profile are also so weak that they would be obscured were it not for relatively low background noise. On 1NW, a straight line with an apparent velocity of 5.8 km/s can be fitted through the scatter of arrivals between 5 and 45 km (figs. 2b and 3). The uncertainty in the latter apparent velocity certainly exceeds 0.1 km/s, and it is our convention to report such velocities to only one decimal place. On this branch note the arrival at 15 km, which is early by 0.2 s, and the arrivals between 25 and 34 km, which are late by up to 0.5 s. The latter arrivals appear to correlate with the part of the profile that lies northeast of the Coyote Creek fault.

On 6NW, the strongest arrivals in the range 39 to 53 km appear to be second arrivals with an apparent velocity of 8.00 km/s (figs. 2a and 3). Beyond a possible offset at 53 km, this branch appears to emerge as a first-arrival branch with an average apparent velocity, through considerable scatter, of 7.2 km/s. Note that the character of the first arrival changes at the 53 km cross-over point from a very weak arrival with a characteristic frequency less than 4 hz to a moderately strong arrival with a characteristic frequency greater than 5 hz. Note also that an arrival 0.4 s early at 69 km correlates well with an early arrival on 1NW, and a region of arrivals late by up to 0.65 s between 75 and 86 km correlate well with a region of late arrivals on 1NW and with the segment of the profile that lies northeast of the Coyote Creek fault. The 7.2-8.00 km/s branch will be referred to as the "subbasement" branch (see discussion in Fuis and others, in press).

One striking feature in fig. 3 is the progressive decrease in intercept times for basement arrivals from 6NW (2.55 s) to 1SE (1.80 s) to 1NW (1.28 s).

The relatively steep slope of the subbasement branch on 6NW combined with an apparent offset near shotpoint 1 produces a reduced traveltime of 2.18 s at shotpoint 1. In order to attempt to match this time on 1SE at shotpoint 6, we drew the steepest branches through the weak arrivals beyond 40 km on 1SE that appear consistent with data on these and other profiles, including a postulated 7.2 km/s subbasement velocity and an offset exceeding 0.18 s across the Imperial fault. The projected reduced traveltime at shotpoint 6 is 2.28 s.

A series of late arrivals are prominent on 6NW and 1SE (figs. 2a, 2b, and 3). On 6NW, second arrivals are prominent from 10 to 21 km, and third arrivals, from 17 to 37 km. Fourth arrivals can be seen from 18 to 27 km. On 1SE, second arrivals are prominent from 7 to 16 km, and third arrivals, from 13 to 18 km. On 1NW, in contrast, only a series of second arrivals are clear, in the range 11 to 18 km (figs. 2b and 3). Questionable third arrivals may be present at 21-22 km. On all three lines, these series of late arrivals are explainable as multiply refracted arrivals (see the next section); that is, their ray paths involve one or more reflections from the free surface during propagation. Consequently, in fig. 3, these arrivals are labeled as "1st", "2nd", and "3rd" multiple refractions. On all three lines, these late arrivals appear to reproduce the first-arrival curve with successively lower curvature, as if the first-arrival curve were being successively stretched out. On 6NW and 1SE, these arrivals have a characteristic frequency of 6 hz and a duration of two wavelengths. On 1NW they are higher in frequency and much longer in duration.

Certain amplitude fluctuations are striking on this profile. On 6NW, first arrivals--that is, the first upswings on the trace--become abruptly weak beyond the Imperial fault (fig. 2a). First arrivals are not strong until the crossover of the subbasement branch at 53 km. The first multiple refraction becomes abruptly weak beyond 21 km and the 2nd multiple refraction may die out beyond 38 km. On 1SE, first arrivals undergo a transition in amplitude from strong, 0-5 km, to moderately strong 5-7 km, to moderate, 7-10 km, to very weak, beyond 10 km (fig. 2b). Beyond 34 km, these arrivals pick up again, becoming weak to moderate in amplitude. The first multiple refraction undergoes a similar but more exaggerated transition from strong, 7-10 km, to moderate, 10-13 km, to weak, 13-18 km, to imperceptible beyond 18 km. A similar transition can be seen in amplitudes of the second multiple refraction. On 1NW, amplitudes also undergo a transition from strong 0-3 km, to moderate, 3-7 km, to weak, beyond 7 km (fig. 2b). On the lower branch of the first multiple, only one trace is pickable. On the upper branch, amplitudes die out at 18 km.

Interpretation

Traveltimes of all perceptible arrivals were used as the primary constraints in modeling velocities along lines 6NW, 1SE, and 1NW. Amplitudes were used as constraints only in a qualitative way.

The starting model was obtained from a flat-layer interpretation[1/] of apparent velocities and intercept times at each shot point. In this starting model a drastic difference in the depth to basement is indicated between 1SE, 3.7 km, and 1 NW, 1.6 km, requiring a basement scarp under shotpoint 1 of about 2 km. From 6NW, one must add as a minimum to the basement intercept time the observed offset across the Imperial fault to obtain a reasonable depth to basement. This depth, 5.55 km, agrees well with the depth calculated from 6NNW (see Mooney and McMechan, in press). The Imperial fault scarp itself has a calculated height

$$\underline{h} = \Delta \underline{t} \bullet \underline{v}_1 \underline{v}_2 / \sqrt{\underline{v}_2^2 - \underline{v}_1^2}$$

where $\Delta \underline{t}$ is the traveltime offset, $\underline{v}_1$ is the velocity of the medium that just buries the scarp, and $\underline{v}_2$ is the velocity of the medium below. Using $\Delta \underline{t}$ = 0.18 s, $\underline{v}_1$ = 3.5 km/s (an average sediment velocity) to 4.85 km/s (the deepest sedimentary layer) and $\underline{v}_2$ = 5.80 km/s, one obtains a scarp height of 0.8 km to 1.6 km.

The final model (fig 2c) was obtained by tracing rays through the starting model and numerous subsequent models (approximately 50) to obtain traveltimes that agreed with the data. This final model produces traveltime agreement with the data that is not worse than 0.05 s in most places and nowhere is worse than 0.15 s except along the lines northwest of shotpoint 1, where no attempt was made to model the bumpy arrival times. (The latter modeling exercise is rather straightforward, once the basic velocity model has been established.)

The final model consists of two sections of sediments, a sediment-basement transition zone, a basement, a basement-subbasement transition zone, and a subbasement. Cross sections through this model at various points, or velocity-depth curves, can be compared to the original velocity model obtained from flat-layer interpretation (fig. 8a, table 3). The cross section 1 km northwest of shotpoint 1 (labeled -1 in fig. 8a) and the cross section at shotpoint 6 (labeled 53 in fig. 8a) appear to be averages of the flat-layer models. Note that in both cases the flat-layer depth to basement falls within the transition zone of our model. The velocity-depth curve at shotpoint 6 is, $\underline{v}$ = 1.8 km/s + 0.69 km/s/km·$\underline{z}$, which agrees well with the curve obtained from velocity logs to a depth of 2.4 km in the Grupe-Engebretson well, 13 km northwest of shotpoint 6 (Kovach and others, 1962: $\underline{v}$ = 1.76 km/s + 0.65 km/s/km·$\underline{z}$). The cross

---

[1/] Flat-layer interpretation assumes all apparent velocities are true velocities and all interfaces are horizontal. Layer thicknesses are calculated from intercept times in a standard fashion.

sections 1 km and 17 km southeast of shotpoint 1 (labeled 1 and 17 in fig. 8a) appear to be averages of the upper 1.3 km of the flat-layer curve, but diverge below this depth to form extremes that bracket this curve. If one considers the center of the transition zone as a depth to basement, then this depth is 2.8 km at 1 km southeast of shotpoint 1 and 4.3 km at 17 km southeast of shotpoint 1. The average of these depths agrees within 0.15 km with the flat-layer depth. Thus, flat-layer interpretation is seen to provide average velocities and depths in a case of laterally varying structure. In the region southeast of shotpoint 1, our model indicates a dip of 5.4° to the southeast; under shotpoint 1, a scarp of about 1 km in height is indicated.

In the following discussion, we shall describe features of the model (fig. 2c) in terms of the observations that lead to them (figs. 2a and 2b), beginning at the top of the model and progressing downward.

The sediments were modeled in two sections with a boundary between them at 1.2 to 1.3 km. Total sediment thickness ranges from about 4.8 km at shotpoint 6 to about 1.4 km northwest of shotpoint 1. The velocity increases with depth through both sections, but the gradients are different and change from place to place. The upper section has very low velocity and in most places a lower gradient (0.4 to 0.7 km/s/km) than the lower section (0.7 to 1.8 km/s/km). Surficial velocity of 1.7 to 1.9 km/s is seen near shotpoint 1, with the higher surficial velocity at the shotpoint. The velocity at the base of the sediments is about 5 km/s in the valley, at depths ranging from 2.5 to 4.8 km but is about 2.4 km/s on West Mesa at a depth of about 1.4 km.

On 1SE, arrivals corresponding to rays that bottom in the upper sedimentary section lie on curves labeled AB, AL, and AP; arrivals corresponding to rays that bottom in the lower sedimentary section lie on curves CD, MN, and QR (fig. 2b). A sharp change in gradient between the two sections along 1SE would, in theory, give rise to triplications ABCD, ALMN, and APQR. Only along ALMN does there appear to be evidence in the data for such a triplication. On 6NW and 1NW the upper section is apparently indistinguishable in gradient from the lower section. Arrivals corresponding to rays in both sedimentary sections lie on curves labeled AB, AN, and AP (fig. 2a) and AB, AI, and AL (fig. 2b).

The multiple refractions in these profiles provide powerful constraints on the velocity model, because a ray that bottoms at a given horizon emerges at an even multiple of the traveltime and distance of a first-arrival ray bottoming at that same horizon (see figs. 9c and 9f). Thus, time and distance scales are multiplied and velocity resolution is enhanced. Hence the "stretched-out" appearance of the multiple refractions. Lateral velocity changes alter this picture, and only the multiple refractions can reveal these. To illustrate how sensitive multiple refractions are to small model changes, one discovers that moving the boundary between the upper and lower sedimentary section up or down 0.1 km, keeping the sediment velocity constant at the boundary,

produces a traveltime disagreement between model and data of up to 0.15 s on the second multiple refraction. Changing the local surficial velocity by 0.1 km/s also produces disagreement of up to 0.15 s on the second multiple refraction. Agreement with well data discussed above is primarily due to the constraints provided by these multiple refractions.

Velocity contours in both sections of sediments dip to the southeast from shotpoint 1 (fig. 2c). In the lower section, they apparently pinch out at the basement scarp at shotpoint 1. The contours appear to be offset at the Imperial fault by about 1 km at the base of the sedimentary section and progressively less upward in the section.

A transition zone, ranging in thickness from 0.6 km to 1 km, is modeled between the sediments and basement. On 1NW, beneath West Mesa, this zone has a velocity discontinuity at its upper boundary, but in the Imperial Valley the discontinuity is small or nonexistent, with velocity increasing from about 5 km/s at the base of the sediments to that of basement, 5.65 to 5.80 km/s. The gradient, 0.5 to 1.1 km/s/km, is in all cases somewhat lower than that in the sediments, but considerably higher than that in the basement. Arrivals corresponding to refracted rays that bottom in the transition zone lie on curve segments DE, NO, and RS on 1SE (fig. 2b), CD, JK, and MN on 1NW (fig. 2b), and BC, NO, and PQ on 6NW (fig. 2a). On 1SE and 6NW, these curve segments appear to be smooth continuations of the traveltime curves for sediment arrivals, with no clear evidence of reflections that would result from a velocity discontinuity between sediments and basement. In contrast, on 1NW, the sharp kink in the travel-time curve at 4-5 km requires such a discontinuity. The associated reflections are permitted by the data, but are not easy to pick out because of other high amplitude energy on the seismograms.

At this point, it becomes necessary to use amplitudes in a qualitative way to put limits on the thickness of and velocity gradient within the transition zone. Wesson (1970) described a method for determining amplitudes based on the spreading of seismic rays. Basically, for a solid angle defined by a bundle of rays taking off from the source, seismic intensity will be inversely proportional to the area of the wavefront defined by this bundle as the rays spread. A correction must, of course, be made for transmission losses at boundaries. Thus, in our ray diagrams (fig. 9), amplitudes will be inversely correlated to the separation of rays emerging at the surface. One perceives at a glance that rays bottoming in the transition zone (figs. 9a, 9c, 9d and 9f) are expected to be intermediate in amplitude between those bottoming in sediments and those bottoming in the basement. The velocity gradient in the transition zone determines the spreading of the rays and hence the amplitudes, and the combination of velocity gradient and layer thickness determines the distance interval over which these arrivals will persist. For example, decreasing the gradient in the transition zone by an average of 0.4 km/s/km southeast of shotpoint 1 would extend the distance

interval for transition-zone arrivals by about 2 km for the first arrival, 4 km for the first multiple, and so forth. The data do not appear to favor this large a change in gradient. On the other hand, if the gradient is held constant and the thickness is decreased, then the distance interval shrinks in proportion to this decrease. For example, halving the thickness of the transition zone southeast of shotpoint 1 would halve the intervals DE, NO, and RS on 1SE (fig. 2b). Again, the data do not appear to favor this large a change in thickness. Note that multiple refractions on 1SE that sample the transition zone have only their first path leg actually penetrating this zone owing to the southeast dip of the zone (fig. 9c). The opposite is true on 6NW, where the only second and successive paths legs actually penetrate this zone owing to the presence of the Imperial fault scarp (fig. 9f). Note that there are some features in the transition zone northwest of shotpoint 6 that are not adequately modeled. For example, arrivals along the curve BC of 6NW (fig. 2a) become successively late compared to the model curve, with a maximum disgreement of 0.1 s. Perhaps delays near the fault would improve the fit. In addition, the first and second multiple refractions, which sample the transition zone northwest of the fault appear to disagree on the velocity gradient and (or) thickness of the transition zone there: the distance interval NO for arrivals sampling this zone appears to be consistent with the data, but the interval PQ appears too short. The disagreement could be caused by lateral variation in the sediments and (or) transition zone northwest of the fault.

Upper basement velocity ranges from 5.6 km/s southeast of the Imperial fault to 5.8 km/s northwest of the fault. Depth to the basement-transition zone boundary ranges from about 5.8 km southeast of the Imperial fault to about 2.1 km northwest of shotpoint 1. As noted above, the depth to basement that one calculates from a flat-layer interpretation of the traveltime curves lies within the transition zone. The velocity gradient in the basement ranges from 0.15 km/s/km under shotpoint 6 to about 0.08 km/s/km northwest of shotpoint 1, although, as discussed below, these gradients are not certain. The velocity of lower basement, at 12.5 km, is 6.6 km/s in this model.

Arrivals that bottom in the basement lie along curves DEFGH on 6NW, FGHI on 1SE, and DEFG on 1NW. Rays corresponding to these arrivals are shown in figs 9a, 9b, and 9d. Owing to the wide spacing of rays emerging from the basement compared to those from the transition zone and sediments, one expects, and sees, a lower amplitude for these arrivals. In fact a lack of energy in the intervals CD on 6NW and EF on 1SE is consistent with a shadow or scattering effect of the Imperial fault scarp and a southeast dip, respectively. The shadow effect due to a southeast dip is illustrated in fig. 9b, where the increment for take-off angle is reduced to nearly the smallest allowable increment in our program, and yet a shadow still exists between successive rays at about 10 and 30 km from shotpoint 1. Note that some very low-amplitude arrivals are seen in the predicted shadow between 10 and 16 km on 1SE. These could be

diffracted energy. Similarly on 6NW, low-amplitude arrivals (referring to the first peak only) are seen in the predicted shadow between 18 and 27 km.

Perceptible multiple refractions from the basement are not expected on 6NW and 1SE owing to the shadow effects of the Imperial fault and the southeast dip (refer to figs. 9c and 9f). This shadow is predicted beyond O and Q on 6NW (fig. 2a) and beyond O and S on 1SE (fig. 2b). There appears to be reasonable agreement with the data except at Q on 6NW, as discussed above. On the other hand, very low-amplitude multiple refractions from basement are predicted on 1NW along the branches northwest of K and N, but the seismic traces are too noisy to see them.

Scarps on the transition zone and basement are located near the Imperial fault and under shotpoint 1; each appears to be about 1 km in height (fig. 2c). The scarp near the Imperial fault was located in our model halfway between the offsets in the arrivals at C on 6NW (fig. 2a) and H on 1SE (fig. 2b). This location is about 3.8 km southeast of the surface expression of the Imperial fault. This distance interval is close to the horizontal distance (4.5 km) between the emergence of a ray from the transition zone to its emergence at the surface. The offset appears to affect primarily the lower sediments, transition zone, and basement, as the multiple refractions, which travel in the upper sediments through this area (fig. 9f), are not conspicuously offset. The apparent dip of the fault that one calculates from the model is about 52^{0}. Correcting for the angle at which line 6NW crosses the fault, about 30^{0}, gives a true dip of about 68^{0} to the northeast. A northeast fault dip is consistent with earthquake epicenters that are located consistently northeast of the fault (see Johnson, 1979, and Johnson and Hutton, in press). A scarp height of 1 km is intermediate between the extremes (0.8 km and 1.6 km) calculated from the traveltime offset and is also required, in combination with a 5.8 km/s velocity for upper basement, to fit the arrival times along the branch FGH on 1SE (fig. 2b).

The location and height of the scarp under shotpoint 1 is a bit more uncertain, because lacking identifiable near-vertical reflections, shotpoint 1 is not in an advantageous position to resolve structure directly beneath it. The scarp could be moved southeastward a maximum of about 1 km if its slope were lessened and its height increased to about 2 km. This configuration would fit better the early arrival at 53 km on 6NW (fig. 2a), but would produce a shadow for basement arrivals 15 to 20 km longer than the observed one on 1SE (fig. 2b) without an unreasonably high velocity gradient in the basement.

There appears to be a slight difference in basement velocity across the Imperial fault. An upper basement velocity of 5.6 km/s was chosen for the region southeast of the fault to be consistent with analysis of the profile 6NNW-13SSE (Mooney and McMechan, in press) where this velocity is well constrained. Northwest of the fault, however, an upper basement velocity of 5.8 km/s appears necessary to fit branches EF on 6NW

(fig. 2a) and FGH on 1SE (fig. 2b), although the structural complexity between shotpoints 1 and 6 make this velocity uncertain by at least 0.1 km/s. Northwest of shotpoint 1, a 5.8 km/s velocity fits the branch DEFG on 1NW (fig. 2b), but owing to lack of reversal on this branch and to considerable scatter, this velocity is also uncertain by at least 0.1 km/s. Upper basement velocity on West Mesa is best determined from lines 5N and 13S, west of shotpoint 1 (fig. 1), which record blasts at shotpoints 5 and 13 (fig. 7). As on 1NW, arrivals on these lines define bumpy traveltime curves, but average basement branches can fitted through them with apparent velocities of 5.96 and 5.90 km/s, (fig. 7, solid lines), or, if one considers only stations recording both blasts, 6.1 and 5.9 km/s (fig. 7, dashed lines). True upper basement velocity, then appears to range from 5.93 to 6.00 km/s. Hamilton (1970) obtained an average basement velocity of 5.92 km/s from time-term analysis of a slightly larger region on the west flank of the Salton Trough. In conclusion, upper basement velocity in the central Imperial Valley east of the Imperial fault appears to be resolvably different from that on West Mesa, 5.6 km/s compared to 5.93-6.00 km/s. Between the Imperial fault and West Mesa, upper basement velocity may or may not be intermediate between these two velocities.

It is interesting to note that the bumpiness in the arrival times on 5N and 13S also shows up in arrivals in this area from shotpoint 1, which are contoured in fig. 10 (see section on a traveltime contour map). Contouring indicates that northeast-trending grabens and horsts on West Mesa are responsible for this bumpiness. Note the change to low frequency for late arrivals above grabens.

The velocity gradient in basement for profile 6NW-1SE-1NW ranges from 0.08 to 0.15 km/s/km (fig. 2c) and is considerably above the range in gradient, 0.02 to 0.05 km/s/km, determined by Mooney and McMechan (in press) for basement along the axis of the Salton Trough on profile 6NNW-13SSE. On line 6NW, a higher gradient is required to fit the weak first arrivals EF (fig. 2a) and is also required on 1SE to turn rays back to the surface at F (fig. 2b; fig. 9b). If one discounts the weak arrivals at EF on 6NW, then one must attempt to explain the sudden change of character in the first arrivals at G on 6NW as an effect of structure rather than an effect of crossover between basement and subbasement arrivals. One does not, however, see a strong structural effect on ray spacing, and hence amplitudes, on either side of G (fig. 9e), and we favor the interpretation that the change at G is due to arrival crossover. On 1SE one might be able to produce the arrivals beyond F by diffracted, rather than refracted energy as we have done. It is not clear, however, that diffracted arrivals would produce the observed shadow EF. In summary, although we favor a relatively higher velocity gradient in the basement on profile 6NW-1SE-1NW than on 6NNW-13SSE, the evidence is not compelling. The higher gradient on 6NW-1SE-1NW results in a velocity for lower basement of 6.6 km/s, compared to 5.85 km/s on 6NNW-13SSE.

A subbasement represented by a velocity step from 6.6 km/s, that of lower basement, to 7.0 km/s is present at about 12.5 km depth (fig. 2c). Within 1 km, the velocity of this layer increases to 7.2 km/s. Arrivals corresponding to refractions in this layer lie along the curve IGJKL on 6NW (fig. 2a) and JI on 1SE (fig. 2b). Reflections from the top of this body are seen along the dashed curve IH on 6NW and JI on 1SE, with critical reflections predicted at I and J, respectively. Moving the top of the subbasement up or down by 1 km, keeping the basement velocity gradient constant, advances or delays the arrivals about 0.1 s and moves the critical reflection toward or away from the shotpoint by 3 to 5 km. The position of the critical point can, of course, be adjusted by changing the velocity step at the top of the layer, but a velocity of at least 7.2 km/s must be reached somewhere within the upper kilometer or so of the layer to satisfy the data (figs. 2a and 3). Refractions from the subbasement cross over basement refractions at about shotpoint 1 (G on 6NW, fig. 2a) and may be responsible for the change in character of the first arrival here. Note the prominent jump in arrival time at this point due to the basement scarp under shotpoint 1. Note also that the presence of the subbasement cuts off basement refractions and supercritical reflections at H on 6NW (fig. 2a).

Hamilton (1970) detected a subbasement with an apparent velocity of 7.1 km/s and calculated a depth of 14 km at a location about 50 km northwest of shotpoint 1. The models developed in this report and that of Mooney and McMechan (in press), appear consistent with Hamilton's interpretation.

Profile 1E-2W

Data

Explosions at shotpoints 1 and 2 were recorded along lines 1E and 2W, which cross the Imperial Valley and East Mesa (fig. 1). Shotpoint 2 is 21 km east of Brawley, on the edge of East Mesa. Geologically, the shotpoints are on opposite shorelines of ancient Lake Cahuilla and penetrate basin sediments. The parts of the lines between shotpoints cross, at the extreme west end, the Superstition Mountain and Superstition Hills faults, and in the center, the Imperial and Brawley faults. Near shotpoint 2, they cross a seismicity lineament along the East Highline canal that is interpreted as a fault (see Johnson and Hutton, in press). East of shotpoint 2, 1E crosses several inferred faults including the Sand Hills and the Algodones faults(?).

Line 1E is 84 km long and contains 93 seismograms, of which 77 are shown (fig. 4b). This line was recorded on three occasions, as records from the first occasion were complicated by the occurrence of a small earthquake. Line 2W is 40 km long and contains 24 traces, all of which are shown (fig. 4a). 1E extends 40 km east of shotpoint 2, but 2W stops about 5 km east of shotpoint 1, leaving the region below shotpoint 1 unsampled.

As on lines 6NW and 1SE, all arrivals on 1E and 2W define smooth traveltime curves with little scatter where these lines cross the Imperial Valley. On 1E east of shotpoint 2, however, the arrivals define a bumpy travel-time curve. Bumps are seen on all scales. On one hand, adjacent traces in many places differ in traveltime by over 0.1 s, measured from the local average traveltime curve. On the other hand, a major offset in the traveltime curve exceeding 0.2 s is seen between arrivals at 61 and 64 km, near the proposed trace of the Algodones fault(?), indicating a larger structure there.

Between 0 and 18 km on 1E, and 0 and 13 km on 2W arrivals are strong and lie along a smooth traveltime curve with strong curvature. Apparent velocities along these curves range progressively from 1.9 to 4.66 km/s indicating sediment arrivals. Beyond these distances, arrivals are moderately strong to weak and can easily be fitted by straight lines out to about 33 km having similar apparent velocities on both profiles of about 5.55 km/s. Beyond 33 km on both profiles, the apparent velocity increases. Beginning at about 30 km on 1E, some coherent second arrivals are apparent. These arrivals are most strikingly coherent between 39 and 43 km where some 15 hz energy appears to ride on a 5 to 6 hz wavelet that is several wavelengths long. East of shotpoint 2 the first arrivals have the same distinctive appearance as on 6 NW beyond shotpoint 1: they consist of a 5-6 hz wavelet about 2 wavelengths long. The second arrivals from 30 to 45 km and the first arrivals beyond 45 km appear to have similar apparent velocities of around 8.5 km/s. Unfortunately, 2W is not long enough or recorded densely enough to see clearly a second arrival similar to the one on 1E.

First, second, and third multiple refractions are seen on both 1E and 2W. Their amplitude behavior is similar to, but more complicated than, that of the first arrivals.

Note that no clear offsets (exceeding a few hundredths of a second) appear to be associated with the any of the faults crossed, with the possible exceptions of the Sand Hills and Algodones faults(?).

Some clear differences are seen between 1E and 1SE (figs. 4b and 2b). When superimposed, the traveltime curves cross each other at about 8 km: arrivals on 1E are earlier from 0 to 8 km by as much as 0.18 s and later beyond 8 km by up to 0.4 s at 35 km. The basement intercept time for 1E is later by 0.3 s. Of course, multiple refractions on 1E and 1SE diverge from each other at multiples of 8 km. There is no prominent first-arrival shadow on 1E and hence no cutoff in the multiple refractions, as was seen on 1SE. These differences lead to marked model differences at shotpoint 1, as discussed below.

Interpretation

The starting model for 1E and 2W was obtained from a flat-layer interpretation of the traveltime curves. In addition, flat-layer interpretations of profiles reported by Kovach and others (1962) along the East Highline canal south of shotpoint 2 and along the Coachella canal 10 km east of shotpoint 2 were used to control relevant segments of the model. Depths to basement inferred from such interpretations are: 4.8 km (1E), 4.3 km (2W), 3.1 km (East Highline canal), and 2.8 km (Coachella canal).

The final model (fig. 4c) is similar in its major features to that for profile 6NW-1SE-1NW, in that it contains two sections of sediments, a transition zone, a basement, a second transition zone, and a subbasement. Cross sections through the model, or velocity-depth curves, indicate some similarities and some differences when compared to 6NW-1SE-1NW (figs. 8b and 8c, table 3). There is an overall similarity in the shape of the velocity-depth curves between the two models. In particular, the velocity-depth curve near shotpoint 2 (labeled 43, fig. 8c) is intermediate between the curves 1 and 17 km southeast of shotpoint 1 (1 and 17, fig. 8b) The curve 25 km east of shotpoint 1, in the center of the Imperial Valley, is essentially the same as that at shotpoint 6 which is in the center of the Salton Trough. Differences include a higher velocity gradient in the upper section of sediments (1.0 km/s/km versus 0.7 km/s/km), a lower velocity gradient in the basement (0.05/s versus 0.1/s), and a different velocity step at the top of the subbasement (5.95 to 6.6 km/s versus 6.6 to 7.0 km/s). Note that the velocity-depth curve 2.5 km east of shotpoint 1 is very different from those 1 km northwest and 1 km southeast of shotpoint 1, reflecting the extreme structural complexity beneath shotpoint 1. Note also that the two sections of sediments are distinguishable only at shotpoint 1 (and east of shotpoint 2, where we must rely entirely on the data of Kovach and others (1962).

Total sediment thickness ranges from about 4.55 km just east of shotpoint 1 to a feather edge on the east side of the Salton Trough (fig. 4c). Velocity contours dip toward the center of the Imperial Valley from both sides of the model. The small oscillation in the contours just west of shotpoint 2 may correlate with a fault along the East Highline canal that is inferred from seismicity. The surficial velocity is 1.8 km/s everywhere except at shotpoint 1 where it is higher (similar to the model for 6NW-1SE-1NW). The velocity at the base of the sediment apparently reaches about 5 km/s everywhere but at the east edge of the Salton Trough.

Arrivals from rays that bottom in the upper sediments on 1E lie along curve segments AB, AI, and AL, and those from the lower sediments, along segments BC, IJ, and LM (fig. 4b). On 2W, where there is apparently no distinction between upper and lower sediments, arrivals from the sediments lie along segments ABC, AGH, and AJK. A change to lower amplitudes is expected for arrivals on 1E bottoming in the lower sediments between 0 and 15 km owing to the change to a lower velocity gradient in this region. This predicted reduction is difficult to test on the first arrivals in the region BC, as most are clipped. One might expected this effect to be smaller on the first multiple refraction (IJ) and smaller yet on the second (LM), as more of these ray paths are out of this region. In fact, amplitudes on the second multiple refraction (LM) appear quite high.

A transition zone, 1 km in thickness under the Imperial Valley and tapering to a feather edge on the east side of the Salton trough, is included in the model between the sediments and basement. Except on the edge of the trough where velocity discontinuities are seen, this zone involves an increase in velocity from about 5 km/s at the base of the sediments to 5.65 km/s in the upper basement. Arrivals corresponding to rays bottoming in this zone lie along curve segments CD, JK, and M+ on 1E (fig. 4b) and along CD, HI, and K+ on 2W (fig. 4a). As on 6NW and 1SE, these segments appear to be smooth continuations of the traveltime curves for the sediments with no clear evidence for reflections that would result from a velocity discontinuity between the sediments and basement. As on 6NW and 1SE, one expects a reduction in amplitudes owing to a reduction in velocity gradient to 0.55 km/s/km in this zone. This reduction might not be dramatic in the first arrivals on 1E, owing to the fact that the lower-sediment gradient in the region 0-15 km ranges through the value of the gradient in the transition zone, but the reduction might be more prominent in the first and second multiple refractions owing to longer path legs in the region beyond 15 km. The data is roughly consistent with these expectations, but irregularities are apparent, such as the abrupt increase in amplitudes at K and persistence of high amplitudes beyond M (fig. 4b). Arguments similar to those in the discussion of the transition zone for 6NW-1SE-1NW can be made here justifying the thickness and gradient chosen for this zone.

Upper basement has a model velocity of about 5.65 km/s, which is consistent with an observed apparent velocity of 5.55 km/s on both 1E and 2W coupled with dips of velocity contours in the sediments toward the center of the valley. Higher apparent velocities beyond 33 km on both lines are also consistent with this model. On 1E, basement apparently rises from its depth of about 5.6 km in the center of the valley to a plateau at about 4.3 km depth under shotpoint 2. If one takes the center of the transition zone to be the equivalent of a flat-layer interpretation of depth to basement, then this depth under shotpoint 2, 3.8 km, is somewhat deeper than that of Kovach and others (1962), 3.1 km, for their profile south of shotpoint 2. The velocity gradient in basement, 0.05 km/s/km is lower than that found for 6NW-1SE-1NW, bringing the velocity at the bottom of the basement layer, at 11.3 km depth, up to only 5.95 km/s.

Arrivals that bottom in the basement lie along curve DE and beyond K on 1E (fig. 4b) and along curve DE and beyond I on 2W (fig. 4a). The reduction in amplitude that one expects from the reduction in velocity gradient is clearly seen.

A subbasement, represented by a velocity step from 5.95 km/s, that of lower basement, to 6.6 km/s is present at about 11.3 km depth (fig. 4c). Within 1 km, the velocity of this layer increases to 7.2 km/s. Arrivals corresponding to refractions from this layer lie along curve GEH on 1E (fig. 4b) and along FE on 2W (fig. 4a). Reflections from the top of this layer are predicted along the dashed curve GF on 1E and beyond F on 2W, with critical reflections at G and F, respectively. As appeared to be the case on 6NW, the cross-over of subbasement arrivals on 1E at E may be responsible for the change in character of the first arrival there. Note the scattering of arrival times on 1E along curve EH (fig. 4b). Like the structure northwest of shotpoint 1, the structure here appears complicated, but was not modeled in detail.

Profile 10SE-2NW

Data

Explosions at shotpoints 2 and 10 were recorded along lines 2NW and 10SE, which cross the northern part of the Imperial Valley obliquely (fig. 1). Shotpoint 10 is 14 km northwest of Brawley, within Imperial Valley, but slightly west of the axis of the Salton Trough. Both shotpoints penetrate basin sediments. Shotpoint 10 is located in the Westmorland geothermal area and is 9 km south of Obsidian Butte, a Holocene rhyolite extrusion. The refraction lines cross the Brawley seismic zone and the East Highline canal seismicity lineament.

Line 2NW is 38 km long and contains 38 traces of which 34 are shown (fig. 5a). 10SE is 34 km long and contains 34 traces of which 32 are shown (fig. 5b). 2NW extends beyond shotpoint 10 and samples the region under that shotpoint; 10SW does not extend beyond shotpoint 2, leaving the region below unsampled.

As on segments of other lines within the Imperial Valley, arrivals on 2NW and 10SE show little scatter (figs. 5a and 5b). Except for the kinks at 4 to 5 km on each line, first arrivals lie on smooth traveltime curves. Apparent velocities ranging progressively from 1.6 to 4.9 km/s are seen from 0 to 20 km on 2NW and from 0 to 16 km on 10SE; dominant velocities are 2.1 and 4.3 km/s, on either side of the kink. Apparent velocities of around 5.6 km/s are seen between 20 and 26 km on 2NW and between 16 and 21 km on 10SE, and higher apparent velocities, 6.6 km/s on 2NW and 6.5 km on 10SE, are seen beyond those points. It is noteworthy that first arrivals beyond the kinks are generally later on 10SE than on 2NW by a maximum of 0.4 sec. at 7 km. Reciprocal travel times at the shotpoints are the same on both lines, however. In contrast to the overall continuity of the traveltime curves, there are marked fluctuations in amplitude on all arrival branches on both lines.

Comparing the traveltime curve of 2NW with that of 2W, one notes similarity with the exception that sedimentary arrivals are slightly later on 2W by a maximum of 0.15 s at 10 km; the basement intercept time on 2W is 0.1s later.

Interpretation

We obtain the starting model for profile 10SE-2NW from flat-layer interpretation of the traveltime curves, which gives a depth to basement of 4.3 km for both lines.

The final model (fig 5c) is similar to previously described models, but sediments are modeled in 3 sections rather than 2 owing primarily to the observed kinks in the traveltime curves. Velocity-depth curves (fig. 8d) can be compared and contrasted with the other models. The velocity-depth curve at shotpoint 2 (labeled 33, fig. 8d, table 3) should

agree closely with the one near shotpoint 2 for 1E-2W (43, fig. 8c), and it does. The curve 15 km southeast of shotpoint 10 (15, fig. 8d) is essentially the same as the one in the center of valley for 1E-2W (25, fig. 8c) and the one at shotpoint 6 (53, fig. 8b), although it involves a few slight changes in gradient. The velocity profile at shotpoint 10 (0, fig. 8d) is essentially the same as the one 17 km southeast of shotpoint 1 (17, fig. 8b). One can thus begin to classify the profiles as shown in fig 8 according to geologic setting in the Imperial Valley region. The reader is referred to the summary at the end of this report for this classification.

Total sediment thickness ranges from 4.6 km halfway between shotpoints 2 and 10 to about 4 km at shotpoint 10 and 3 km at shotpoint 2, although the depth under shotpoint 2 is not constrained by our data owing to the lack of data beyond it from shotpoint 10. Velocity contours have an apparent dip generally northwest. As in the model for 6NW-1SE-1NW, the upper section of sediments, here 0.6 to 1.2 km thick, are characterized by a low velocity, 1.9 to 2.0 km/s at the surface in most places, and a low gradient, 0.2 to 0.3 km/s/km. These sediments overlie a section characterized by a higher gradient of about 1.3 km/s/km. This section in turn overlies a section whose gradient is lower again and variable from place to place, 0.5 km/s/km to 0.8 km/s/km. The large bump in the contours in this section centered about 7 km southeast of shotpoint 10, appears significant and may reflect a structure (fold, fault, or intrusion) associated with the Brawley seismic zone. At the base of the sediments, the velocity is about 5 km/s, as in the other models.

First arrivals from rays bottoming in the upper sediments lie along curves ABC in both profiles (figs. 5a and 5b) and those bottoming in sediments below lie along curves DBE. The large increase in velocity gradient at about 1 km depth produces a marked triplication reflected by the kink in the traveltime curve at about 5 km on both profiles. This triplication is repeated in each of the traveltime curves for the multiple refractions, creating a locus AJ (10SE) and AK (2NW) of stretched-out and overlapping triplications, along which many arrivals having nearly the same travel time interfere with one another. A similar but less prominent triplication is consistent with the data on profile 1SE (fig. 2b) and perhaps also on 2W (fig. 4a), although the latter profile was modeled without one.

A transition zone, ranging in thickness from 0.5 to 1.4 km, is included in this model, as in the other models, to produce the observed smooth transitions EF and HI (figs. 5a and 5b) on the traveltime curves from sediment to basement arrivals. An increase in velocity from around 5 km/s at the base of the sediments to 5.65 km/s in the upper basement is accomplished by gradients which in the southeast half of the model are lower (.5 -.6 km/s/km) and in the northwest half are higher (1.0-1.3 km/s/km) than those in the sediments immediately above. For arrivals

from this zone, one might expect lower amplitudes on 2NW and higher amplitudes on 10SE compared to adjacent arrivals from the sediments, but instead the observed amplitude fluctuations are somewhat erratic, indicating complications that are not modeled.

The upper basement has an average model velocity of 5.65 km/s, consistent with observed apparent velocities of around 5.6 km/s past F on both profiles (figs. 5a and 5b). The model produces this apparent velocity by the competing effects of an apparent dip on basement of about 1 southeast from shotpoint 10 and an apparent dip on sediments of about 1.5 northwest from shotpoint 2. A marked reversal in basement dip near shotpoint 2 gives rise to an observed 6.5 km/s velocity on 10SE and a slight increase in dip near shotpoint 10 give a similar high apparent velocity on 2NW. (Refer to arrivals near G on both profiles). Thus the overall basement structure appears to be a slightly assymmetric basin with its deepest part, 5.4 km, located 10 to 15 km northwest of shotpoint 2.

Comparing this model with the one for 1E-2W in the vicinity of shotpoint 2, one notes some similarities and some differences. All velocity contours from 2.0 to 4.5 km/s are similar to a distance of about 10 km from shotpoint 2. The 5.0 km/s contour, however, is depressed about 0.4 km in depth for 10SE-2NW compared to 1E-2W, but has a similar shape, deepening more or less gradually to the northwest. Worse yet, the 5.5 km/s contour, along with the upper-basement interface appears to be nearly a kilometer deeper on 10SE-2NW than on 1E-2W at a point 5 km from shotpoint 2. As pointed out in the discussion of the scarp under shotpoint 1, it is difficult to model uniquely a structure directly beneath a shotpoint, as the data are unreversed, if the region is sampled at all. In the case of shotpoint 1, we were able to move the scarp a kilometer or so outward and lessen its slope while still satisfying the data. Perhaps we have an analogy at shotpoint 2, where models for 1E-2W and 10SE-2NW represent the two extremes in modeling the region below. This possibility has not yet been tested. On the other hand, the discrepancy may be in part real and related to faulting along the East Highline canal seismicity lineament.

The large bump in the velocity contours centered 7 km southeast of shotpoint 10 (fig. 5c) results from an attempt to model a region of apparently highly complicated structure. The data from shotpoint 10 require a local high velocity in this region to fit first arrivals near 10 km (fig. 5b), whereas arrivals from shotpoint 2, which sample this region less comprehensively, indicate a normal regional average velocity (fig. 5a). This feature is, thus, relatively localized and possibly related to the Brawley seismic zone.

Profile 1ESE

Data and Interpretation

Description and analysis of unreversed profile 1ESE is included primarily because this profile exhibits the most dramatic evidence of arrivals from the subbasement. Refractions and reflections from the subbasement lie along model curves CD and CB, respectively (fig. 6a).

This profile extends 60 kilometers east-southeast of shotpoint 1 through the central Imperial Valley, intermediate in azimuth between 1SE and 1E (fig. 1). It was recorded on two separate occasions. On the first occasion, it was recorded, from 12 to 60 km and contains 26 traces (fig. 6a). On the second occasion it was recorded from 0 to 25 km and contains 400 traces, which are not shown here but which were used to constrain the sedimentary sections of the model. The second recording was part of an effort, still under way, to trace reflections from the subbasement to subcritical distances.

The subbasement arrivals on 1ESE are interesting not only because they are so strong but also because they are seen first at a range of 25 km from the shotpoint, 5 km ahead of similar arrivals on 1E and 6NNW (see Mooney and McMechan, in press) and more than 10 km ahead of similar arrivals on 6NW. All of these lines sample nearby parts of the central Imperial Valley, and it is of interest to compare inferred depths to subbasement for consistency. In addition to the strong subbasement arrivals, other features on 1ESE that are of interest in modeling include the offset in the first arrivals, and in the second multiple refraction at about 25 km, just past the Imperial fault, and also the amplitude decrease in all arrivals (except those from the subbasement) beginning at about the Imperial fault.

Comparing the record sections of 1ESE with nearby 1SE and 1E similarities and contrasts are noted. The first arrivals of 1ESE are very similar in time to those of 1SE except that they diverge at about 8 km to become 0.25 s later; basement intercept time is correspondingly later. Basement apparent velocity on 1ESE is nearly 6.00 km/s, compared to 5.67 km/s on 1SE. First arrivals on 1ESE do not show the abrupt amplitude drop at 10 km seen on 1SE. First arrivals on 1E diverge in turn from 1ESE beyond 8 km, becoming 0.2 s later, but are markedly earlier from 0 to 8 km. Basement apparent velocity on 1E is only 5.55 km/s. Beyond the Imperial fault, which produces a traveltime offset of about 0.18 s, (similar to that on 6NW), arrival times on 1ESE and 1E agree well. The multiple refractions on 1ESE agree in time with those of 1SE, where they overlap, but continue considerably farther. They are generally slightly earlier than those of 1E and do not continue as far. In summary, data suggests that the correct model for 1ESE might be one with velocity gradients similar to 6NW-1SE-1NW, but interface depths that are intermediate between those of 6NW-1SE-1NW and 1E-2W.

TRAVELTIME CONTOUR MAP

A few shotpoints were recorded widely enough to permit contouring of reduced travel time. To date, only the contour map for shotpoint 1 has been constructed (fig. 10). A reducing velocity of 6 km/s is used, similar to (but not identical to) basement velocity. Such a contour map is roughly similar to a sedimentary isopach map, where greater reduced travel time correlates with greater sediment thickness.

In constructing the map, all reduced arrival times from shotpoint 1 with estimated errors less than 0.1 s were plotted at their respective locations on a map. Triangles were drawn among triads of locations which were judged to be nearest neighbors. Contour intervals were then interpolated on the legs of the triangles, and contour lines were drawn. A contour interval of 0.1 s was chosen equivalent to the maximum estimated reading error. In interpreting the map, then, one must keep in mind that at distances beyond about 30 to 50 km, depending on background noise, reading error increases (refer to figs. 2,4,5,6, and 7), and contours could be in error by an amount estimated to be one contour interval.

Interpretation of this map is made difficult by the complex structure beneath shotpoint 1. The reduced travel time of the first basement-refracted arrival varies drastically with azimuth: 1.35 s on 1NW, 1.9 s on 1SE, 2.25 s on 1ESE, and 2.4 s on 1E. (refer to figs. 2b,6a, and 4b) Such variation precludes the use of the map as an equivalent of a time-term map, as the fundamental assumption of time-term analysis is that "down-times" be independent of azimuth at each source and receiver site (Berry and West, 1966). Furthermore, traveltimes for rays bottoming in several different refractors are represented, and the reducing velocity of 6 km/s does not exactly match that of any one refractor. Thus in interpreting the map one must also keep the following facts in mind:

1) At different azimuths, a given contour does not reflect the same depth to a refractor. Indeed, even along a single azimuth structural complications in the media above the refractor must be modeled first before a depth to the refractor can be inferred (as is evident in the first part of this report).
2) At different azimuths, arrivals from different refractors are seen in different distance intervals from shotpoint 1:
   a) At azimuths from northwest counter-clockwise (CCW) to south, basement arrivals are seen at distances beyond 7 km.
   b) At azimuths from south CCW to north, basement arrivals are seen in distance intervals from between 11 and 18 km to between 45 and 55 km. Beyond 45 to 55 km, arrivals from the subbasement refractor are seen.
   c) At azimuths from north CCW to northwest the interval in which arrivals from a basement refractor are seen is uncertain due to structural complexity in the San Jacinto fault zone.
3) Within the distance interval in which basement arrivals are seen in the central Imperial Valley, a slow drift to higher contours is expected with distance, even with no increase in depth to basement, owing to the choice of 6 km/s reducing velocity.

The starting model for 1ESE was the final model for 6NW-1SE-1NW with the scarp on the transition zone and basement associated with the Imperial fault moved to a position about 1 km east of the surface trace of the Imperial fault on 1ESE. In the final model for 1ESE (fig. 6b), velocity gradients like those in 6NW-1SE-1NW do indeed fit the data, and transition zone and basement interfaces are intermediate in depth between models for 6NW-1SE-1NW and 1E-2W. In particular, the scarp height under shotpoint 1 is increased by 1.4 km over that of 6NW-1SE-1NW, making basement 4.5 deep east of the shotpoint The height of the Imperial fault scarp is apparently less than that in 6NW-1SE-1NW, and a zone of lower velocity (4 percent lower) through the fault zone was required to fit multiple refraction times at around 30 km. Note that in the model for 6NW-1SE-1NW a scarp height of 1 km was used with no decrease in the fault-zone velocity to model the same traveltime offset of 0.18 s. To some extent models for 1ESE and 6NW-1SE-1NW may represent extremes in modeling possibilities, although this idea has not been tested. The apparent dip on the fault on 1ESE is 75^{0} northeast. Correcting for the angle at which the profile crosses the fault, a true dip of about 78^{0} northeast is calculated.

Amplitudes of the multiple refractions do fall off at F and I as one would predict from entry of ray paths into the basement where the velocity gradient drops. Upper-basement velocities are similar to those for 6NW-1SE-1NW, but the basement velocity gradient is lower, leading to a lower-basement velocity of only 6.15 km/s, in rough agreement with that found on 1E. Most importantly, a subbasement depth of 11.3 km agrees exactly with that found along nearby 1E. The reflection from the subbasement is so strong that it shows up as a multiple reflection at G.

In summary, the model for 1ESE is a blend of many features of both those for 6NW-1SE-1NW and 1E-2W which lie to either side. In spite of the differing strength and onset distance for subbasement arrivals on 1E and 1ESE, similar subbasement depths are indicated.

4) Features in the contours are displaced radially away from shotpoint 1 from the structures that cause them. The amount of displacement depends on the depth of the structure and the ray path sampling it (eg. for a structure in the upper basement in the center of the valley, the distance is generally 6 to 8 km).

Even with this burdensome list of things to keep in mind, a number of simple and interesting observations can be easily made from the map.

The contour map (fig. 10) is roughly an inverse of the surficial topography, with a "ridge" of reduced traveltimes as high as 2.5 s along the axis of the Salton Trough and a "valley" of low values, around 1.3 s, on West Mesa. The southwest flank and crest of the "ridge" are within the interval where first arrivals are from basement. The northeast flank of the ridge is within the interval for subbasement first arrivals. If one assumes the "ridge" crest represents the axis of a sedimentary trough and translates all points of this crest radially toward shotpoint 1 by about 8 km (the horizontal distance an upcoming ray would travel through these sediments), this axis coincides roughly with the seismogenic belt in the Imperial Valley (see Johnson, 1979, and Johnson and Hutton, in press).

The "valley" of low contour values on West Mesa is separated from the "ridge" by a steep slope which trends north-south south of shotpoint 1 but is deflected northwest by both the Superstition Mountain and Superstition Hills faults to the north. To the south, this slope presumably reflects the buried basement scarp discovered under shotpoint 1, and to the north, it probably reflects basement scarps along the faults. Superstition Mountain, an uplifted basement block, shows up clearly as a small area of depressed contours northwest of shotpoint 1. It appears to be part of a somewhat larger basement block near the surface as indicated by the region of low contour values between the northwest segments of the Superstition Hills and Superstition Mountain faults. Northwest of Superstition Mountain, a very steep gradient, resulting in a jump of up to 0.7 s in traveltime, appears to trend east to northeast from near the end of the Coyote Creek fault. This feature roughly parallels the northwest boundary of the Superstition Hills. Steep contour gradients are also observed along the Elsinore fault system. The northeast trend of contours in the area to the west of shotpoint 1 suggests basement structures at right angles to the San Jacinto and Elsinore fault systems. One such structure was noted by Kovach and others (1962).

Closer examination of the map reveals some subtle features. The "ridge" in the center of the trough is indented by "valleys" and "saddles" that trend northeast. These features are perpendicular to the major faults and have linear dimensions exceeding 15 km in some cases. They correlate with four of the major geothermal resource areas in the Imperial Valley. The geothermal areas plotted in fig. 10 include all those in the Imperial Valley listed in Renner and others (1975) and Brook and others (1978) with indicated subsurface temperatures above 150^{0} C.

The Salton Sea and Westmorland geothermal areas (S, W, fig. 10) are associated with the strongest of the features on the map, a "saddle" with a relief of up to 0.3 s. These areas also have the largest estimated heat reservoirs (Brook and others, 1975). The Heber area (H, fig. 10), with the next largest heat reservoir, is associated with a "valley" that also has a relief of about 0.3 s. The Brawley and East Mesa areas (B, EM, fig. 10), with the smallest heat reservoirs, are the weakest features, "saddles" having a relief of 0.1 s, which is barely resolvable given the reading error. Note the apparent connection between the East Mesa and Heber areas, as well as the apparent right-lateral offset between these areas across the Imperial fault.

A GRAVITY MODEL ACROSS THE IMPERIAL VALLEY REGION

The velocity structure derived from lines 1NW, 1E, and 2W has been used to constrain a gravity model across the Imperial Valley region. This model supercedes previous ones (Kovach and others, 1962; Biehler and others, 1964; Plawman, 1978) in that it includes a high density subbasement (3.1 g/cc) beneath the region.

A gravity profile across southernmost California taken from Oliver and others (in press) shows that the central Imperial Valley is characterized by a slightly negative Bouguer anomaly of -30 to -40 mgal, the Chocolate Mountains by an anomaly of -50 mgal, and the Peninsular Ranges (west of fig. 1) by an anomaly of up to -90 mgal (fig. 11a). Therefore the Imperial Valley, despite its thick sediments, is a slight gravity high relative to the regions which flank it. Previous gravity models across the valley have explained the lack of a strong negative anomaly by a mantle upwelling whose high density compensates for the light sediments. We here present a model in which the subbasement compensates for the light sediments.

In constructing the gravity model (fig. 11b), compressional wave velocities were converted to densities using the relationships summarized by Hamilton (1978) and Batemen and Eaton (1967) and layers with differences in P-wave velocity of less than 0.5 km/s were assigned the same density. For example, the crustal structure of western Arizona consists of "layers" with velocities of 5.8, 6.1, and 6.3 km/s (Warren, 1969; Keller, personal communication, 1980). The average of these crustal velocities is 6.1 km/s and the entire crustal section has been assigned a density of 2.75 g/cc. The complex gravity field over the California Borderland has not been modeled in detail because this is outside the region of present concern; the interested reader is referred to Plawman (1978) for a detailed model of that region.

The gravity calculation presumes a two-dimensional structure and a standard mass column of 70 km with a zero Bouguer gravity anomaly of 9255 mgal (Baraday, 1974; Whitsett, 1975). Iterative adjustments of layer boundaries, constrained by surface geology and seismic refraction data were made until the computed gravity agreed with the observed Bouguer gravity.

It is evident from the computed gravity model (fig. 11b) that the subbasement (3.1 g/cc) compensates gravitationally for both the valley sediments (2.3 and 2.55 g/cc) and the low density basement (2.65 g/cc). Furthermore, it is of particular note that the scarp in the basement under shotpoint 1 (distance 0 km in fig. 11) is mirrored in both the subbasement and mantle. Also note that the negative anomalies over the Chocolate Mountains and Peninsular Ranges require that the subbasement deepen and (or) pinch out in those directions.

Mantle is modeled at an average depth of 23 km beneath the Imperial Valley, the same depth as is reported for western Arizona from seismic refraction measurements (Warren, 1969; Keller, personal communication, 1980). Because of the uncertainties inherent in any gravity model, the depth to mantle needs to be confirmed by seismic refraction measurements.

SUMMARY

A combination of new instrumentation and improved methods of analysis have enabled us to conduct a extensive and detailed seismic refraction survey of the Imperial Valley region, California. The use of 100 cassette-tape-recorded seismometers that can be programmed to turn on at prearranged shot times, deployed rapidly, and played back in the field enabled us to cover an extensive area in the Imperial Valley region with dense lines and arrays of instruments recording shots in numerous places. In addition, with the ability to produce digital record sections in the field, we could modify the survey as it progressed. In all, more than 1300 recording locations were occupied and more than 3000 usable seismograms obtained. With the adaptation of a standard method of ray-tracing to interactive computing, numerous models could be quickly tested for traveltime consistency with the data. Not only first arrivals but, importantly, multiple refractions were used to constrain the model. In addition, this method of interactive ray tracing enabled us to use amplitudes in a qualitative way (and, with some modification, in a quantitative way; Mooney and McMechan, in press) to further constrain the models. Our models are not unique but are largely consistent with one another where profiles cross.

Models are developed for four profiles that cross the Imperial Valley and bordering mesas at several angles. (A model is developed for a fifth profile along the axis of the Salton trough by Mooney and McMechan, in press). All models have in common a sedimentary section (modeled in one to three parts), a transition zone, a basement, and a subbasement.

Sediment velocity appears to increase with depth without discontinuities but with changes in gradient. Velocity-depth curves in the sediments differ somewhat from place to place, but one can classify them. Referring to fig. 8, they can be grouped as follows:

1) Velocity curves from the platforms along the border of the Salton Trough (East and West Mesas) are typified by the curve labeled -1, although these curves change considerably from place to place. On this curve the velocity ranges from 1.7 km/s at the surface to 2.4 km/s at the base of the sediments (1.4 km deep) with a low gradient of 0.5 km/s/km.
2) Velocity curves from the deepest parts of the trough, including those labeled 53, 25, and 15, show velocity gradients that are nearly linear at 0.67 km/s/km from a velocity of 1.8 km/s at the surface to about 5 km/s at the base, over 4.5 km deep.
3) Velocity curves in intermediate regions include those labeled 1, 17, 43, and 0. On these curves the velocity increases from 1.8 km/s at the surface to about 5 km/s at the base, which varies in depth from place to place. The velocity gradient is generally lower in the upper kilometer or so of sediments (0.4 to 0.7 km/s/km) and steeper in lower sections (0.7 to 1.8 km/s/km).

The velocity curve 2.5 km east of shotpoint 1 (labeled 2.5) is the only

one that does not fall into one of these categories; it apparently reflects a structural complication. Velocity contours generally dip toward the center of the valley.

Along the axis of the trough, sediment thickness ranges from about 4.8 km at the U.S.-Mexican border to 3.7 km along the southwest shore of the Salton Sea with an overall plunge along the axis of about 0.8^{o} southeast (Mooney and McMechan, in press). Across the trough between Brawley and El Centro, sediment thickness undergoes more or less abrupt changes from an average of around 1.4 km on West Mesa to 4.5 km in the center of the valley to around 3 km on East Mesa. The changes in thickness occur at buried scarps located at or near the shore lines of ancient Lake Cahuilla, which separate the Imperial Valley from the mesas.

In the Imperial Valley the smooth continuity of the traveltime curves from low apparent velocities (less than 5 km/s) to higher ones (5.55 km/s to 5.80 km/s) is modeled by a transition zone generally 1 km thick in which velocity increases from that at the base of the sediments, about 5 km/s, to an upper basement velocity of 5.65 km/s in most places. In most places, the velocity gradient in this zone decreases slightly from that in the sediments above. On West Mesa and in other places where the sediments thin to less than about 2.5 km, a prominent velocity discontinuity is present at the top of this zone.

Basement has a velocity of 5.65 km/s in most places in the Imperial Valley, based on several reversed profiles, but on West Mesa it has a velocity of 5.92-6.00 km/s based on a reversed profile segment and a time-term study by Hamilton (1970).

No evidence of velocity anisotropy has been found among the five profiles analyzed. Azimuths sampled in the central valley, however, range only from 80^{o} to 130^{o}; northerly and northeasterly azimuths have not yet been sampled. Because of structural complications on profiles crossing the valley, it is probably not possible to distinguish a difference of less than 0.2 km/s in basement velocity, representing a change of 3.5 percent.

Basement velocity gradients may differ between the central valley and West Mesa areas. In the central valley, the velocity gradient is low, around 0.04 km/s/km; a velocity of 5.85-5.95 km/s is attained in the lower basement at depths ranging from 10 to 16 km. Southwest of the Imperial fault and on West Mesa, there is weak evidence for a higher gradient of around 0.1 km/s/km, corresponding to a lower-basement velocity of 6.6 km/s at 12.5 km.

Several structures are seen which affect the basement and transition-zone boundaries as well as deeper velocity contours in the sediments.

1) A scarp is present along the Imperial fault from at least 12 km southeast of El Centro to about 9 km north-northeast of El Centro. Its height apparently decreases from about 1 km at the southeast end to

less than 0.5 km at the northwest end. A dip on the fault of about 70^{o} north-east fits data at the southeast end and 78^{o} fits data at the north-west end; uncertainty in dip is estimated to be less than 10^{o}. No scarp was detected across the fault where it splays out southwest of Brawley. A decrease in velocity for waves passing through the fault zone was needed in the model for 1ESE and would probably have improved the fit in model for 6NW-1SE-1NW.

2) An anomalous bump in the velocity contours in the lower sediments 10 km north of Brawley correlates spacially with the Brawley seismic zone of Johnson (1979).

3) A large scarp beneath shotpoint 1 is required because of the drastic difference in inferred depth to basement east and west of the shotpoint. The precise height, shape, and location of this scarp is more uncertain than most features in the models. Scarp height appears to increase from 1 km, southeast of shot point 1, to 3.5 km, east and northeast of shotpoint 1. Southeast of the shotpoint, the scarp appears to be part of a north-south trending bench on basement and transition-zone rocks which does not correlate with any structure mappable at the surface. East and northeast of the shotpoint, the scarp may be associated with the Superstition Mountain fault.

4) There are no conspicuous scarps in the models along other mapped faults, although the Brawley, Sand Hills, and Algodones faults appear to correlate with changes in slope on basement and transition-zone rocks.

Evidence for a subbasement is seen on all profiles longer than about 40 km. Strong to weak secondary arrivals at distances beginning between 25 and 40 km followed by cross-overs at between 40 and 55 km to branches having apparent velocities of 7.2 to 8.5 km/s indicate the presence of a subbasement at depths ranging from 10 to over 15 km. This layer can be modeled by a velocity step from a velocity between 5.85 and 6.6 km/s, that of lower basement, to a velocity between 6.6 and 7.0 km/s. Below this step is a 1-km-thick zone in which velocity increases rapidly to 7.2 km/s. Such a model is consistent with an interpretation by Hamilton (1970) of a 14 km depth to a 7.1 km/s subbasement in the Borrego Valley-West Mesa area. Plotting only the best-determined depths to subbasement to obtain a rough picture of its topography, one sees a dome between Brawley and El Centro, where the top of the dome is situated at a depth of about 11 km. This dome has a relief on its south side of about 1 km, an amount barely resolvable, and on its north side of about 5 km. Gravity indicates a sharp step downward of the subbasement on the west side and a more gradual deepening to the east. Thus the vicinity of the convergence of the Imperial, Brawley, Superstition Hills, and Superstition Mountain faults appears to be subbasement high.

A contour map of reduced traveltime from shotpoint 1 is roughly equivalent to a sediment isopach map, where greater reduced travel time correlates with greater sediment thickness. This map is difficult to interpret quantitatively, however, because of structural complexity beneath shotpoint 1. Qualitatively it reveals some intriguing features. The map mirrors the surficial topography, in that a "ridge" of high reduced traveltime corresponds to the Imperial Valley, and a "valley" of

low reduced traveltime correponds to West Mesa. The "ridge" reflects a sedimentary trough whose axis coincides roughly with the seismogenic belt in the Imperial Valley. A steep gradient in the contours separates the "ridge" from the "valley". This steep gradient has a roughly north-south trend south of shotpoint 1 and is interpreted to correspond to a buried scarp with this trend. North of shotpoint 1 this gradient appears deflected successively along the Superstition Mountain and Superstition Hills faults, probably reflecting buried scarps along those faults. Steep gradients are also associated with the Coyote Creek fault and the northwest margin of the Superstition Hills and with the Elsinore fault.

Small "valleys" and "saddles" indent the "ridge" in northeast directions, with relief up to 0.3 s and linear dimensions up to 15 km. These features correlate accurately with five of the six geothermal areas in the Imperial Valley having indicated reservoir temperatures exceeding 150^{0} C. The strongest features correlate with areas having the largest estimated heat reservoirs. The traveltime map shows an apparent connection between the Salton and Westmorland areas and between the Heber and East Mesa areas. The latter two appear to be right-laterally offset across the Imperial fault.

Using the new velocity structure for the Imperial Valley region to constrain a gravity model, we discover that a) gravitational compensation for the sediments is accomplished largely by the subbasement (lower crust), with a model density of 3.1 g/cc, b) the relatively flat gravity profile across the Salton Trough requires that the upper surface of this subbasement largely mirror the contact between sediments and basement, and c) the negative gravity anomalies over the Peninsular Ranges and Chocolate Mountains require that the subbasement deepen and (or) pinch out in those directions.

The reader is referred to Fuis and others (in press) for petrologic and tectonic implications of the models developed here.

ACKNOWLEDGMENTS

We estimate that data collection, analysis, and writing of this paper consumed over 10 man-years of effort since the beginning of 1979. About half of this effort was expended by persons other than the authors of this paper. Thus, we wish to express our indebtedness to S. K. Gallanthine, L. R. Hoffman, Barry Keller, J. N. Roloff, and V. C. Sutton, who, together with W. J. Lutter, one of the authors, deployed the instruments; to W. M. Kohler and L. E. Leone, who digitized the data and kept the field computers and plotters running; to D. E. Taylor who permitted the shotpoints; to Bruce Echols and S. S. Wegener who managed the drilling and loading of shot holes; to R. D. Jones, Harry Tostado, and D. L. Styles, who drilled many of the shotholes; to P. T. German and Victor Lamanuzzi, who assisted with the surveying of instrument sites; to R. M. Kaderabek and Robert McClearn, who kept the instruments running; to V. Barba and Elsie Hirscher, who typed the manuscript; and to K. B. Berg, N. C. Crossley, Herbert Mills, and J. R. Van Schaack who provided administrative assistance. In addition, a number of persons facilitated this survey in various ways. Land owners who permitted us to drill and shoot on their properties include R. E. Casey and Wendell Finley (shotpoint 8[1/]) and John Elmore (shotpoint 10). Permission to drill and shoot on government land was granted or expedited by Lieutenant Commander W. F. Ellis of the U.S. National Parachute Test Range (shotpoints 1 and 13), S. L. Johnson of the U.S. Bureau of Land Management (shotpoints 2, 3[1/], 5, 6, 7), and several persons at the U.S. Department of Interior Fish and Wildlife Service (shotpoint 4 [1/]). Clifford Brown, of the U.S. Department of Agriculture graciously allowed us to use the building at their Brawley facility for our field headquarters. Senior Chief C. W. Franklin at the U.S. National Parachute Test Facility kindly permitted us to store explosives at the facility. James Cantrell of the Southern Pacific Railroad Company held up trains for one of our shots. In addition, we wish to express our appreciation to the many people, public and private, of Imperial County who helped us in countless ways.

This paper was improved by many discussions with D. P. Hill and P. A. Spudich. V. Červený kindly provided the ray-tracing code used. R. L. Nowack provided an interactive version of the code.

[1/]These shotpoints were not used and are not shown in fig. 1.

REFERENCES CITED

Baraday, R. J., 1974, Structure of the Panama Basin from marine gravity data: M. S. thesis, Oregon State University, Corvallis, 99 p.

Bateman, P. C., and Eaton, J. P., 1967, Sierra Nevada Batholith: Science, v. 158, p. 1407-1417.

Berry, M. J., and West, G. F., 1966, An interpretation of the first arrival data of the Lake Superior experiment by the time-term method: Seismological Society of America Bulletin, v. 56, p. 141-171.

Biehler, Shawn, Kovach, R. L., and Allen, C. R., 1964, Geophysical framework of northern end of Gulf of California structural province, in van Andel, T. H., and Shor, G. G., Jr., eds., Marine geology of the Gulf of California: American Association of Petroleum Geologists, Memoir 3, p. 126-143.

Blank, H. R., Healy, J. H., Roller, John, Lamson, Ralph, Fisher, Fred, McClearn, Robert, and Allen, Steve, 1979, Seismic refraction profile, Kingdom of Saudi Arabia, field operations, instrumentation, and initial results: U.S. Geological Survey Saudi Arabian Mission, Project Report 259, 49 p.

Brook, C. A., Mariner, R. H., Mabey, D. R., Swanson, J. R., Guffanti, Marianne, and Muffler, L. J. P., 1978, Hydrothermal convection systems with reservoir temperatures $\geq 90^{\circ}$ C, in Muffler, L. J. P., ed., Assessment of geothermal resources of the U.S.--1978: U.S. Geological Survey Circular 790, p. 18-85.

Červený, Vlastilav, Molotkov, I. A., and Pšenčík, Ivan, 1977, Ray methods in seismology: Prague, Karlova University, 214 p.

Fuis, G.S., Mooney, W.D., Healy, J.H., McMechan, G.A., and Lutter, W.J., Crustal structure of the Imperial Valley region, in The Imperial Valley earthquake of October 15, 1979: U.S. Geological Survey Professional Paper (in press).

Hamilton, E. L., 1978, Sound velocity-density relations in sea-floor sediments and rocks: Journal of the Acoustical Society of America, v. 63, no. 2, p. 366-377.

Hamilton, R. M., 1970, Time-term analysis of explosion data from the vicinity of the Borrego Mountain, California, earthquake of 9 April, 1968: Seismological Society of America Bulletin, v. 60, p. 367-381.

Johnson, C. E., 1979, I. Cedar--an approach to the computer automation of short-period local networks II. Seismotectonics of the Imperial Valley of southern California: Ph.D. thesis, California Institute of Technology, Pasadena, 332 p.

Johnson, C. E., and Hutton, L. K., The 15 October 1979 earthquake: a study of aftershocks and prior seismicity, in The Imperial Valley earthquake of October 15, 1979: U.S. Geological Survey Professional Paper (in press).

Kovach, R. L., Allen, C. R., and Press, Frank, 1962, Geophysical investigations in the Colorado delta region: Journal of Geophysical Research, v. 67, p. 2845-2871.

Mooney, W. D., and McMechan, G. A., Synthetic seismogram modeling for the laterally varying structure in the central Imperial Valley, in The Imperial Valley earthquake of October 15, 1979: U.S. Geological Survey Professional Paper (in press).

Oliver, H. W., Chapman, R. H., Biehler, Shawn, Robbins, S. L., Hanna, W. F., Griscom, Andrew, Beyer, L., and Silver, E. A., Preliminary gravity map of California and its continental margin: California Division of Mines and Geology, scale 1:750,000 (in press).

Plawman, T. L., 1978, Crustal structure of the continental borderland and the adjacent portion of Baja California between latitudes 30° N and 33° N: M. S. thesis, Oregon State University, Corvallis, 72 p.

Renner, J. L., White, D. E., and Williams, D. L., 1975, Hydrothermal convection systems, in White, D.E., and Williams, D. L., eds., Assessment of geothermal resources of the U.S.--1975: U.S. Geological Survey Circular 726, p. 5-57.

Warren, D. H., 1969, A seismic-refraction survey of crustal structure in central Arizona: Geological Society of America Bulletin, v. 80, p. 257-282.

Wesson, R. L., 1970, A time integration method for computation of the intensities of seismic rays: Seismological Society of America Bulletin, v. 60, p. 307-316.

Whitsett, R. M., 1975, Gravity measurements and their structural implications for the continental margin of southern Peru: M. S. thesis, Oregon State University, Corvallis, 82 p.

Table 1. Shot list, giving shotpoint locations, origin times (GMT), and yield (lbs of high explosive).

	DEG	MIN	SEC		YR	MON	DAY	HR	MIN	SECOND	YIELD (LBS)
SHOTPOINT 1											
	32	53	4.2	NLAT	79	JAN	23	23	0	0.026	30
	115	46	20.4	WLONG	79	JAN	26	12	30	2.939	1000
					79	FEB	2	13	0	0.010	500
					79	FEB	5	11	30	0.009	1000
					79	FEB	8	10	30	0.016	2000
					79	FEB	18	10	30	0.010	1000
					79	FEB	21	12	0	0.015	1500
					79	MAR	10	10	30	0.015	1000
					79	MAR	14	9	30	0.020	*
					79	MAR	24	10	0	0.013	2000
					79	MAR	31	11	0	0.012	*
					79	NOV	17	9	0	0.002	1440
					79	NOV	17	10	0	0.003	1500
					79	NOV	17	11	0	0.002	240
SHOTPOINT 2											
	32	58	58.8	NLAT	79	MAR	14	11	30	0.016	2000
	115	17	34.8	WLONG	79	MAR	27	11	0	0.013	*
					79	MAR	31	10	30	0.010	*
SHOTPOINT 5											
	32	38	48.8	NLAT	79	FEB	2	11	0	0.009	2000
	115	50	37.8	WLONG	79	FEB	5	11	0	0.015	2000
					79	FEB	8	11	0	0.015	2000
					79	MAR	9	11	0	0.013	400
SHOTPOINT 6											
	32	41	39.7	NLAT	79	FEB	5	12	0	0.020	2000
	115	15	4.1	WLONG	79	FEB	8	11	30	0.011	2000
					79	FEB	18	10	0	0.014	1500
					79	FEB	21	10	0	0.016	2000
					79	MAR	6	10	30	0.006	*
					79	MAR	14	9	0	0.020	2000
SHOTPOINT 7											
	32	42	59.0	NLAT	79	FEB	8	10	0	0.011	2000
	114	58	18.2	WLONG	79	MAR	14	10	30	0.020	2000
SHOTPOINT 10											
	33	5	10.0	NLAT	79	MAR	6	11	0	0.010	1500
	115	37	20.0	WLONG	79	MAR	9	10	0	0.013	*
					79	MAR	14	11	0	0.021	*
					79	MAR	24	10	30	0.014	*
					79	MAR	27	10	30	0.018	1800
					79	MAR	31	11	30	13.818	*
					79	APR	1	8	0	0.010	350
SHOTPOINT 12											
	33	10	36.6	NLAT	79	FEB	21	12	30	0.011	*
	115	52	2.7	WLONG							
SHOTPOINT 13											
	33	10	36.6	NLAT	79	FEB	18	11	0	0.014	2000
	115	52	21.6	WLONG	79	MAR	6	10	0	0.011	2000
SHOTPOINT 14											
	33	10	35.5	NLAT	79	MAR	9	11	30	0.013	*
	115	51	32.4	WLONG	79	MAR	10	10	0	0.014	2000
					79	MAR	27	10	0	0.008	*

* NOT AVAILABLE

STOP --

Table 2. Recorder locations and shots recorded at each.

LOCATION	FIELD ID	LATITUDE DEG	MIN	SEC	LONGITUDE DEG	MIN	SEC	NUMBER OF TIMES SHOTPOINT WAS RECORDED BY A STATION SP1	SP2	SP5	SP6	SP7	SP10	SP12	SP13	SP14
1	HUD0	32	53	4.2	115	46	20.4	80								
2	SS02	32	58	58.8	115	17	34.8	1	1				1			
10	TS00	33	6	10.0	116	37	28.0						1			
80	CM03	33	26	8.3	115	40	42.6		1				1			
81	OW01	33	7	38.0	116	3	49.2	1		1						
82	OW02	33	7	33.6	116	2	47.1	1		1						
83	OW03	33	7	33.5	116	1	46.0	1		1						
84	OW04	33	7	33.5	116	0	44.4	1		1						
85	OW05	33	7	33.9	115	59	42.4	1		1						
86	OW06	33	7	33.9	115	58	40.4	1		1						
87	OW07	33	7	33.9	115	57	38.8	1		1						
88	OW08	33	7	33.9	115	56	36.3	1		1						
89	OW09	33	7	33.8	115	55	34.2	1		1						
90	OW10	33	7	33.9	115	54	32.7	1		1						
91	OW11	33	7	33.9	115	53	31.1	1		1						
92	OW12	33	7	34.7	115	52	34.2	1		1						
93	OW13	33	7	34.3	115	51	32.1	1		1						
101	SS04	33	10	8.4	114	43	38.8	2		1						
102	MIDV	33	14	30.2	114	50	21.8	2		1						
103	OGIL	33	5	28.6	114	54	37.1	2		1						
104	SS03	32	59	10.1	115	2	4.1	2		1						
105	EC19	33	0	12.3	115	18	50.4	2		1						
106	EC18	32	58	3.7	115	20	49.1	2		1						
107	EC17	32	56	45.4	115	22	30.5	2		1						
108	EC16	32	55	54.4	115	24	16.8	2		1						
109	EC15	32	54	57.8	115	25	16.5	2		1						
110	EC14	32	54	6.5	115	27	10.2	2		1						
111	EC0B	32	53	4.0	115	27	54.8	2		1						
112	EC13	32	51	60.0	115	28	29.8	2		1						
113	EC12	32	51	13.1	115	30	2.8	2		1						
114	EC11	32	50	10.8	115	31	7.1	2		1						
115	EC10	32	49	30.9	115	31	52.0	2		1						
116	EC09	32	48	49.6	115	33	36.4	2		1						
117	EC08	32	47	41.9	115	35	54.1	2		1						
118	EC07	32	47	18.7	115	37	20.7	2		1						
119	EC06	32	45	33.7	115	38	16.0	2		1						
120	EC05	32	44	14.8	115	40	30.2	2		1						
121	RR40	33	17	17.4	116	58	44.2	2		2			1			1
122	RR39	33	13	48.3	115	58	41.7	1		1			1			1
123	RR38	33	9	43.6	115	58	33.0	1		1			1			1
124	RR36	33	7	6.7	115	58	32.3	2		2			1			1
125	RR34	33	6	13.3	115	58	33.3	2		2			1			1
126	RR33	33	6	47.0	115	58	32.6	2		2			1			1
127	RR32	33	5	21.6	115	58	33.0	2		2			1			1
128	RR31	33	4	55.8	115	58	32.6	2		2			1			1
129	RR30	33	4	29.7	115	58	33.2	2		2	1		1			1
130	RR29	33	4	0.4	115	58	37.6	2		2	1		1			1
131	RR28	33	3	34.1	115	58	37.1	2		2			1			1
132	RR27	33	3	8.4	115	58	36.8	2		2	2		1			1
133	RR26	33	2	42.1	115	58	36.8	2		2	1		1			1

LOCATIONS AND RECORDED SHOTPOINTS

LOCATION	FIELD ID	LATITUDE DEG	MIN	SEC	LONGITUDE DEG	MIN	SEC	NUMBER OF TIMES SHOTPOINT WAS RECORDED BY A STATION SP1	SP2	SP6	SP6	SP7	SP10	SP12	SP13	SP14
134	RR25	33	2	20.5	115	58	37.2	2		2	1		1			1
135	RR24	33	1	52.3	115	58	38.1	2		2	1		1			1
136	RR23	33	1	24.1	115	58	36.4	1		1			1			1
137	RR22	33	1	3.7	115	58	13.2	1		1			1			1
138	RR21	33	0	40.1	115	57	52.4	1		1			1			1
139	RR19	33	0	7.6	115	57	9.9	1		1			1			1
141	OB01	33	2	47.6	115	41	22.3	2		1	1		1		1	
142	OB02	33	4	7.0	115	40	20.3	2		1	1		1		1	
143	OB03	33	5	56.5	115	38	0.3	3	1	1	1		3		1	
144	OB04	33	7	24.0	116	37	52.1	2		1						
145	OB05	33	7	55.7	115	36	20.6	2		1						
146	OB06	33	8	53.2	115	35	46.5	2		1	1		1		1	
147	OB07	33	9	5.0	115	34	14.5	2		1	1		1		1	
148	OB08	33	10	36.9	115	34	35.8	2		1	1		1		1	
149	OB09	33	11	26.3	115	33	43.2	2		1	1		1		1	
150	OB10	33	12	45.6	115	32	33.7	2		1						
151	OB11	33	14	8.6	115	32	7.5	2		1						
152	OB12	33	15	23.8	115	30	30.4	2		1						
153	OB13	33	16	49.3	115	29	36.9	2		1						
154	OB14	33	18	1.4	115	29	38.1	2		1						
155	OB15	33	19	20.1	115	29	25.5	2		1						
156	OB16	33	22	47.0	115	28	38.0	2		1						
157	SS12	33	5	14.9	115	37	44.5	3	1	1			2			
158	SS10	33	16	25.2	115	29	31.7	2		1						
159	SS08	33	26	33.9	115	50	22.1	2		1						
160	SS09	33	10	35.0	115	51	17.4	2		1	1		1		1	
161	RR17	32	59	16.8	115	56	43.2	2		2			1			1
162	COYT	32	46	13.0	116	0	8.3	3		2			1			2
163	DAVI	32	42	11.6	115	59	1.0	2		1						
164	SS05	32	38	50.5	115	50	33.6	6		5	2	1	2			4
165	SS06	32	41	40.4	115	14	54.0	2		1						
166	SS07	32	42	57.7	114	58	15.4	2		1						
167	EC01	32	40	40.8	115	45	56.3	2		1						
168	EC02	32	40	48.5	115	44	38.4	2		1						
169	EC03	32	41	35.6	115	42	38.9	2		1						
170	EC04	32	42	47.9	115	41	10.3	2		1						
171	RR05	32	51	26.8	115	52	5.7	3		1						1
172	RR06	32	52	6.6	115	52	31.2	2		2			1			1
173	RR12	32	56	51.0	115	55	28.1	2		2			1			1
174	RR13	32	57	38.4	115	56	58.1	2		2			1			1
175	RR14	32	58	18.7	115	56	11.7	2		2			1			1
176	RR15	32	58	36.2	115	56	23.5	2		2			1			1
177	RR16	32	59	56.5	115	56	35.4	2		2			1			1
178	SH21	32	53	37.8	115	46	4.8	2		1	1		1		1	
179	SH23	32	51	34.2	115	47	56.2	3		1	1		1		1	1
180	SS01	32	53	10.4	115	46	14.8	4	1	2	1		1			
181	SH01	33	2	5.6	115	42	38.6	2		1	1		1		1	
182	SH02	33	1	26.7	115	42	34.9	2		1	1		1		1	
183	SH03	33	1	2.2	115	42	52.1	2		1	1		1		1	
184	SH04	33	0	47.3	115	43	7.0	2		1	1		1		1	

LOCATIONS AND RECORDED SHOTPOINTS

LOCATION	FIELD ID	LATITUDE DEG	MIN	SEC	LONGITUDE DEG	MIN	SEC	NUMBER OF TIMES SHOTPOINT WAS RECORDED BY A STATION SP1	SP2	SP5	SP6	SP7	SP10	SP12	SP13	SP14
185	SH05	33	0	30.3	115	43	22.9	2		1	1		1		1	
186	SH06	33	0	4.0	115	43	40.3	2		1	1		1		1	
187	SH07	32	59	33.8	115	43	39.4	2		1	1		1		1	
188	SH08	32	59	12.1	115	43	38.6	2		1	1		1		1	
189	SH09	32	58	43.3	115	43	59.8	2		1	1		1		1	
190	SH10	32	58	25.2	115	44	19.4	2		1	1		1		1	
191	SH11	32	58	5.8	115	44	41.6	2		1	1		1		1	
192	SH12	32	57	56.6	115	45	8.9	2		1	1		1		1	
193	SH13	32	57	28.1	115	45	8.0	2		1						
194	SH14	32	56	57.7	115	45	10.0	2		1	1		1		1	
195	SH15	32	55	46.1	115	45	40.4	2		1	1		1		1	
196	SH16	32	56	28.7	115	45	10.2	2		1	1		1		1	
197	SH17	32	55	16.5	115	46	1.9	2		1	1		1		1	
198	SH18	32	54	49.7	115	45	40.2	2		1	1		1		1	
199	SH19	32	54	25.3	115	45	14.8	2		1	1		1		1	
200	SH20	32	53	59.8	115	45	39.7	2		1	1		1		1	
201	SH22	32	52	15.2	115	47	43.1	1		2	2		2		1	1
202	SS01	32	53	4.9	115	48	19.8				1		1		1	
207	RR11	32	55	57.4	115	54	53.3	1		2	1		1			1
208	RR10	32	56	11.7	115	54	25.3	1		2	1		1			1
209	RR09	32	54	26.0	115	53	56.4	1		2	1		1			1
210	RR08	32	53	40.7	115	53	28.4	1		2	1		1			1
211	RR07	32	52	53.6	115	52	59.8	1		2	1		1			1
212	RR04	32	50	34.5	115	51	33.8	1		1	1					
213	RR03	32	49	46.8	115	51	7.3	1		1	1					
214	RR20	33	0	28.2	115	57	26.9			1			1			1
215	RR35	33	6	37.3	115	58	38.3	1		2			1			1
216	BX29	32	41	40.4	115	15	54.0	1		1	1					
217	BD29	32	42	3.8	115	16	43.2	1		1	1					
218	BX28	32	42	31.1	115	17	38.4	1		1	1					
219	BD28	32	42	30.9	115	18	42.0	1		1	1					
220	BX27	32	42	54.2	115	19	55.2	1		1	1					
221	BD27	32	43	19.6	115	20	22.8	1		1	1					
222	BX26	32	43	24.6	115	21	28.8	1		1	1					
223	BD26	32	43	26.7	115	22	6.0	1		1	1					
224	BX25	32	43	42.9	115	22	60.0	1		1	1					
225	BD25	32	43	44.9	115	23	13.2	1		1	1					
226	BX24	32	44	13.3	115	23	39.6	1		1	1					
227	BD24	32	44	46.8	115	24	14.4	1		1	1					
228	BX23	32	45	1.5	115	24	44.3	1		1	1					
229	BD23	32	45	5.4	115	25	43.3	1		1	1					
230	BX22	32	45	32.7	115	28	44.8	1		1	1					
231	BD22	32	48	0.8	115	27	27.2	1		1	1					
232	BD21	32	47	6.8	115	28	21.6	1		1	1					
233	BX20	32	47	30.0	115	29	11.0	1		1	1					
234	BD20	32	47	49.9	115	29	28.1	1		1	1					
235	BX19	32	47	32.8	115	30	23.8	1		1	1					
236	BD19	32	47	14.1	115	31	7.5	1		1	1					
237	BX18	32	47	18.1	115	31	46.1	1		1	1					
238	BD18	32	48	26.5	115	32	22.0	1		1	1					

>

LOCATIONS AND RECORDED SHOTPOINTS

LOCATION	FIELD ID	LATITUDE DEG	MIN	SEC	LONGITUDE DEG	MIN	SEC	NUMBER OF TIMES SHOTPOINT WAS RECORDED BY A STATION SP1	SP2	SP5	SP6	SP7	SP10	SP12	SP13	SP14
239	BX17	32	48	40.4	115	32	59.6	1		1	1					
240	BD17	32	48	48.6	115	33	38.4	1		1	1					
241	BX16	32	48	36.8	115	34	21.2	1		1	1					
242	BD16	32	48	53.2	115	35	7.5	1		1	1					
243	BX15	32	49	8.5	115	35	50.8	1		1	1					
244	BD09	32	49	6.2	115	36	42.2	1		1	1					
245	BX08	32	49	0.1	115	37	28.6	1		1	1					
246	BD08	32	49	24.5	115	37	44.0	1		1	1					
247	BX07	32	49	43.5	115	38	15.0	1		1	1					
248	BY07	32	50	26.5	115	38	45.2	1		1	1					
249	BD07	32	50	40.0	115	39	13.2	1		1	1					
250	BX06	32	50	44.6	115	39	47.1	1		1	1					
251	BD06	32	50	45.7	115	40	43.3	1		1	1					
252	BD05	32	50	56.7	115	41	45.8	1		1	1					
253	BX04	32	51	13.1	115	42	34.3	1		1	1					
254	BD04	32	51	46.1	115	42	33.6	1		1	1					
255	BD03	32	52	19.5	115	43	35.7	1		1	1					
256	BD02	32	52	48.2	115	44	25.2	1		1	1					
257	BD01	32	53	12.1	115	45	23.5	1		1	1					
258	FC01	32	54	16.4	115	47	26.7	2		2	1		1			2
259	FC02	32	54	53.2	115	48	44.6	1		2	1		1			1
260	FC03	32	55	19.4	115	49	40.5	1		2	1		1			1
261	FC04	32	55	43.9	115	50	33.2	1		1	1					
262	FC05	32	56	10.3	115	51	26.1	1		1	1					
263	FC06	32	56	36.5	115	52	19.6	1		1	1					
264	FC07	32	57	3.4	115	53	15.7	1		1	1					
265	FC08	32	57	29.1	115	54	10.1	1		1	1					
266	FC09	32	58	5.9	115	55	1.6	1		1	1					
267	FC10	32	58	47.3	115	55	42.7	1		1	1					
268	FC11	32	58	25.2	115	56	23.3	1		1	1					
269	FC12	33	0	7.6	115	57	8.9	1		1	1					
270	FC13	33	0	40.1	115	57	52.4	1		1	1					
271	FC14	33	1	24.1	115	58	35.4	1		1	1					
272	FC16	33	2	47.7	115	59	53.2	1		1	1					
273	FC18	33	4	7.0	116	1	18.0	1		1	1					
274	FC20	33	4	47.0	116	3	11.7	1		1	1					
275	FC22	33	5	87.7	116	5	8.9	1		1	1					
276	FC24	33	6	5.1	118	7	8.9	1		1	1					
277	FC25	33	7	3.4	116	9	60.0	1		1	1					
280	MP02	32	56	56.9	116	43	13.0	1		1	1					
281	MP03	32	56	53.6	116	44	22.8	1		1	1					
282	MP05	32	57	2.8	115	46	4.1	1		1	1					
283	MP06	32	56	37.5	115	46	52.9	1		1	1					
284	MP07	32	56	38.0	115	47	51.5	1		1	1					
285	MP12	32	58	21.8	115	48	44.7	1		2	1		1			1
286	MP13	32	57	41.0	115	48	56.6	1		2	1		1			1
287	MP11	32	57	16.3	116	49	18.8	1		2	1		1			1
288	MP15	32	59	11.6	115	49	2.4	1		2	1		1			1
289	MP16	33	0	1.8	116	49	2.0	1		2	1		1			1
290	MP17	33	0	56.9	116	48	46.1	1		2	1		1			1

LOCATIONS AND RECORDED SHOTPOINTS

LOCATION	FIELD ID	LATITUDE DEG	MIN	SEC	LONGITUDE DEG	MIN	SEC	NUMBER OF TIMES SHOTPOINT WAS RECORDED BY A STATION SP1	SP2	SP5	SP6	SP7	SP10	SP12	SP13	SP14
291	KS01	32	53	28.5	115	38	33.4	1		1	1					
292	KS04	32	55	28.9	115	40	4.8	1		1	1					
293	KS07	32	57	25.1	115	41	35.0	1		1	1					
294	KS10	32	58	29.4	115	43	10.0	1		1	1					
295	KS13	33	1	52.4	115	45	8.6	2		2	1		1			2
296	KS14	33	2	21.5	115	45	46.4	2		2	1		1			2
297	KS15	33	3	4.1	115	46	28.1	2		2	1		1			2
298	KS16	33	3	44.9	115	47	9.2	1		1	1					
299	KS17	33	4	31.2	115	47	58.5	1		1	1					
301	YM56	32	40	46.7	115	28	11.4	1		1	1	1				
302	YM57	32	40	43.3	115	27	34.4	1		1	1	1				
303	YM58	32	40	45.3	115	27	9.1	1		1	1	1				
304	YM59	32	40	32.4	115	26	29.5	1		1	1	1				
305	YM60	32	40	15.3	115	25	48.2	1		1	1	1				
306	YA61	32	40	17.7	115	25	23.9	1		1	1	1				
307	YA62	32	40	20.3	115	24	59.4	1		1	1	1				
308	YA63	32	40	22.3	115	24	20.1	1		1	1	1				
309	YA64	32	40	23.9	115	23	56.0	1		1	1	1				
310	YA65	32	40	26.1	115	23	14.4	1		1	1	1				
311	YA66	32	40	27.8	115	22	44.3	1		1	1	1				
312	YA67	32	40	30.1	115	22	14.9	1		1	1	1				
313	YA68	32	40	32.7	115	21	44.3	1		1	1	1				
314	YA69	32	40	35.0	115	21	11.6	1		1	1	1				
315	YA70	32	40	36.5	115	20	51.0	1		1	1	1				
316	YA71	32	40	37.6	115	20	16.8	1		1	1	1				
317	YA72	32	40	44.4	115	18	46.8	1		1	1	1				
318	YA73	32	40	56.4	115	19	12.1	1		1	1	1				
319	YA74	32	41	3.9	115	18	46.0	1		1	1	1				
320	YA75	32	41	13.6	115	18	19.3	1		1	1	1				
321	YA76	32	41	26.1	115	17	51.8	1		1	1	1				
322	YA77	32	41	37.0	115	17	23.7	1		1	1	1				
323	YM73	32	41	35.0	115	18	52.0	1		1	1	1				
324	YM74	32	41	40.9	115	16	21.5	1		1	1	1				
325	YM75	32	41	40.5	115	15	49.7	1		1	1	1				
327	YM77	32	41	40.9	115	14	49.9	1		1	1	1				
328	YM78	32	41	40.9	115	14	18.5	1		1	1	1				
329	YM79	32	41	40.5	115	13	47.2	1		1	1	1				
330	YM80	32	41	40.5	115	13	16.8	1		1	1	1				
331	YM81	32	41	40.8	115	12	45.9	1		1	1	1				
332	YM82	32	41	40.5	115	12	15.1	1		1	1	1				
333	YM83	32	41	40.5	115	11	44.8	1		1	1	1				
334	YM84	32	41	40.5	115	11	13.0	1		1	1	1				
335	YM85	32	41	40.5	115	10	42.6	1		1	1	1				
338	YM86	32	41	40.5	115	10	10.8	1		1	1	1				
337	YM87	32	41	40.5	115	9	39.9	1		1	1	1				
338	YM88	32	41	40.9	115	9	7.2	1		1	1	1				
339	YM89	32	41	40.5	115	8	37.7	1		1	1	1				
340	YM90	32	41	40.5	115	8	6.4	1		1	1	1				
341	YM35	32	40	40.1	115	40	26.5	1		1	1	1				
342	YM34	32	40	43.2	115	40	57.9	1		1	1	1				

LOCATIONS AND RECORDED SHOTPOINTS

LOCATION	FIELD ID	LATITUDE DEG	MIN	SEC	LONGITUDE DEG	MIN	SEC	NUMBER OF TIMES SHOTPOINT WAS RECORDED BY A STATION SP1	SP2	SP5	SP6	SP7	SP10	SP12	SP13	SP14
343	YM33	32	40	46.8	115	41	29.6	1		1	1	1				
344	YM32	32	40	43.6	115	41	57.7	1		1	1	1				
345	YM31	32	40	43.6	115	42	25.8	1		1	1	1				
346	YM30	32	40	42.1	115	43	2.2	1		1	1	1				
347	YM29	32	40	46.3	115	43	33.5	1		1	1	1				
348	YM28	32	40	40.9	115	44	5.8	1		1	1	1				
349	YM27	32	40	52.6	115	44	39.9	1		1	1	1				
350	YM26	32	40	40.9	115	45	6.9	1		1	1	1				
351	YM25	32	40	41.3	115	45	57.6	1		1	1	1				
352	YM24	32	40	36.2	115	46	26.4	1		1	1	1				
353	YM23	32	40	36.6	115	47	0.5	1		1	1	1				
354	YM22	32	40	32.7	115	47	35.0	1		1	1	1				
355	YM21	32	40	31.2	115	48	2.2	1		1	1	1				
356	YM20	32	40	29.6	115	48	35.4	1		1	1	1				
357	YM19	32	40	27.3	115	49	8.4	1		1	1	1				
358	YM18	32	40	26.9	115	49	37.9	1		1	1	1				
359	YM17	32	40	24.9	115	50	7.4	1		1	1	1				
360	YM16	32	40	22.2	115	50	39.6	1		1	1	1				
362	YM15	32	40	15.8	115	51	11.7	1		1	1	1				
363	YMYM	32	40	11.5	115	51	41.2	1		1	1	1				
364	YM13	32	40	5.1	115	52	13.9	1		1	1	1				
365	YM12	32	40	6.2	115	52	40.4	1		1	1	1				
366	YM11	32	40	12.5	115	53	9.9	1		1	1	1				
367	YM10	32	40	29.8	115	53	30.4	1		1	1	1				
368	YM09	32	40	50.7	115	53	51.1	1		1	1	1				
369	YM08	32	40	58.3	115	54	19.8	1		1	1	1				
370	YM07	32	41	4.3	115	54	49.2	1		1	1	1				
371	YM06	32	41	11.1	115	55	21.0	1		1	1	1				
372	YM05	32	41	33.1	115	55	39.9	1		1	1	1				
373	YM04	32	41	56.1	115	55	53.5	1		1	1	1				
374	YM03	32	42	20.3	115	56	6.7	1		1	1	1				
375	YM01	32	42	52.8	115	56	39.1	1		1	1	1				
376	YC01	32	43	12.7	115	57	32.3	1		1	1	1				
377	YC02	32	43	24.5	115	58	33.8	1		1	1	1				
378	YC03	32	43	28.4	115	59	43.2	1		1	1	1				
379	YC04	32	43	35.1	116	0	44.2	1		1	1	1				
380	YC05	32	42	12.5	116	1	46.2	1		1	1	1				
381	YM36	32	40	16.4	115	39	59.1	1		1	1	1				
382	YM37	32	39	26.6	115	39	41.3	1		1	1	1				
383	YM38	32	39	15.2	115	39	16.1	1		1	1	1				
384	YM39	32	39	17.3	115	38	50.0	1		1	1	1				
385	YM40	32	39	19.9	115	38	18.2	1		1	1	1				
386	YM41	32	39	21.7	115	37	44.3	1		1	1	1				
387	YM42	32	39	23.5	115	37	17.6	1		1	1	1				
388	YM43	32	39	26.5	115	36	42.0	1		1	1	1				
389	YM44	32	39	28.5	115	36	9.6	1		1	1	1				
390	YM45	32	39	31.0	115	35	38.6	1		1	1	1				
391	YM46	32	39	33.5	115	35	4.3	1		1	1	1				
392	YM47	32	38	36.8	115	34	32.4	1		1	1	1				
393	YM48	32	39	38.6	115	34	3.4	1		1	1	1				

>

LOCATIONS AND RECORDED SHOTPOINTS

LOCATION	FIELD ID	LATITUDE DEG	MIN	SEC	LONGITUDE DEG	MIN	SEC	NUMBER OF TIMES SHOTPOINT WAS RECORDED BY A STATION SP1	SP2	SP5	SP6	SP7	SP10	SP12	SP13	SP14
393	YM48	32	39	38.8	116	34	3.4	1		1	1	1				
394	YM49	32	39	41.2	116	33	38.3	1		1	1	1				
395	YM50	32	39	44.9	116	32	48.2	1		1	1	1				
396	YM51	32	39	47.0	116	32	18.0	1		1	1	1				
397	YM52	32	39	56.2	116	31	32.8	1		1	1	1				
398	YM53	32	39	59.1	116	31	2.8	1		1	1	1				
399	YM54	32	40	0.9	116	30	25.6	1		1	1	1				
400	YM55	32	40	20.6	116	29	28.2	1		1	1	1				
401	BR41	32	58	1.6	116	36	41.4	1			1				1	
402	BR42	32	57	47.2	116	35	11.1	1			1				1	
403	BR43	32	57	55.8	116	34	25.6	1			1				1	
404	BR44	32	58	18.2	116	33	26.8	1			1				1	
405	BR45	32	57	48.7	116	33	34.7	1			1				1	
406	BR46	32	57	22.2	116	34	13.9	1			1				1	
407	BR47	32	56	56.7	116	32	49.7	1			1				1	
408	BR48	32	56	31.2	116	32	39.0	1			1				1	
409	BR49	32	56	30.8	116	33	20.3	1			1				1	
410	BR50	32	58	1.2	116	33	13.5	1			1				1	
411	BR51	32	56	28.5	116	31	59.3	1			1				1	
412	BR52	32	56	16.0	116	32	35.5	1			1				1	
413	BR53	32	55	37.0	116	32	11.3	1			1				1	
414	BR99	32	56	0.8	116	31	3.1	1			1				1	
415	BR54	32	55	14.3	116	31	34.2	2	1		1		1		1	
416	BR55	32	54	57.3	116	31	2.8	1			1				1	
417	BR56	32	54	31.7	116	30	41.6	1			1				1	
418	BR57	32	54	18.8	116	30	1.8	1			1				1	
419	BR58	32	55	14.0	116	30	0.9	1			1				1	
420	BR59	32	54	43.7	116	29	28.8	1			1				1	
421	BR80	32	48	34.7	116	23	26.3	1			1				1	
422	BR81	32	48	22.2	116	22	14.8	1			1				1	
423	BR82	32	48	3.1	116	21	58.2	1			1				1	
424	BR83	32	47	49.1	116	21	27.7	1			1				1	
425	BR84	32	47	30.3	116	20	56.4	1			1				1	
426	BR85	32	47	14.0	116	20	8.4	1			1				1	
427	BR86	32	47	17.1	116	19	19.4	1			1				1	
428	BR87	32	47	17.9	116	18	36.5	1			1				1	
429	BR88	32	45	36.6	116	21	6.9	1			1				1	
430	BR89	32	46	30.8	116	20	10.1	1			1				1	
431	BR90	32	46	33.5	116	19	5.2	1			1				1	
432	BR91	32	44	59.2	116	18	38.0	1			1				1	
433	BR92	32	44	41.3	116	17	60.0	1			1				1	
434	BR93	32	44	15.2	116	17	36.0	1			1				1	
435	BR94	32	43	48.3	116	17	4.6	1			1				1	
436	BR96	32	43	20.3	116	18	31.0	1			1				1	
437	BR96	32	42	59.2	116	16	16.7	1			1				1	
438	BR97	32	42	33.1	116	15	58.7	1			1				1	
439	BR98	32	42	13.3	116	15	43.3	1			1				1	
441	BR21	33	4	29.6	116	42	28.6	1			1				1	
442	BR22	33	3	47.5	116	42	24.0	1			2		1		2	
443	BR23	33	3	40.1	116	41	54.4	1			1				1	

>

LOCATIONS AND RECORDED SHOTPOINTS

LOCATION	FIELD ID	LATITUDE DEG	MIN	SEC	LONGITUDE DEG	MIN	SEC	NUMBER OF TIMES SHOTPOINT WAS RECORDED BY A STATION SP1	SP2	SP5	SP6	SP7	SP10	SP12	SP13	SP14
445	BR25	33	8	48.3	115	41	22.8	1			1				1	
446	BR26	33	2	30.4	115	40	52.7	1			1				1	
447	BR27	33	3	15.7	115	40	19.4	1			1				1	
448	BR28	33	2	36.2	115	39	48.4	1			1				1	
449	BR29	33	2	24.2	115	39	19.3	1			1				1	
450	BR30	33	1	56.9	115	40	27.3	1			1				1	
451	BR31	33	1	42.1	115	39	48.4	1			1				1	
452	BR32	33	1	8.4	115	39	24.9	1			1				1	
453	BR33	33	1	12.3	115	38	47.8	1			1				1	
454	BR34	33	0	47.9	115	38	48.0	1			1				1	
455	BR35	33	0	28.8	115	38	25.2	1			1				1	
456	BR36	33	0	10.9	115	37	44.8	1			1				1	
457	BR37	32	59	57.3	115	37	5.5	1			1				1	
458	BR38	32	59	20.3	115	36	45.6	1			1				1	
459	BR39	32	58	55.3	115	36	11.4	1			1				1	
460	BR40	32	58	32.0	115	35	41.4	1			1				1	
461	BR01	33	10	38.0	115	52	2.7	1			1				1	
462	BR02	33	10	3.8	115	50	20.8	1			1				1	
463	BR03	33	9	18.9	115	50	20.8	1			1				1	
464	BR04	33	8	50.8	115	49	57.0	1			1				1	
465	BR05	33	8	38.1	115	49	17.1	1			1				1	
466	BR06	33	8	25.1	115	48	45.0	1			1				1	
467	BR07	33	7	52.8	115	48	42.7	1			1				1	
468	BR08	33	7	32.0	115	48	7.1	1			1				1	
469	BR09	33	7	10.8	115	47	44.3	1			1				1	
470	BR10	33	6	49.8	115	46	59.9	1			1				1	
471	BR11	33	6	38.8	115	46	14.5	1			1				1	
472	BR12	33	6	12.1	115	45	39.8	1			1				1	
473	BR13	33	6	2.5	115	45	5.8	1			1				1	
474	BR14	33	5	48.3	115	44	36.3	1			1				1	
475	BR15	33	5	51.4	115	44	5.4	1			1				1	
476	BR16	33	5	23.0	115	44	4.2	1			1				1	
477	BR17	33	5	31.8	115	43	36.8	1			1				1	
478	BR18	33	4	58.2	115	43	36.9	1			1				1	
479	BR19	33	4	47.1	115	43	1.6	1			1				1	
480	BR20	33	4	58.2	115	42	31.8	1			1				1	
481	BR60	32	54	19.9	115	28	3.2	1			1				1	
482	BR61	32	53	54.9	115	29	46.2	1			1				1	
483	BR62	32	53	27.6	115	29	30.0	1			1				1	
484	BR63	32	53	23.4	115	29	0.4	1			1				1	
485	BR64	32	52	57.3	115	28	50.8	1			1				1	
486	BR65	32	52	56.8	115	28	23.0	1			1				1	
487	BR66	32	53	45.2	115	28	28.6	1			1				1	
488	BR67	32	53	4.3	115	27	56.4	1			1				1	
489	BR68	32	53	8.9	115	26	60.0	1			1				1	
490	BR69	32	52	31.5	115	27	38.9	1			1				1	
491	BR70	32	52	7.4	115	27	31.4	1			1				1	
492	BR71	32	51	38.7	115	26	47.0	1			1				1	
493	BR72	32	51	18.7	115	26	38.3	1			1				1	
494	BR73	32	50	50.6	115	26	18.1	1			1				1	

>

LOCATIONS AND RECORDED SHOTPOINTS

LOCATION	FIELD ID	LATITUDE DEG	MIN	SEC	LONGITUDE DEG	MIN	SEC	NUMBER OF TIMES SHOTPOINT WAS RECORDED BY A STATION SP1	SP2	SP5	SP6	SP7	SP10	SP12	SP13	SP14
496	BR74	32	50	35.8	115	35	46.2	1			1				1	
498	BR75	32	50	22.2	115	25	21.3	1			1				1	
497	BR76	32	50	2.3	115	24	50.8	1			1				1	
498	BR77	32	49	32.7	115	24	30.9	1			1				1	
499	BR78	32	49	34.3	115	23	48.0	1			1				1	
500	BR79	32	48	54.8	115	24	12.0	1			1				1	
501	GL21	32	58	4.7	115	31	57.7	4			1			1		
502	GL22	32	55	24.5	116	32	11.5	4			1			1		
503	GL23	32	54	58.5	115	32	55.4	5	1		1		1	1		
504	GL24	32	54	41.3	116	31	34.2	4			1			1		
505	GL25	32	54	41.3	115	31	4.2	4			1			1		
506	GL26	32	54	32.3	115	30	38.5	4			1			1		
507	GL27	32	55	37.0	115	30	26.8	5	1		1		1	1		
508	GL28	32	55	37.0	115	30	49.9	4			1			1		
509	GL29	32	56	37.0	116	31	18.5	4			1			1		
510	GL30	32	54	30.8	115	30	3.2	4			1			1		
511	GL31	32	54	33.9	115	30	2.3	4			1			1		
512	GL32	32	55	35.1	115	29	29.5	5	1		1		1	1		
513	GL33	32	54	31.2	115	29	29.5	4			1			1		
514	GL34	32	54	38.2	115	29	0.4	4			1			1		
515	GL35	32	55	29.2	115	28	54.4	4			1			1		
516	GL36	32	55	55.7	115	28	27.2	4			1			1		
517	GL37	32	55	39.3	115	27	55.7	6	1		1		1	1		
518	GL38	32	54	49.1	115	27	54.4	4			1			1		
519	GL39	32	55	0.0	115	28	23.5	4			1			1		
520	GL40	32	54	37.8	115	32	31.4	4			1			1		
521	GL61	32	58	46.0	115	22	30.0	5	1		1		1	1		
522	GL62	32	58	51.4	115	21	42.1	5	1		1		1	1		
523	GL63	32	56	50.7	115	21	11.5	4			1			1		
524	GL64	32	56	48.4	115	20	40.8	5	1		1		1	1		
525	GL65	32	56	49.8	115	20	10.8	4			1			1		
526	GL66	32	58	48.2	115	19	40.6	6	1		1		1	1		
527	GL67	32	58	48.5	115	19	10.1	4			1			1		
528	GL68	32	56	51.4	116	18	38.1	5	1		1		1	1		
529	GL69	32	57	32.0	115	18	8.3	5	1		1		1	1		
530	GL70	32	57	56.5	116	17	20.3	4			1			1		
531	GL71	32	58	12.5	115	16	54.4	4			1			1		
532	GL72	32	58	12.5	115	16	16.7	5	1		1		1	1		
533	GL73	32	58	12.8	116	15	38.6	4			1			1		
534	GL74	32	58	12.7	115	15	5.5	6	1		1		1	1		
535	GL75	32	58	11.7	115	14	28.6	4			1			1		
536	GL76	32	58	12.7	116	13	43.8	5	1		1		1	1		
537	GL77	32	58	11.7	116	12	59.1	4			1			1		
538	GL78	32	58	7.4	116	11	55.3	4			1			1		
539	GL79	32	58	21.0	115	10	59.9	5	1		1		1	1		
540	GL80	32	58	38.2	115	10	13.2	4			1			1		
541	GL41	32	55	8.6	116	27	26.7	4			1			1		
542	GL42	32	55	51.8	115	27	30.0	4			1			1		
543	GL43	32	55	0.8	116	26	60.0	4			1			1		
544	GL44	32	56	1.8	116	26	54.4	5	1		1		1	1		

LOCATIONS AND RECORDED SHOTPOINTS

LOCATION	FIELD ID	LATITUDE DEG	MIN	SEC	LONGITUDE DEG	MIN	SEC	NUMBER OF TIMES SHOTPOINT WAS RECORDED BY A STATION SP1	SP2	SP5	SP6	SP7	SP10	SP12	SP13	SP14
545	GL45	32	55	60.0	115	26	23.9	4			1			1		
546	GL46	32	55	59.2	115	25	52.6	5	1		1		1	1		
547	GL47	32	55	59.2	115	25	20.8	4			1			1		
548	GL48	32	56	59.2	115	24	50.8	5	1		1		1	1		
549	GL49	32	56	54.3	115	24	17.5	4			1			1		
550	GL50	32	56	0.8	115	23	49.8	5	1		1		1	1		
551	GL51	32	55	58.4	115	23	18.6	4			1			1		
552	GL52	32	55	59.6	115	22	46.5	5	1		1		1	1		
553	GL53	32	55	5.8	115	22	48.4	4			1			1		
554	GL54	32	55	5.8	115	23	17.5	4			1			1		
555	GL56	32	55	5.6	115	24	20.7	4			1			1		
556	GL57	32	56	1.2	115	24	50.9	4			1			1		
557	GL58	32	55	6.8	115	25	21.0	4			1			1		
558	GL59	32	56	6.2	115	25	52.6	4			1			1		
559	GL60	32	54	58.0	115	26	36.8	4			1			1		
560	GL56	32	55	13.6	115	23	49.5	4			1			1		
561	GL01	32	55	37.0	115	37	41.0	5	1		1		1	1		
562	GL02	32	56	31.1	115	38	43.3	5	1		1		1	1		
563	GL03	32	56	35.6	115	39	41.1	4			1			1		
564	GL04	32	55	35.8	115	40	38.7	5	1		1		1	1		
565	GL05	32	55	28.6	115	41	38.7	4			1			1		
566	GL06	32	54	51.6	115	42	22.4	5	1		1		1	1		
567	GL07	32	54	9.3	115	42	53.8	4			1			1		
568	GL08	32	54	57.3	115	38	80.0	5	1		1		1	1		
569	GL09	32	54	55.9	115	36	28.1	4			1			1		
570	GL10	32	54	51.1	115	38	8.9	5	1		1		1	1		
571	GL11	32	56	11.1	115	35	24.8	5	1		1		1	1		
572	GL12	32	55	37.0	115	35	23.2	4			1			1		
573	GL13	32	56	38.0	115	34	54.2	4			1			1		
574	GL14	32	56	11.1	115	34	48.1	5	1		1		1	1		
575	GL15	32	56	12.3	115	34	24.7	4			1			1		
576	GL16	32	56	38.2	115	34	26.3	4			1			1		
577	GL17	32	55	36.4	115	33	45.0	4			1			1		
578	GL18	32	55	9.7	115	33	35.0	5	1		1		1	1		
579	GL19	32	56	50.3	115	33	7.3	4			1			1		
580	GL20	32	55	55.7	115	32	39.4	4			1			1		
581	GL81	32	58	45.8	115	9	46.1	4			1			1		
582	GL82	32	58	50.3	115	8	13.8	4			1			1		
583	GL83	32	58	50.5	115	8	41.4	4			1			1		
584	GL84	32	59	8.9	115	8	13.7	4			1			1		
585	GL85	32	58	12.1	115	7	48.3	4			1			1		
586	GL86	32	59	18.3	115	7	13.4	4			1			1		
587	GL87	32	59	35.4	115	6	41.8	4			1			1		
588	GL88	32	58	38.5	115	6	7.7	4			1			1		
589	GL89	32	58	40.9	115	5	35.4	4			1			1		
590	GL90	32	59	38.5	115	5	6.8	4			1			1		
591	GL91	32	59	39.3	115	4	36.2	4			1			1		
592	GL92	32	58	56.5	115	4	2.9	4			1			1		
593	GL93	33	0	14.8	115	3	35.7	4			1			1		
594	GL94	33	0	32.5	115	3	11.7	4			1			1		

LOCATIONS AND RECORDED SHOTPOINTS

LOCATION	FIELD ID	LATITUDE DEG	MIN	SEC	LONGITUDE DEG	MIN	SEC	NUMBER OF TIMES SHOTPOINT WAS RECORDED BY A STATION SP1	SP2	SP5	SP6	SP7	SP10	SP12	SP13	SP14
595	GL95	33	0	48.7	115	2	34.3	4			1			1		
596	GL96	33	1	21.1	115	1	52.2	4			1			1		
597	GL97	33	1	55.6	115	1	6.4	4			1			1		
598	GL98	33	2	34.2	115	0	24.2	4			1			1		
599	GL99	33	3	11.7	114	59	35.9	4			1			1		
600	GL10	33	5	29.8	114	54	37.1	4			1			1		
601	SS10	33	5	13.7	115	37	20.7				1		1		1	
602	OX10	33	6	52.2	115	35	18.1				1		1		1	
603	OX19	33	7	26.0	115	35	48.2				1		1		1	
604	OX13	33	8	25.3	115	36	13.1				1		1		1	
605	OS05	33	7	58.0	115	36	18.9				1		1		1	
606	OX12	33	7	50.8	115	36	51.6				1		1		1	
607	OX11	33	7	46.0	115	37	19.0				1		1		1	
608	OS04	33	7	25.7	115	37	52.2				1		1		1	
609	OX10	33	7	6.6	115	38	0.1				1		1		1	
610	OX09	33	6	44.0	115	38	28.9				1		1		1	
611	US05	33	6	20.7	115	40	18.5				1		1		1	
612	US06	33	7	9.6	115	39	40.5				1		1		1	
613	US07	33	7	37.9	115	39	22.5				1		1		1	
614	US08	33	7	56.9	115	39	0.7				1		1		1	
615	US09	33	8	19.5	115	38	39.0				1		1		1	
617	US11	33	8	16.4	115	37	54.5				1		1		1	
618	US12	33	8	54.5	115	37	48.0				1		1		1	
619	US13	33	9	44.8	115	38	15.4				1		1		1	
620	US14	33	10	17.5	115	37	31.4				1		1		1	
625	OX14	33	8	51.8	115	36	41.4				1		1		1	
626	OX15	33	8	14.0	115	35	16.8				1		1		1	
627	OX16	33	10	36.2	115	35	47.8				1		1		1	
628	OX17	33	10	9.0	115	34	45.2				1		1		1	
629	OX20	33	11	2.3	115	33	56.5				1		1		1	
630	OX21	33	11	58.6	115	33	8.8				1		1		1	
631	OX22	33	12	26.1	115	33	9.7				1		1		1	
632	US15	33	9	17.5	115	37	22.1				1		1		1	
633	US16	33	10	7.8	115	37	3.1				1		1		1	
634	US17	33	10	34.3	115	36	38.5				1		1		1	
635	US18	33	10	56.9	115	36	18.7				1		1		1	
636	US19	33	11	39.1	115	35	47.8				1		1		1	
637	US20	33	11	59.5	115	35	46.9				1		1		1	
638	US21	33	12	19.5	115	34	52.6				1		1		1	
639	US22	33	12	47.9	115	34	28.4				1		1		1	
640	US23	33	13	12.1	115	34	5.3				1		1		1	
645	OX01	33	2	10.1	115	42	8.7				1		1		1	
646	OX02	33	2	29.8	115	41	37.7				1		1		1	
648	OX03	33	3	14.0	115	40	51.0				1		1		1	
649	OX04	33	3	41.7	115	40	34.9				1		1		1	
651	OX05	33	4	44.0	115	39	54.4				1		1		1	
652	OX09	33	5	9.9	115	39	30.4				1		1		1	
653	OX07	33	5	34.7	115	39	15.6				1		1		1	
655	US04	33	0	9.8	115	40	25.0				1		1		1	
656	US03	33	5	47.0	115	40	47.8				1		1		1	

>

LOCATIONS AND RECORDED SHOTPOINTS

LOCATION	FIELD ID	LATITUDE DEG	MIN	SEC	LONGITUDE DEG	MIN	SEC	NUMBER OF TIMES SHOTPOINT WAS RECORDED BY A STATION SP1	SP2	SP5	SP6	SP7	SP10	SP12	SP13	SP14
657	WS02	33	5	22.2	115	41	13.1				1		1		1	
658	WS01	33	4	49.5	115	41	29.8				1		1		1	
661	WS26	33	14	31.2	115	32	53.8				1		1		1	
662	WS25	33	14	3.5	115	33	17.2				1		1		1	
663	WS24	33	13	38.3	115	33	36.8				1		1		1	
664	OB10	33	18	46.0	115	32	33.6				1		1		1	
665	OX23	33	13	18.5	115	32	17.8				1		1		1	
666	OX24	33	13	33.0	115	32	9.0				1		1		1	
667	OB11	33	14	9.4	115	32	7.7				1		1		1	
668	OX25	33	14	8.6	115	31	34.9				1		1		1	
669	OX26	33	14	53.8	115	30	4.3				1		1		1	
670	OB12	33	15	23.3	115	30	29.7				1		1		1	
671	OX27	33	15	48.6	115	29	33.0				1		1		1	
672	OX28	33	16	23.5	115	29	38.7				1		1		1	
673	OB13	33	16	47.4	115	28	36.8				1		1		1	
674	OX29	33	17	19.9	115	28	43.1				1		1		1	
675	OB14	33	18	0.8	115	28	37.6				1		1		1	
676	OX30	33	18	45.4	115	28	33.9				1		1		1	
677	OB15	33	19	17.5	115	28	25.7				1		1		1	
678	OX31	33	20	22.2	115	28	11.8				1		1		1	
679	OX32	33	21	33.2	115	28	55.2				1		1		1	
680	OB16	33	23	5.8	115	28	33.4				1		1		1	
701	PC01	32	47	21.4	116	41	36.5			1			1			1
702	PC02	32	47	30.0	116	42	36.0			1			1			1
703	PC03	32	47	38.6	115	43	34.6			1			1			1
704	YH06	32	45	14.2	116	53	26.4	1		1			1			2
705	YH07	32	46	15.1	116	52	35.9	1		1			1			2
706	RR04	32	50	24.3	115	51	32.6			1			1			1
707	RR03	32	49	46.8	116	51	7.3			1			1			1
708	RR02	32	48	47.0	115	50	58.9			1			1			1
709	RR01	32	47	53.2	115	51	2.5			1			1			1
710	PR21	32	52	44.8	116	4	49.4	1		1			1			2
711	PR20	32	52	42.5	116	3	24.6	1		1			1			2
712	PR19	32	52	57.7	116	1	31.4	1		1			1			2
713	PR18	32	52	55.3	116	0	8.0	1		1			1			2
714	PR17	32	52	21.4	115	59	5.6	1		1			1			2
715	PR16	32	52	5.1	115	58	3.2	1		1			1			2
716	PR15	32	51	59.6	115	57	8.7	1		1			1			2
717	PR14	32	51	39.8	115	56	3.2	1		1			1			2
718	PR13	32	51	33.5	115	54	80.0	1		1			1			2
719	PR12	32	51	33.9	115	54	6.5	1		1			1			2
720	PR11	32	51	38.0	115	53	9.2	1		1			1			2
741	PR05	32	51	35.1	115	48	43.8			1			1			1
742	PR07	32	51	30.4	115	48	57.7			1			1			1
743	PR09	32	51	28.4	115	51	2.8			1			1			1
756	RR18	32	50	40.9	115	56	55.8			1			1			1
759	SS02	32	50	34.3	115	17	51.2	1		1			1			2
761	PC17	32	44	59.1	115	57	10.6			1			1			1
762	PC16	32	45	32.3	115	56	19.9			1			1			1
763	PC15	32	45	59.7	115	55	28.3			1			1			1

LOCATIONS AND RECORDED SHOTPOINTS

LOCATION	FIELD ID	LATITUDE DEG	MIN	SEC	LONGITUDE DEG	MIN	SEC	NUMBER OF TIMES SHOTPOINT WAS RECORDED BY A STATION SP1	SP2	SP5	SP6	SP7	SP10	SP12	SP13	SP14
764	PC14	32	46	27.7	115	54	34.1			1			1			1
765	PC13	32	46	55.4	115	53	42.9			1			1			1
766	PC12	32	47	25.8	115	52	56.2			1			1			1
767	PC11	32	47	30.8	115	51	49.8			1			1			1
768	PC10	32	47	28.8	115	50	31.6			1			1			1
769	PC09	32	47	30.7	115	49	45.3			1			1			1
770	PC08	32	47	29.6	115	48	47.0			1			1			1
771	PC07	32	47	30.4	115	47	44.8			1			1			1
772	PC06	32	47	29.9	115	46	55.8			1			1			1
773	PC05	32	47	31.4	115	45	57.3			1			1			1
774	PC04	32	47	32.9	115	44	51.3			1			1			1
781	PR01	32	51	48.7	116	42	33.7			1			1			1
782	PR03	32	51	35.0	116	44	36.9			1			1			1
784	SX22	32	53	7.4	115	47	43.8			1			1			1
785	SX20	32	53	59.6	115	47	43.8			1			1			1
789	NX02	32	56	11.7	115	49	33.2	1		1			1			2
790	NX03	32	58	35.8	115	49	30.0	1		1			1			2
801	PX01	32	47	29.2	115	42	8.8	1								1
802	PX02	32	47	28.6	115	43	6.9	1								1
803	PX03	32	47	26.6	115	44	21.6	1								1
806	RX04	32	50	57.8	115	51	59.0	1								1
807	RX03	32	50	12.2	115	51	31.3	1								1
808	RX02	32	49	48.8	115	51	3.7	1								1
809	RX01	32	48	18.5	115	50	58.9	1								1
821	RX20	33	0	34.7	115	57	42.5	1								1
822	RX21	33	0	53.8	115	58	2.8	1								1
823	RX22	33	1	13.6	115	58	23.2	1								1
824	RX23	33	1	41.3	115	58	36.6	1								1
825	RX24	33	2	5.8	115	58	30.6	1								1
826	RX25	33	2	33.9	115	58	37.1	1								1
827	RX26	33	2	58.1	115	58	36.3	1								1
828	RX27	33	3	21.4	115	58	36.3	1								1
829	RX28	33	3	47.9	115	58	31.2	1								1
830	RX29	33	4	14.0	115	58	32.1	1								1
831	RX30	33	4	43.6	115	58	39.5	1								1
832	RX31	33	5	9.3	115	58	39.0	1								1
833	RX32	33	5	34.3	115	58	33.0	1								1
834	RX33	33	5	60.0	115	58	33.0	1								1
835	RX34	33	6	26.1	115	58	33.5	1								1
836	RX35	33	6	51.8	115	58	34.8	1								1
837	RX36	33	7	19.1	115	58	33.0	1								1
838	RX38	33	8	53.0	115	58	32.5	1								1
839	RX39	33	13	18.7	115	58	41.2	1								1
840	RX40	33	17	18.3	115	58	44.9	1								1
842	PR08	32	61	29.2	115	49	59.1	1								1
844	RX08	32	52	31.6	115	52	45.2	1								1
845	RX07	32	53	18.7	115	52	59.6	1								1
846	RX08	32	54	3.5	115	53	48.9	1								1
847	RX09	32	54	48.7	115	54	12.0	1								1
848	RX10	32	55	33.9	115	54	40.1	1								1

LOCATIONS AND RECORDED SHOTPOINTS

LOCATION	FIELD ID	LATITUDE DEG	MIN	SEC	LONGITUDE DEG	MIN	SEC	NUMBER OF TIMES SHOTPOINT WAS RECORDED BY A STATION SP1	SP2	SP5	SP6	SP7	SP10	SP12	SP13	SP14
849	RX11	32	56	19.1	115	55	7.4	1								1
850	RX12	32	57	18.9	115	55	41.6	1								1
851	RX13	32	57	47.6	115	55	59.1	1								1
852	RX14	32	58	25.3	115	56	18.5	1								1
853	RX15	32	58	50.3	115	56	30.8	1								1
854	RX16	32	59	9.4	115	56	40.1	1								1
855	RX17	32	59	30.8	115	56	50.2	1								1
856	RX18	32	59	51.8	115	57	1.3	1								1
857	RX19	33	0	16.8	115	57	18.9	1								1
858	PR06	32	52	0.4	115	47	48.4	1		1			1			2
862	PX17	32	44	48.0	115	57	31.8	1								1
863	PX16	32	45	10.2	115	58	41.1	1								1
864	PX15	32	45	40.8	115	55	53.4	1								1
865	PX14	32	46	9.5	115	54	66.9	1								1
866	PX13	32	46	39.8	115	54	12.7	1								1
867	PX12	32	47	7.8	115	53	18.1	1								1
868	PX11	32	47	29.0	115	52	25.0	1								1
869	PX10	32	47	31.8	115	50	51.6	1								1
870	PX09	32	47	30.4	115	50	9.6	1								1
871	PX08	32	47	29.7	115	49	30.0	1								1
872	PX07	32	47	38.7	115	48	22.5	1								1
873	PX06	32	47	28.2	115	47	22.7	1								1
874	PX05	32	47	36.6	115	46	27.3	1								1
875	PX04	32	47	34.9	115	45	22.5	1								1
876	YH05	32	44	22.9	115	53	24.6	1		1			1			2
877	YH03	32	42	58.2	115	52	38.1	1		1			1			2
878	YH02	32	41	28.7	115	53	15.4	1		1			1			2
879	YH01	32	40	23.7	115	52	52.1	1		1			1			2
881	PR02	32	51	35.8	115	43	36.4	1								1
882	PR04	32	51	36.6	115	45	39.7	1								1
883	SX23	32	52	48.9	115	47	45.7	1								1
884	SX21	32	53	33.9	115	47	43.8	1								1
885	FX01	32	54	28.1	115	48	4.6	1								1
887	FX02	32	56	3.5	115	48	17.1	1								1
888	MX01	32	55	45.2	115	49	36.0	1								1
891	MX15	32	59	38.5	115	49	4.1	1								1
892	MX16	33	0	28.8	115	49	6.4	1								1
893	MX17	33	1	49.8	115	48	45.1	1								1
894	MX11	32	58	49.5	115	49	3.2	1								1
895	MX12	32	57	57.3	115	48	35.7	1								1
896	MX13	32	57	32.0	115	49	2.8	1								1
901	CC01	32	57	39.0	115	10	34.7	1	1		1	1	1			
902	CC02	32	58	2.3	115	9	48.8	1	1		1	1	1			
903	CC03	32	54	24.2	115	9	2.7	1	1		1	1	1			
904	CC04	32	52	50.3	115	8	4.2	1	1		1	1	1			
905	CC05	32	51	30.0	115	6	53.1	1	1		1	1	1			
906	CC06	32	50	6.8	115	5	38.3	1	1		1	1	1			
909	CC09	32	47	80.8	115	1	18.9	1	1		1	1	1			
910	CC10	32	46	32.7	114	58	55.5	1	1		1	1	1			
911	CC11	32	45	3.6	114	57	52.1	1	1		1	1	1			

>

LOCATIONS AND RECORDED SHOTPOINTS

LOCATION	FIELD ID	LATITUDE DEG	MIN	SEC	LONGITUDE DEG	MIN	SEC	NUMBER OF TIMES SHOTPOINT WAS RECORDED BY A STATION SP1	SP2	SP5	SP6	SP7	SP10	SP12	SP13	SP14
912	CC12	32	43	30.0	114	56	54.0	1	1		1	1	1			
914	YM96	32	41	37.0	115	5	10.6	1	1		1	1	1			
915	YM98	32	41	41.3	115	4	8.7	1	1		1	1	1			
916	AZ01	32	41	45.6	115	3	6.0	1	1		1	1	1			
917	AZ03	32	41	49.5	115	2	5.1	1	1		1	1	1			
918	AZ05	32	41	53.8	115	1	1.7	1	1		1	1	1			
919	AZ06	32	41	56.5	115	0	31.6	1	1		1	1	1			
920	AZ07	32	41	57.7	115	0	1.4	1	1		1	1	1			
921	AX28	32	42	58.3	114	47	47.2	1	1		1	1	1			
922	AX29	32	42	54.4	114	47	17.8	1	1		1	1	1			
923	AX30	32	42	56.6	114	46	44.6	1	1		1	1	1			
924	AX31	32	42	57.6	114	46	14.0	1	1		1	1	1			
925	AX32	32	42	59.9	114	45	44.7	1	1		1	1	1			
926	AX33	32	43	2.0	114	45	14.5	1	1		1	1	1			
927	AX34	32	43	3.9	114	44	44.0	1	1		1	1	1			
928	AX35	32	43	26.6	114	43	50.7	1	1		1	1	1			
929	KM08	32	43	54.3	114	45	24.3	1	1		1	1	1			
930	AX36	32	46	41.8	114	45	51.9	1	1		1	1	1			
931	AX37	32	45	42.6	114	46	18.0	1	1		1	1	1			
932	AX38	32	45	40.3	114	44	26.3	1	1		1	1	1			
933	AX39	32	45	40.4	114	43	54.4	1	1		1	1	1			
934	AX40	32	45	35.9	114	43	8.0	1	1		1	1	1			
935	AX41	32	46	35.1	114	42	26.1	1	1		1	1	1			
936	AX42	32	45	41.7	114	41	8.8	1	1		1	1	1			
937	AX43	32	45	39.8	114	40	2.3	1	1		1	1	1			
938	AX44	32	45	48.9	114	38	0.3	1	1		1	1	1			
939	AX46	32	45	42.5	114	36	25.5	1	1		1	1	1			
940	AX48	32	46	27.4	114	33	18.1	1	1		1	1	1			
941	HO07	32	51	18.0	115	19	1.4	1	1		1	1	1			
942	HO08	32	51	9.0	115	20	11.5	1	1		1	1	1			
943	HO09	32	51	81.6	115	21	45.0	1	1		1	1	1			
944	HO10	32	51	16.4	115	22	58.9	2	1		1	1	2			
945	EH09	32	50	42.1	115	17	17.5	1	1		1	1	1			
946	EH10	32	51	33.3	115	17	28.8	1	1		1	1	1			
947	EH11	32	52	26.1	115	17	28.2	1	1		1	1	1			
948	EH12	32	53	17.9	115	17	30.0	1	1		1	1	1			
949	EH13	32	54	24.9	115	17	34.1	1	1		1	1	1			
950	EH14	32	55	17.1	115	17	31.8	1	1		1	1	1			
951	EH15	32	56	11.7	115	17	28.6	1	1		1	1	1			
952	EH16	32	57	4.7	115	17	34.6	1	1		1	1	1			
953	EH17	32	57	56.1	115	17	30.8	1	1		1	1	1			
954	SS02	32	58	57.7	115	17	31.8	1	1		1	1	1			
956	EH18	33	1	7.0	115	18	31.3	1	1		1	1	1			
958	EH19	33	3	87.7	115	20	20.4	1	1		1	1	1			
957	EH20	33	6	34.7	115	21	7.8	1	1		1	1	1			
958	EH21	33	8	40.1	115	23	6.1	1	1		1	1	1			
959	EH22	33	11	8.8	115	25	23.1	1	1		1	1	1			
960	EH23	33	13	5.9	115	26	51.7	1	1		1	1	1			
961	AZ08	32	42	0.7	114	59	28.8	1	1		1	1	1			
962	AZ09	32	42	0.7	114	58	57.8	1	1		1	1	1			

LOCATIONS AND RECORDED SHOTPOINTS

LOCATION	FIELD ID	LATITUDE DEG	MIN	SEC	LONGITUDE DEG	MIN	SEC	NUMBER OF TIMES SHOTPOINT WAS RECORDED BY A STATION SP1	SP2	SP5	SP6	SP7	SP10	SP12	SP13	SP14
963	AZ10	32	42	5.1	114	58	87.7	1	1		1	1	1			
964	AZ11	32	42	8.0	114	57	56.0	1	1		1	1	1			
965	AZ12	32	42	3.1	114	57	27.4	1	1		1	1	1			
966	AZ13	32	42	5.1	114	56	55.7	1	1		1	1	1			
967	AX14	32	42	8.7	114	56	24.6	1	1		1	1	1			
968	AX15	32	42	10.8	114	55	53.9	1	1		1	1	1			
969	AX16	32	41	52.2	114	55	16.4	1	1		1	1	1			
970	AX17	32	42	18.1	114	54	50.6	1	1		1	1	1			
971	AX18	32	42	22.4	114	54	10.8	1	1		1	1	1			
972	AX19	32	42	24.6	114	53	37.1	1	1		1	1	1			
973	AX20	32	42	27.1	114	53	18.6	1	1		1	1	1			
974	AX21	32	44	30.3	114	51	41.4	1	1		1	1	1			
975	AX22	32	44	21.9	114	51	13.3	1	1		1	1	1			
976	AX23	32	44	15.9	114	50	41.2	1	1		1	1	1			
977	AX24	32	43	58.0	114	50	4.8	1	1		1	1	1			
978	AX25	32	43	40.1	114	49	23.8	1	1		1	1	1			
979	AX26	32	43	25.6	114	48	51.9	1	1		1	1	1			
980	AX27	32	43	10.9	114	48	22.8	1	1		1	1	1			
981	SS07	32	42	58.5	114	58	18.2	1	1		1	1	1			
982	EH01	32	42	33.1	115	15	58.7	1	1		1	1	1			
983	EH02	32	43	18.1	115	16	31.0	1	1		1	1	1			
984	EH03	32	44	15.6	115	17	36.0	1	1		1	1	1			
985	EH04	32	45	10.9	115	17	4.8	1	1		1	1	1			
986	EH05	32	47	2.7	115	18	34.2	1	1		1	1	1			
987	EH06	32	48	8.6	115	18	37.1	1	1		1	1	1			
988	EH07	32	48	59.6	115	16	51.3	1	1		1	1	1			
989	EH08	32	49	49.0	115	17	6.2	1	1		1	1	1			
990	EM01	32	47	47.3	116	14	48.9	1	1		1	1	1			
991	EM02	32	48	38.9	115	14	48.5	1	1		1	1	1			
992	EM03	32	47	47.1	115	15	43.9	1	1		1	1	1			
993	EM04	32	46	58.3	115	15	45.0	1	1		1	1	1			
994	HO01	32	48	55.6	115	15	52.9	1	1		1	1	1			
995	HO02	32	50	21.3	116	14	44.8	1	1		1	1	1			
996	HO03	32	50	1.3	115	12	42.6	1	1		1	1	1			
997	HO04	32	49	51.4	115	10	41.5	1	1		1	1	1			
998	HO05	32	49	58.8	116	9	4.3	1	1		1	1	1			
999	HO06	32	50	50.5	115	9	14.3	1	1		1	1	1			
1001	HB13	32	42	58.1	116	33	35.4	1					1			
1002	HB12	32	42	60.1	116	33	5.0	1					1			
1003	HB11	32	42	58.1	116	32	39.7	1					1			
1004	HB10	32	42	58.1	116	31	56.8	1					1			
1005	HB09	32	42	53.8	115	31	29.8	1					1			
1006	HB08	32	42	60.5	115	30	56.9	1					1			
1007	HB07	32	43	34.7	116	30	28.6	1					1			
1008	HB06	32	43	22.2	115	28	57.5	1					1			
1009	HB05	32	43	23.4	115	28	0.9	1					1			
1010	HB04	32	43	23.0	115	27	0.0	1					1			
1011	HB03	32	43	20.3	115	25	45.9	1					1			
1012	HB02	32	43	28.5	115	24	56.4	1					1			
1013	DV0D	32	40	40.9	115	32	8.8	1					1			

LOCATIONS AND RECORDED SHOTPOINTS

LOCATION	FIELD ID	LATITUDE DEG	MIN	SEC	LONGITUDE DEG	MIN	SEC	NUMBER OF TIMES SHOTPOINT WAS RECORDED BY A STATION SP1	SP2	SP5	SP6	SP7	SP10	SP12	SP13	SP14
1014	DU08	32	41	38.0	115	31	52.7	1					1			
1015	DU07	32	42	7.8	115	32	1.0	1					1			
1016	DU06	32	42	28.5	115	32	10.8	1					1			
1017	DU05	32	43	24.6	115	32	11.1	1					1			
1018	DU04	32	43	51.0	115	32	10.8	1					1			
1019	DU03	32	44	16.8	115	32	5.1	1					1			
1020	DU01	32	45	0.0	115	32	11.6	1					1			
1021	AM01	33	5	43.2	115	34	43.0	1					1			
1022	AM02	33	5	51.4	115	33	48.3	1					1			
1024	AM04	33	6	10.9	115	31	50.7	1					1			
1026	AM06	33	6	1.1	115	30	25.8	1					1			
1027	AM07	33	5	48.3	115	29	26.8	1					1			
1028	AM08	33	5	47.8	115	28	24.8	1					1			
1029	AM09	33	5	47.5	115	27	23.5	1					1			
1030	AM10	33	5	47.5	115	26	15.0	1					1			
1031	AM11	33	5	47.8	115	25	12.1	1					1			
1033	AM13	33	5	57.8	115	23	17.8	1					1			
1034	AM14	33	5	57.8	115	22	15.7	1					1			
1035	AM15	33	5	8.6	115	20	53.5	1					1			
1037	AM17	33	4	56.3	115	18	48.9	1					1			
1038	AM18	33	5	30.6	115	18	56.5	1					1			
1040	AM20	33	5	8.7	115	17	9.2	1					1			
1042	MO11	32	51	16.0	115	24	4.2	1					1			
1043	MO12	32	51	8.7	115	25	6.9	1					1			
1044	MO13	32	51	17.1	115	26	0.4	1					1			
1045	MO14	32	51	28.7	115	26	39.2	1					1			
1046	MO15	32	52	6.6	115	27	26.9	1					1			
1047	MO16	32	52	9.0	115	28	1.4	1					1			
1048	MO17	32	52	22.4	115	28	32.3	1					1			
1049	MO18	32	52	8.0	115	29	27.2	1					1			
1050	MO19	32	52	8.5	115	30	15.7	1					1			
1051	MO20	32	52	13.6	115	31	3.2	1					1			
1052	MO21	32	52	13.0	115	31	28.6	1					1			
1053	MO22	32	52	22.2	115	32	21.0	1					1			
1054	MO23	32	52	14.0	115	33	5.5	1					1			
1055	MO24	32	51	58.4	115	33	48.1	1					1			
1056	MO25	32	52	14.6	115	34	40.8	1					1			
1057	MO26	32	52	35.1	115	35	28.8	1					1			
1058	MO27	32	52	34.7	115	36	18.9	1					1			
1059	MO28	32	52	51.3	115	37	21.2	1					1			
1060	MO29	32	53	5.5	115	38	21.7	1					1			
1061	IR01	33	10	25.7	115	33	41.5	1					1			
1062	IR02	33	10	36.8	115	32	38.6	2	1				2			
1063	IR03	33	10	34.7	115	31	33.7	1					1			
1064	IR04	33	10	16.8	115	30	26.9	2	1				2			
1065	IR05	33	10	47.1	115	29	33.2	2	1				2			
1066	IR06	33	10	46.0	115	28	29.7	1					1			
1067	IR07	33	10	44.4	115	27	29.8	1					1			
1068	IR08	33	10	43.3	115	26	41.8	1					1			
1069	IR09	33	10	18.8	115	25	54.5	2	1				2			

LOCATIONS AND RECORDED SHOTPOINTS

LOCATION	FIELD ID	LATITUDE DEG	MIN	SEC	LONGITUDE DEG	MIN	SEC	NUMBER OF TIMES SHOTPOINT WAS RECORDED BY A STATION SP1	SP2	SP5	SP6	SP7	SP10	SP12	SP13	SP14
1070	IR10	33	10	49.6	115	36	7.2	2	1				2			
1071	IR11	33	12	19.8	115	35	45.3	1					1			
1072	IR12	33	11	41.2	115	34	17.4	2	1				2			
1073	IR13	33	10	52.7	115	32	55.3	2	1				2			
1074	IR14	33	10	2.0	115	30	35.1	2	1				2			
1075	IR15	33	9	27.4	115	18	12.7	2	1				2			
1076	IR16	33	9	30.2	115	17	38.9	2	1				2			
1077	IR17	33	7	0.0	115	16	21.1	1					1			
1078	IR18	33	5	26.2	115	12	54.8	1					1			
1079	IR19	33	3	55.8	115	10	37.4	1					1			
1080	IR20	33	2	10.5	115	8	7.0	1					1			
1081	MB20	32	42	47.0	115	41	10.3	1					1			
1082	MB19	32	42	44.8	115	39	43.4	1					1			
1083	MB18	32	42	45.5	115	38	22.0	1					1			
1084	MB17	32	42	52.0	115	37	10.4	1					1			
1085	MB16	32	43	6.1	115	36	12.0	1					1			
1086	MB15	32	42	55.2	115	35	9.0	1					1			
1087	MB14	32	42	58.8	115	34	9.8	1					1			
1088	LB10	32	45	8.7	115	34	6.5	1					1			
1089	LB09	32	44	50.6	115	34	37.2	1					1			
1090	LB08	32	44	21.0	115	34	37.0	1					1			
1091	LB07	32	43	57.7	115	34	37.0	1					1			
1092	MB21	32	42	31.0	115	42	89.8	1					1			
1093	MB22	32	42	30.8	115	43	33.2	1					1			
1094	MB23	32	42	30.8	115	44	32.8	1					1			
1095	MB24	32	42	31.4	115	45	35.9	1					1			
1096	LB06	32	43	31.2	115	34	36.8	1					1			
1097	LB05	32	42	36.8	115	34	41.8	1					1			
1098	LB04	32	41	41.2	115	35	6.5	1					1			
1099	LB03	32	40	51.2	115	35	7.2	1					1			
1100	LB02	32	40	0.6	115	35	6.7	1					1			
1101	CA01	33	20	22.3	115	33	28.2		1				1			1
1102	CA02	33	21	20.7	115	34	23.8		1				1			1
1103	CA03	33	22	0.1	115	35	41.6		1				1			1
1104	CA04	33	22	38.2	115	37	25.8		1				1			1
1105	CA05	33	23	38.0	115	38	4.7		1				1			1
1106	CA06	33	24	46.4	115	40	5.1		1				1			1
1107	CA07	33	26	18.1	115	41	35.4		1				1			1
1108	CA08	33	27	5.9	115	42	43.8		1				1			1
1109	CA09	33	27	22.8	115	43	44.8		1				1			1
1110	CA10	33	28	21.7	115	45	53.8		1				1			1
1111	CA11	33	30	10.5	115	46	1.4		1				1			1
1112	CA12	33	30	57.3	115	45	46.5		1				1			1
1113	BR01	33	28	32.3	115	45	24.6		1				1			1
1114	BR02	33	28	14.0	115	45	45.7		1				1			1
1115	BR03	33	27	57.7	115	46	10.8		1				1			1
1116	BR04	33	27	31.2	115	46	16.0		1				1			1
1117	BR05	33	27	10.1	115	46	14.0		1				1			1
1118	BR06	33	26	45.2	115	46	6.4		1				1			1
1119	BR07	33	26	20.2	115	46	5.2		1				1			1

>

LOCATIONS AND RECORDED SHOTPOINTS

LOCATION	FIELD ID	LATITUDE DEG	MIN	SEC	LONGITUDE DEG	MIN	SEC	NUMBER OF TIMES SHOTPOINT WAS RECORDED BY A STATION SP1	SP2	SP5	SP6	SP7	SP10	SP12	SP13	SP14
1120	BM02	33	26	1.0	115	45	55.6		1				1			1
1121	MU01	33	21	20.6	115	30	50.5		1				1			1
1122	MU02	33	21	3.5	115	31	12.0		1				1			1
1123	MU03	33	20	45.5	115	31	47.3		1				1			1
1124	MU05	33	19	54.6	115	32	52.8		1				1			1
1125	MU07	33	18	60.7	115	32	38.8		1				1			1
1126	MU08	33	18	46.4	115	33	29.2		1				1			1
1127	MU09	33	18	16.0	115	33	41.3		1				1			1
1128	BB01	33	21	15.1	115	43	11.2		1				1			1
1129	BB02	33	21	5.7	115	44	31.4		1				1			1
1130	BB03	33	21	16.6	115	43	39.0		1				1			1
1131	BB04	33	22	5.4	115	42	46.7		1				1			1
1132	FK01	33	20	36.0	115	39	49.4		1				1			1
1133	FK02	33	20	57.0	115	39	27.3		1				1			1
1134	FK03	33	21	15.9	115	39	2.8		1				1			1
1135	FK04	33	21	44.7	115	38	49.6		1				1			1
1136	FK05	33	22	0.5	115	38	46.0		1				1			1
1137	FK06	33	22	31.7	115	38	34.3		1				1			1
1138	FK08	33	23	24.1	115	37	59.6		1				1			1
1139	FK09	33	23	52.2	115	37	58.3		1				1			1
1140	FK10	33	24	16.8	115	38	11.9		1				1			1
1141	CL01	33	18	8.6	116	13	42.4		1				1			1
1142	CL02	33	18	15.6	116	12	39.5		1				1			1
1143	CL03	33	18	3.5	116	11	40.8		1				1			1
1144	CL04	33	17	7.4	116	9	28.7		1				1			1
1145	CL05	33	16	46.0	116	8	30.3		1				1			1
1146	CL06	33	16	54.9	116	6	54.1		1				1			1
1147	CL07	33	16	51.8	116	5	54.7		1				1			1
1148	CL08	33	16	37.8	116	3	43.0		1				1			1
1149	CL09	33	16	35.8	116	3	8.4		1				1			1
1150	CL10	33	15	50.6	116	1	1.7		1				1			1
1151	CL11	33	15	59.2	116	0	8.8		1				1			1
1152	CL13	33	17	8.0	115	57	7.3		1				1			1
1153	CL14	33	17	19.5	115	56	8.6		1				1			1
1154	CL15	33	17	48.7	115	55	43.8		1				1			1
1155	MU10	33	18	4.6	115	34	11.7		1				1			1
1156	MU11	33	17	34.2	115	34	37.8		1				1			1
1157	MU13	33	17	5.4	115	35	16.8		1				1			1
1158	MU14	33	16	28.2	115	34	41.9		1				1			1
1159	MU15	33	16	14.0	115	35	19.3		1				1			1
1160	MU16	33	15	49.7	115	35	18.1		1				1			1
1161	BM22	33	21	24.9	115	45	28.7		1				1			1
1162	BM21	33	21	58.1	115	48	18.1		1				1			1
1163	BM20	33	22	28.0	115	46	6.2		1				1			1
1164	BM23	33	22	31.6	115	47	5.0		1				1			1
1165	BM18	33	22	34.1	115	46	4.9		1				1			1
1166	BM18	33	23	1.4	115	46	3.3		1				1			1
1167	BM17	33	23	26.3	115	46	2.3		1				1			1
1168	BM16	33	23	38.6	115	46	1.6		1				1			1
1169	BM15	33	23	55.2	115	46	4.1		1				1			1

>

LOCATIONS AND RECORDED SHOTPOINTS

LOCATION	FIELD ID	LATITUDE DEG	MIN	SEC	LONGITUDE DEG	MIN	SEC	NUMBER OF TIMES SHOTPOINT WAS RECORDED BY A STATION SP1	SP2	SP5	SP6	SP7	SP10	SP12	SP13	SP14
1170	BR14	33	24	14.9	115	46	5.9		1				1			1
1171	BR13	33	24	31.1	115	46	0.6		1				1			1
1172	BR12	33	24	44.4	115	45	57.8		1				1			1
1173	BR11	33	24	56.2	115	45	56.1		1				1			1
1174	BR10	33	25	10.6	115	45	57.8		1				1			1
1175	BR09	33	25	33.4	115	46	7.4		1				1			1
1176	BS01	33	25	36.5	115	49	20.1		1				1			1
1177	BS02	33	25	43.8	115	48	47.1		1				1			1
1178	BS03	33	25	37.0	115	48	15.8		1				1			1
1179	BS04	33	25	37.0	115	47	18.1		1				1			1
1180	BS06	33	25	54.2	115	49	0.0		1				1			1
1181	CR01	33	27	19.7	115	41	29.3		1				1			1
1182	CR02	33	26	57.5	115	41	12.9		1				1			1
1183	CX03	33	26	21.4	115	41	21.7									1
1184	CR04	33	25	41.5	115	40	59.3		1				1			1
1185	CR05	33	25	10.0	115	40	53.4		1				1			1
1186	CR06	33	24	48.1	115	40	55.4		1				1			1
1187	CR07	33	24	16.0	115	40	56.2		1				1			1
1188	CR08	33	23	53.8	115	40	57.7		1				1			1
1189	CR09	33	23	26.9	115	41	1.6		1				1			1
1190	CR10	33	23	4.1	115	41	22.9		1				1			1
1191	CR11	33	22	33.2	115	41	36.1		1				1			1
1192	CR12	33	22	40.7	115	42	12.5		1				1			1
1193	CR13	33	22	25.6	115	42	36.1		1				1			1
1194	CR14	33	22	18.0	115	43	0.4		1				1			1
1195	CR15	33	21	58.1	115	43	26.2		1				1			1
1196	CR16	33	21	41.1	115	43	41.0		1				1			1
1197	CR17	33	21	33.1	115	43	53.6		1				1			1
1198	CR18	33	21	27.2	115	44	0.0		1				1			1
1199	CR19	33	21	25.1	115	44	22.9		1				1			1
1200	CR20	33	21	27.9	115	44	51.1		1				1			1
1201	UL08	33	3	50.6	115	33	6.5	1	1				1			
1202	UL09	33	3	37.6	115	32	36.9	1	1				1			
1203	UL10	33	3	34.7	115	32	18.9	1	1				1			
1204	UL11	33	3	21.7	115	31	31.2	1	1				1			
1205	UL12	33	3	18.5	115	31	3.3	1	1				1			
1206	UL13	33	3	12.6	115	30	40.8	1	1				1			
1207	UL14	33	2	56.1	115	30	15.6	1	1				1			
1208	UL15	33	2	40.9	115	29	38.5	1	1				1			
1209	UL16	33	2	41.3	115	29	0.2	1	1				1			
1210	UL17	33	2	27.7	115	28	40.3	1	1				1			
1211	UL18	33	2	19.1	115	27	55.9	1	1				1			
1212	UL19	33	2	15.0	115	27	21.7	1	1				1			
1213	UL20	33	2	3.9	115	26	54.4	1	1				1			
1214	UL21	33	1	56.1	115	26	24.3	1	1				1			
1215	UL22	33	1	48.6	115	25	50.5	1	1				1			
1216	UL23	33	1	40.6	115	25	18.9	1	1				1			
1217	UL24	33	1	35.5	115	24	52.1	1	1				1			
1219	UL26	33	1	23.0	115	23	59.0	1	1				1			
1220	UL27	33	1	14.0	115	23	14.1	1	1				1			

>

LOCATIONS AND RECORDED SHOTPOINTS

LOCATION	FIELD ID	LATITUDE DEG	MIN	SEC	LONGITUDE DEG	MIN	SEC	NUMBER OF TIMES SHOTPOINT WAS RECORDED BY A STATION SP1	SP8	SP5	SP6	SP7	SP10	SP12	SP13	SP14
1221	KS20	33	6	6.0	115	50	57.6	1	1				1			
1222	KS21	33	5	41.1	115	51	52.5	1	1				1			
1223	KS22	33	5	42.8	115	53	14.2	1	1				1			
1224	KS23	33	5	47.2	115	54	18.4	1	1				1			
1225	KS24	33	5	18.8	115	52	41.2	1	1				1			
1226	KS25	33	4	20.8	115	52	52.9	1	1				1			
1227	GT01	33	2	31.4	115	35	9.9	1	1				1			
1228	GT02	33	2	7.6	115	34	9.1	1	1				1			
1229	GT03	33	1	42.5	115	33	8.8	1	1				1			
1230	GT04	33	1	34.5	115	32	38.9	1	1				1			
1231	GT05	33	1	22.1	115	31	59.7	1	1				1			
1232	GT06	33	1	1.4	115	31	9.4	1	1				1			
1233	GT07	33	0	41.8	115	30	35.0	1	1				1			
1234	GT08	33	1	28.8	115	30	36.1	1	1				1			
1235	GT09	33	2	14.4	115	30	11.8	1	1				1			
1236	GT10	33	0	45.8	115	30	0.8	1	1				1			
1237	GT11	33	0	36.4	115	29	28.4	1	1				1			
1238	GT12	33	0	24.6	115	28	25.7	1	1				1			
1239	GT13	33	0	11.7	115	27	23.7	1	1				1			
1261	WL01	33	4	59.6	115	36	50.9	1	1				2			
1262	WL02	33	4	50.5	115	36	18.6	1	1				1			
1263	WL03	33	4	40.1	115	35	46.8	1	1				1			
1264	WL04	33	4	31.1	115	35	7.4	1	1				1			
1265	WL05	33	4	18.1	115	34	38.2	1	1				1			
1266	WL06	33	4	3.4	115	34	9.0	1	1				1			
1267	WL07	33	3	58.7	115	33	32.5	1	1				1			
1268	WS05	33	6	38.5	115	40	17.7	1	1				1			
1281	WL28	33	0	56.2	115	22	39.5	1	1				1			
1282	WL29	33	0	51.0	115	22	15.0	1	1				1			
1283	WL30	33	0	40.1	115	21	45.3	1	1				1			
1284	WL31	33	0	30.0	115	21	8.1	1	1				1			
1285	WL32	33	0	17.7	115	20	43.9	1	1				1			
1286	WL33	33	0	8.7	115	20	8.8	1	1				1			
1287	WL34	32	59	53.4	115	19	37.4	1	1				1			
1288	WL35	32	59	30.4	115	18	1.7	1	1				1			
1289	WL36	32	59	3.7	115	18	36.3	1	1				1			
1299	WL37	32	59	5.2	115	17	58.0	1	1				1			
1301	TS01	33	5	3.9	115	37	27.2						1			
1302	TS02	33	4	28.9	115	37	26.5						1			
1303	TS03	33	4	16.9	115	37	14.7						1			
1304	TS04	33	4	3.1	115	37	14.7						1			
1305	TS05	33	3	50.1	115	37	14.7						1			
1306	TS06	33	3	37.2	115	37	14.7						1			
1307	TS07	33	3	23.4	115	37	14.7						1			
1308	TS08	33	3	10.1	115	37	14.7						1			

>

Table 3.--Velocity above and below model boundaries at locations of velocity-depth curves in figure 8. Velocity-depth curves in figure 8 were constructed from values given here. Curve numbers are same as in that figure; they indicate distance (in km) southeast or east of first-named shotpoint (SP) in respective section of table. Approximate geographic location for curve is given (in N. Lat. and W. Long.). Double slash between two velocities indicates discontinuity; slash preceded by or followed by dash indicates top or bottom of model, respectively.

SP1 to SP6

Depth to boundary (km)	Velocity above/below boundary (km/s)	Inferred geologic unit
Curve -1 32°53.4' 115°46.8'		
0.0	--/1.9	--
1.2	2.3/2.3	sedimentary rocks
1.4	2.35//5.1	--
2.1	5.8/5.8	--transition zone
12.5	6.6//7.0	--basement
13.5	7.2/7.2	subbasement
20.0	8.0/--	
Curve 1 32°52.9' 115°45.7'		
0.0	--/1.9	--
1.3	2.8/2.8	sedimentary rocks
2.5	5.0//5.1	--
3.1	5.8/5.8	--transition zone
12.5	6.6//7.0	--basement
13.5	7.2/7.2	subbasement
20.0	8.0/--	
Curve 17 32°49.3' 115°37.1'		
0.0	--/1.8	--
1.3	2.6/2.6	sedimentary rocks
3.8	4.8//5.1	--
4.8	5.8/5.8	--transition zone
12.5	6.6//7.0	--basement
13.5	7.2/7.2	subbasement
20.0	8.0/--	
Curve 53 (SP6) 32°41.7' 115°15.1'		
0.0	--/1.8	--
1.2	2.6/2.6	sedimentary rocks
4.75	5.1/5.1	--
5.75	5.6/5.6	--transition zone
12.5	6.6//7.0	--basement
13.5	7.2/7.2	subbasement
20.0	8.0/--	

SP1 to SP2

Depth to boundary (km)	Velocity above/below boundary (km/s)	Inferred geologic unit
Curve 2.5 32°53.6' 115°44.7'		
0.0	--/1.8	--
1.8	3.7/3.7	sedimentary roc
4.55	5.1/5.1	--
5.55	5.65/5.65	--transition zone
11.4	5.95//6.6	--basement
12.4	7.2/7.2	subbasement
20.0	7.76/--	
Curve 25 32°55.3' 115°30.5'		
0.0	--/1.8	--
1.8	3.0/3.0	sedimentary roc
4.55	5.1/5.1	--
5.55	5.65/5.65	--transition zone
11.3	5.95//6.60	--basement
12.3	7.2/7.2	subbasement
20.0	7.76/--	
Curve 43 32°57.1' 115°19.1'		
0.0	--/1.8	--
1.8	3.5/3.5	sedimentary roc
3.3	5.0/5.0	--
4.3	5.65/5.65	--transition zone
11.3	5.95//6.6	--basement
12.3	7.2/7.2	subbasement
20.0	7.76/--	

SP10 to SP2

Depth to boundary (km)	Velocity above/below boundary (km/s)	Inferred geologic unit
Curve 0 (SP10) 33°05.2' 115°37.5'		
0.0	--/1.8	--
1.0	2.3/2.3	sedimentary rocks
2.5	3.8/3.8	--
3.95	5.0/5.0	--transition zone
4.45	5.65/5.65	basement
13.0	7.0/--	
Curve 15 33°02.4' 115°28.5'		
0.0	--/1.95	--
1.0	2.3/2.3	sedimentary rocks
2.2	3.6/3.6	--
4.6	4.8/4.8	--transition zone
5.3	5.5/5.5	basement
13.0	7.0/--	
Curve 33 (SP2) 32°59.0' 115°17.6'		
0.0	--/1.90	--
0.6	2.1/2.1	sedimentary rocks
1.8	3.8/3.8	--
3.1	5.0/5.0	--transition zone
4.1	5.65/5.65	basement
13.0	7.0/--	

Figure Captions

Figure 1. Index map showing shotpoints, recorder locations, and profiles analyzed. Profiles that are modeled are indicated by outline and stipple; profile segment 5N-13S, indicated by outline only, is discussed in the text but not modeled. Mapped faults are indicated by solid lines, inferred faults by queried lines, and seismicity lineaments by dashed lines. Names for these structures are abbreviated A, Algodones fault; B, Brawley fault; BZ, Brawley seismic zone (as defined in Johnson, 1979); CC, Coyote Creek fault; E, Elsinore fault; EH, East Highline canal seismicity lineament; I, Imperial fault; SA, San Andreas fault; SdH, Sand Hills fault(?); SH, Superstition Hills fault; SM, Superstition Mountain fault. The shoreline of ancient Lake Cahuilla are indicated by a light dotted line. South of the Salton Sea this shoreline separates the Imperial Valley from East and West Mesas. The axis of the Salton Trough, as defined in this report, is a line that bisects the Salton Sea and projects southward. Note that this axis does not coincide with the topographic axis of the Imperial Valley. Sup. H., Superstition Hills; Sup. M., Superstition Mountains.

Figure 2. Record sections for lines 6NW (a) and 1SE and 1NW (b). Traveltime is reduced by Δ(distance in km)/6km/s. The amplitude of each seismic trace is scaled by the maximum amplitude on that trace in the first 10 s of the record. The final model (c) for this profile is plotted below at the same distance scale; vertical exaggeration is 2.2x. Velocity boundaries in the model are indicated by heavy lines, dashed where uncertain, and velocity contours by light dashed lines with values given in km/s. Velocity contour interval is 0.5 km/s. Shotpoint locations are indicated as well as fault traces and seismicity lineaments crossed. Refer to caption of figure 1 for fault name abbreviations. Traveltime curves generated by the model are indicated on the record sections by smooth curves. For letter labels refer to the text. Refractions are indicated by solid lines and reflections by dashed lines.

Figure 3. Traveltime pick diagram for lines 6NW, 1SE, and 1NW, taken from figures 2a and 2b. Picks for arrivals from shotpoint 6 are indicated with solid symbols and from shotpoint 1 with open symbols: circles for first arrivals from sediments and basement, squares for arrivals from subbasement, and triangles for "1st", "2nd", and "3rd" multiple refractions. Arrivals uncertain to more than 0.1 s are queried. Apparent velocities in km/s are indicated for each line fitted to the data. Apparent velocities uncertain to more than 0.1 km/s are given to only one decimal place.

Figure 4. Record sections for 2W (a) and 1E (b), and final model (c). For further explanation see caption for figure 2.

Figure 5. Record sections for 2NW (a) and 10SE (b) and final model (c). For further explanation see caption for figure 2.

Figure 6. Record section for 1ESE (a) and final model (b). For further explanation see caption for figure 2.

Figure 7. Record sections for 13S (a) and 5N (b). Solid lines are traveltime curves averaged for all arrivals. Dashed lines are traveltime curves for arrivals (heavy black dots) at the three stations that recorded both blasts. These record sections indicate a true basement velocity of 5.9 to 6.0 km/s under West Mesa in contrast to the relatively low basement velocity of 5.65 km/s in most places in the Imperial Valley.

Figure 8. Velocity-depth curves at various locations along the profiles analyzed. These are cross sections of the final models at the indicated distances from the shotpoints.

Figure 9. Ray diagrams. The final model for 6NW-1SE-1NW is shown with no vertical exaggeration. Ray termini are labeled to correspond with labeled arrivals on figure 2. Rays for first arrivals were plotted in angular increments of 0.01 radian, and rays for first multiple refractions were plotted in increments of 0.05 radian. Exceptions are in (a) the last ray represents an angular increment of 0.004 radian rather than 0.01 radian, in (b) the angular increment is 0.0002 radian for all rays rather than 0.01 radian, in (c) the last two rays represent angular increments of 0.01 and 0.02 radian, respectively, rather than 0.05 radian, and in (f) the last ray represents an increment of 0.04 radian rather than 0.05 radian. These diagrams are used to determine traveltimes for first and multiple arrivals. In addition, seismic amplitude behavior can be inferred qualitatively from them. Seismic intensity observed at the surface is inversely correlated to the spacial separation of emerging rays.

Figure 10. Contour map of reduced traveltime for first arrivals from shotpoint 1. Reducing velocity is 6 km/s. The region of contours around shotpoint 1 (the black dot) with reduced traveltimes of less than 1.2 s is indicated with a light stipple pattern surrounded by a hashured contour. The faults shown are the same as in figure 1. Geothermal areas are abbreviated B, Brawley; Bd, Border; EM, East Mesa; H, Heber; S, Salton Sea; and W, Westmorland. This map is roughly similar to a sedimentary isopach map, where greater reduced traveltime correlates with greater sediment thickness.

Figure 11. (a) Gravity profile oriented east-northeast across California from La Jolla to the Chocolate Mountains; taken from a gravity map of California by Oliver and others (1979) along a straight line from La Jolla through Glamis. Control on boundaries in model (b) is provided by seismic refraction (see text). Numbers are density in g/cc. The 3.1 g/cc "subbasement" beneath the Imperial Valley, a feature lacking in previous gravity models for the Imperial Valley region, is the material which provides most of the compensation for the valley sediments.

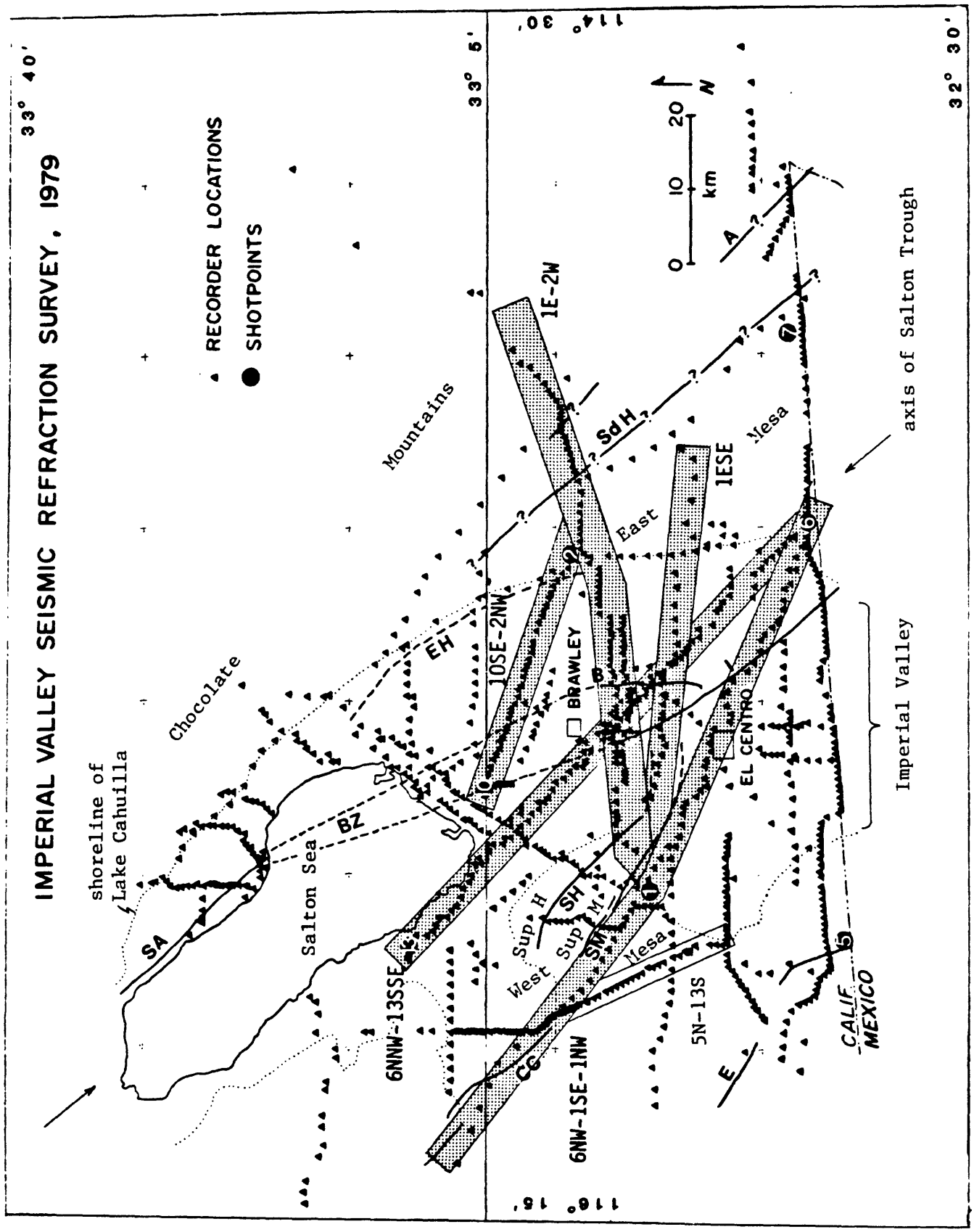
IMPERIAL VALLEY SEISMIC REFRACTION SURVEY, 1979
RECORDER LOCATIONS
SHOTPOINTS
33° 40'
33° 5'
32° 30'
114° 30'
116° 15'
0 10 20 km
N
shoreline of Lake Cahuilla
Chocolate Mountains
Salton Sea
SA
BZ
EH
6NNW-13SSE
10SE-2NW
1E-2W
SdH
East Mesa
1ESE
BRAWLEY
EL CENTRO
axis of Salton Trough
Imperial Valley
West Sup
Sup H
SH
SM
Mesa
6NW-1SE-1NW
5N-13S
CG
E
CALIF
MEXICO

Figure 1

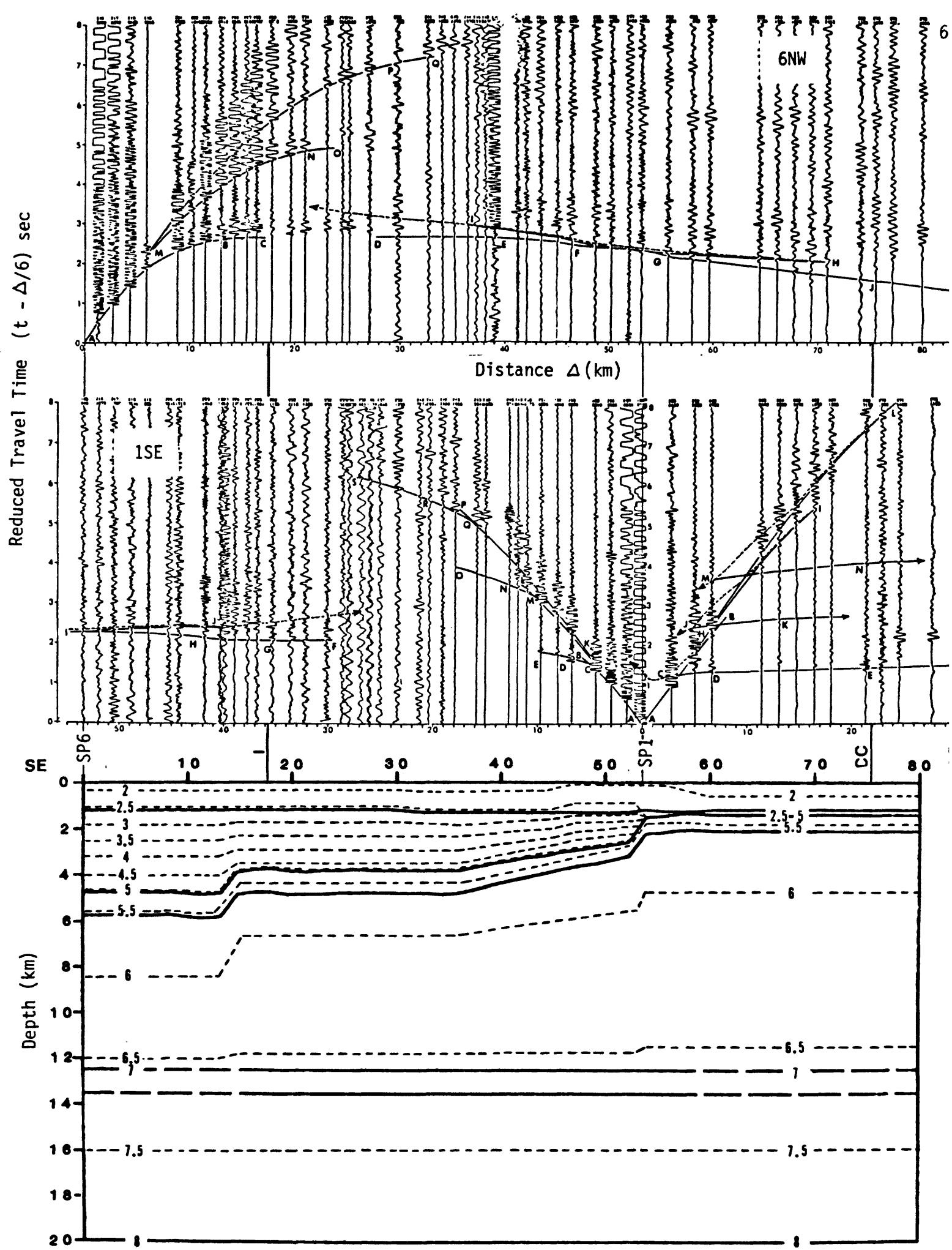
6NW
1SE
Reduced Travel Time (t - Δ/6) sec
Distance Δ (km)
SE
SP6
SP1
CC
Depth (km)
2
2.5
3
3.5
4
4.5
5
5.5
6
6.5
7
7.5
8

Figure 2

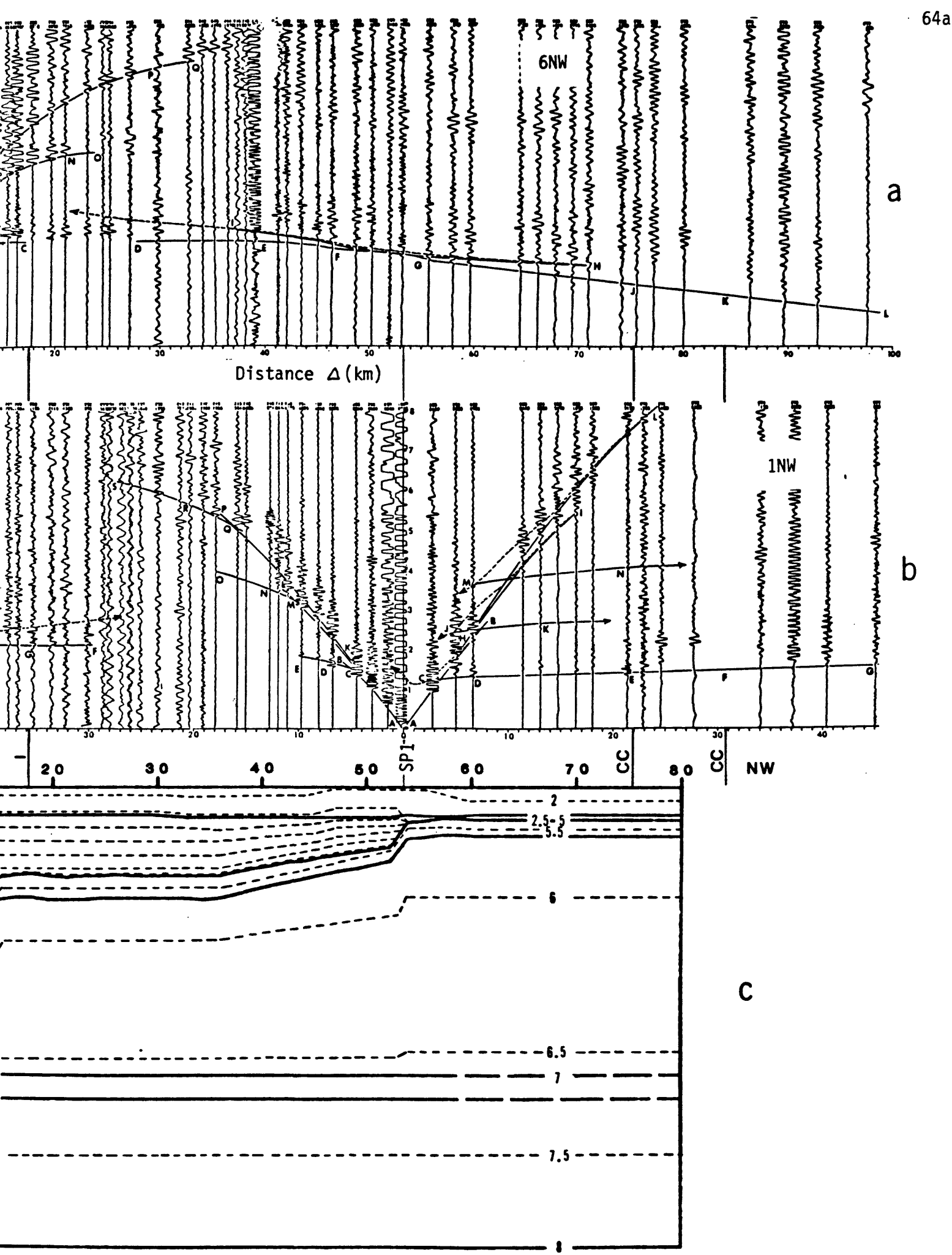

Figure 2

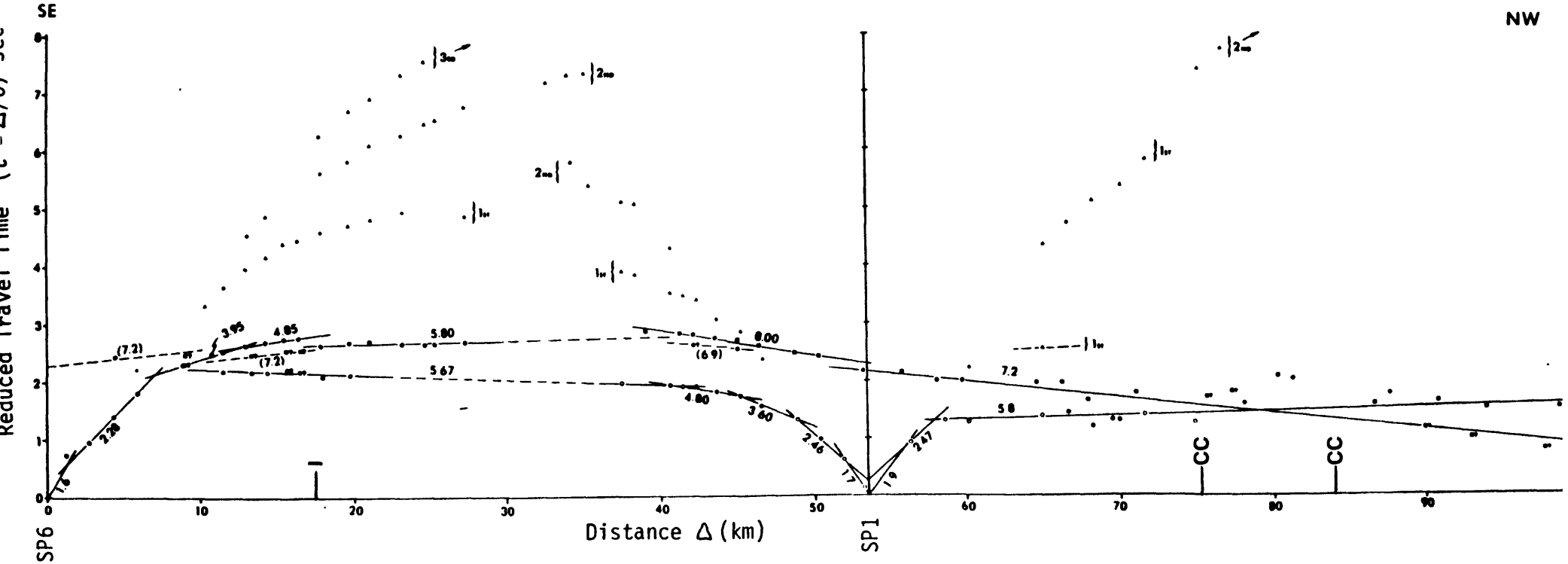
SE
NW
Reduced Travel Time (t - Δ/6) Sec
Distance Δ (km)
SP6
SP1
CC
CC
(7.2)
3.95
4.85
5.80
(7.2)
5.67
(6.9)
8.00
7.2
5.8
4.80
3.60
2.46
2.47
1.7
1.9
2.20
1.6

Figure 3

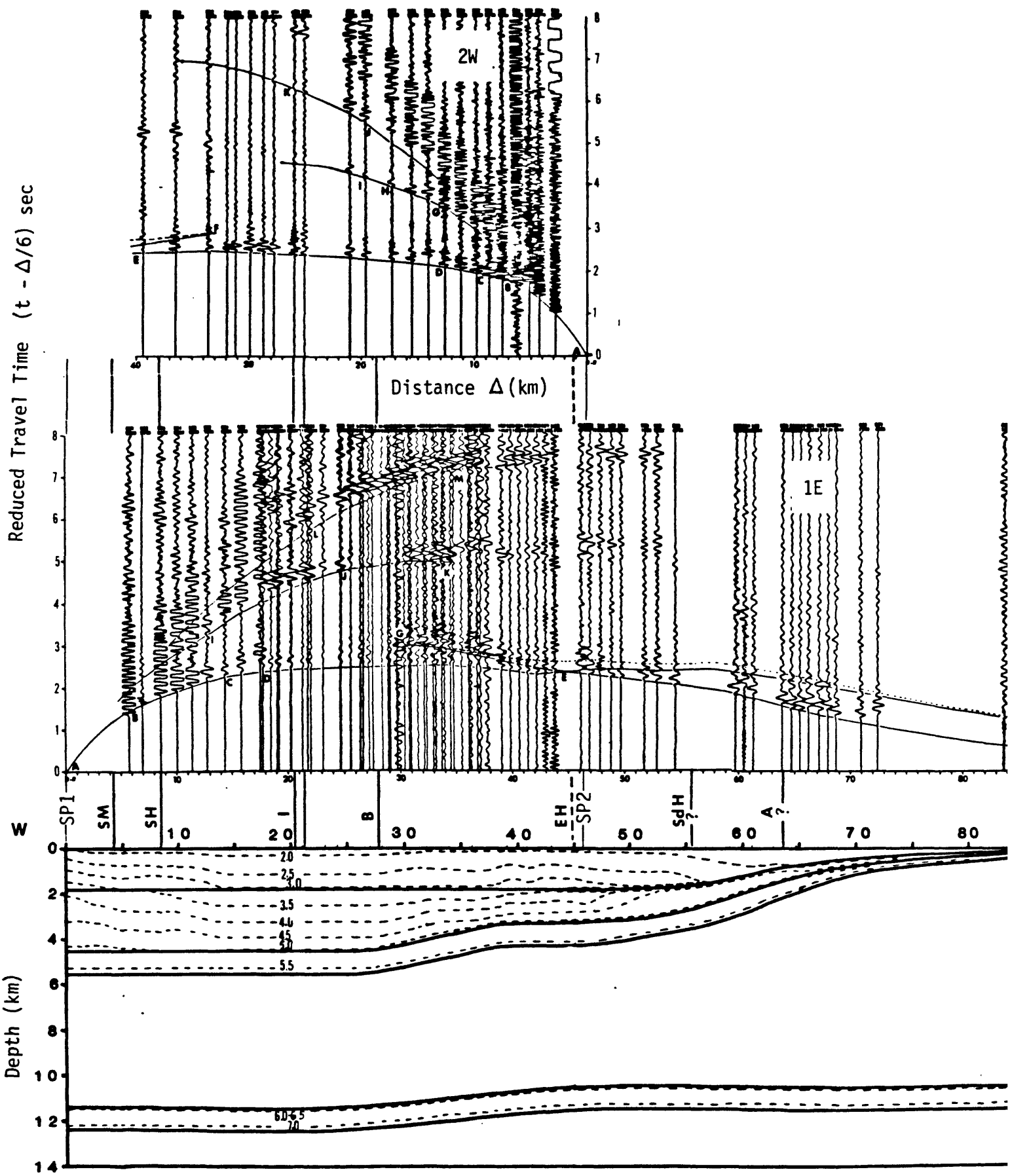
2W
1E
Distance Δ (km)
Reduced Travel Time (t - Δ/6) sec
W
SP1
SM
SH
I
B
EH
SP2
SdH
A
Depth (km)
2.0
2.5
3.0
3.5
4.0
4.5
5.0
5.5
6.0
6.5
7.0

Figure 4

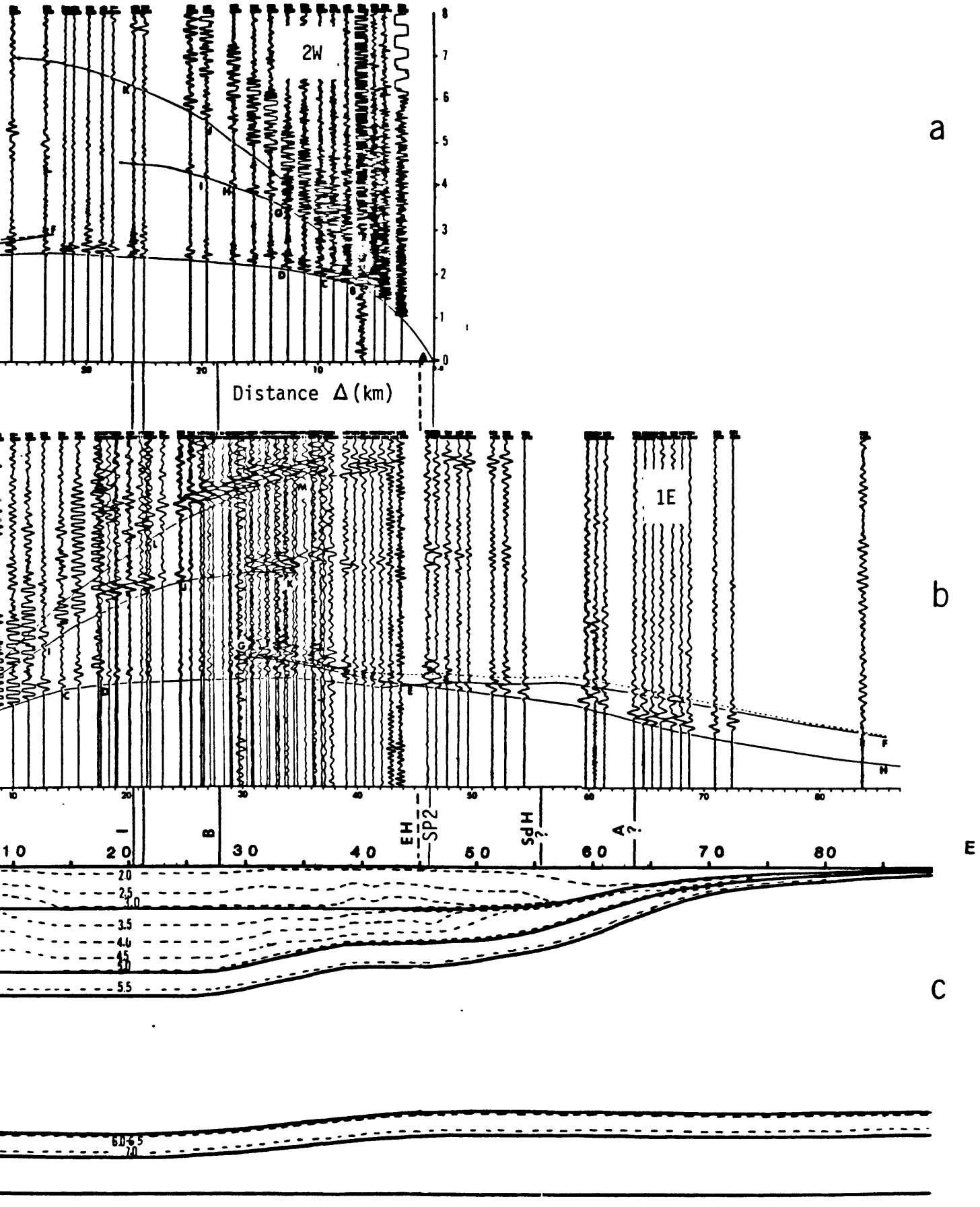

Figure 4

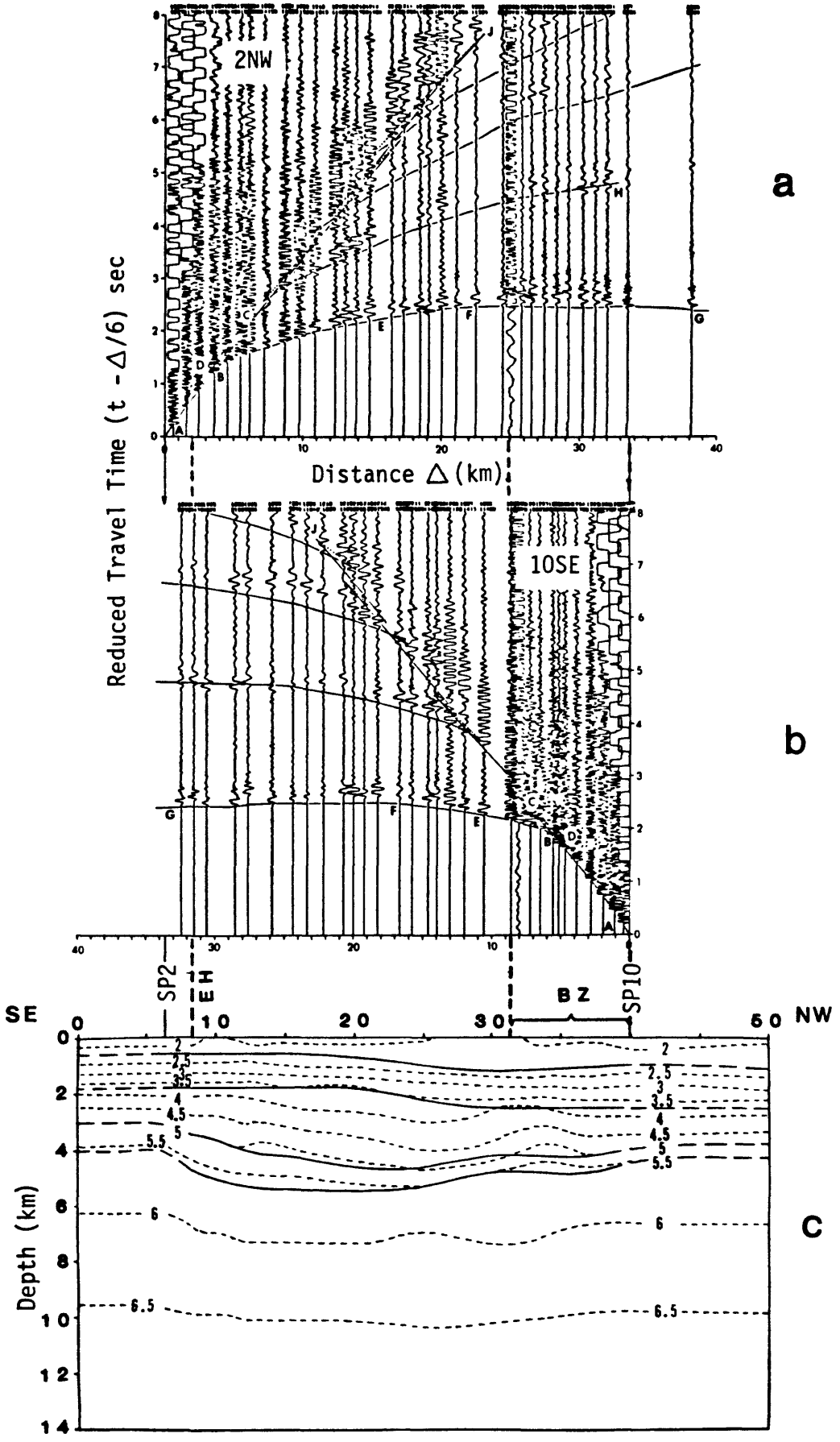
2NW
a
Reduced Travel Time (t -Δ/6) sec
Distance Δ (km)
10SE
b
SE
NW
SP2
EH
BZ
SP10
0
10
20
30
50
Depth (km)
2
2.5
3
3.5
4
4.5
5
5.5
6
6.5
c

Figure 5

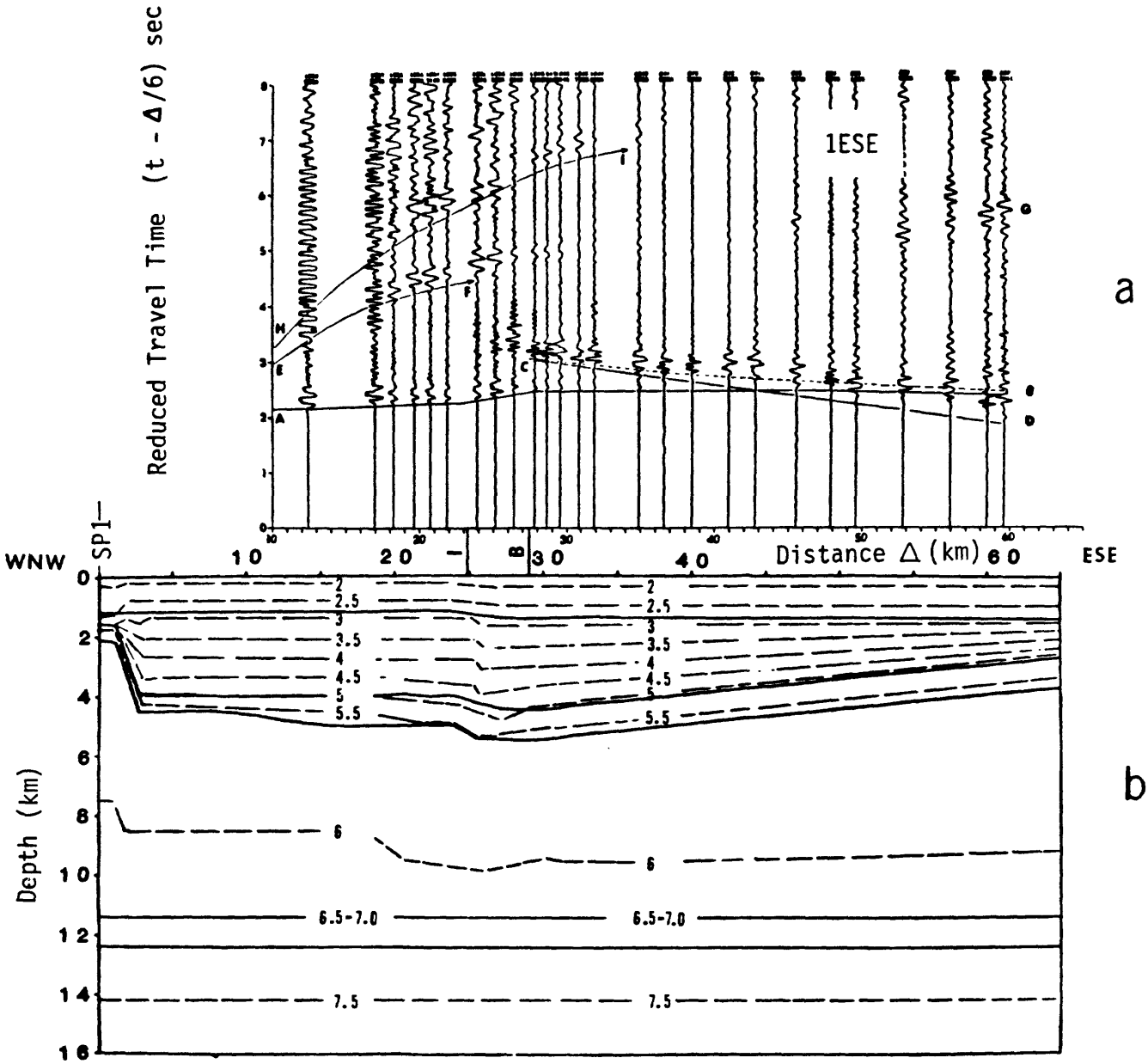
Reduced Travel Time (t - Δ/6) sec
1ESE
a
Distance Δ (km)
WNW
SP1
ESE
Depth (km)
2
2.5
3
3.5
4
4.5
5
5.5
6
6.5-7.0
7.5
b

Figure 6

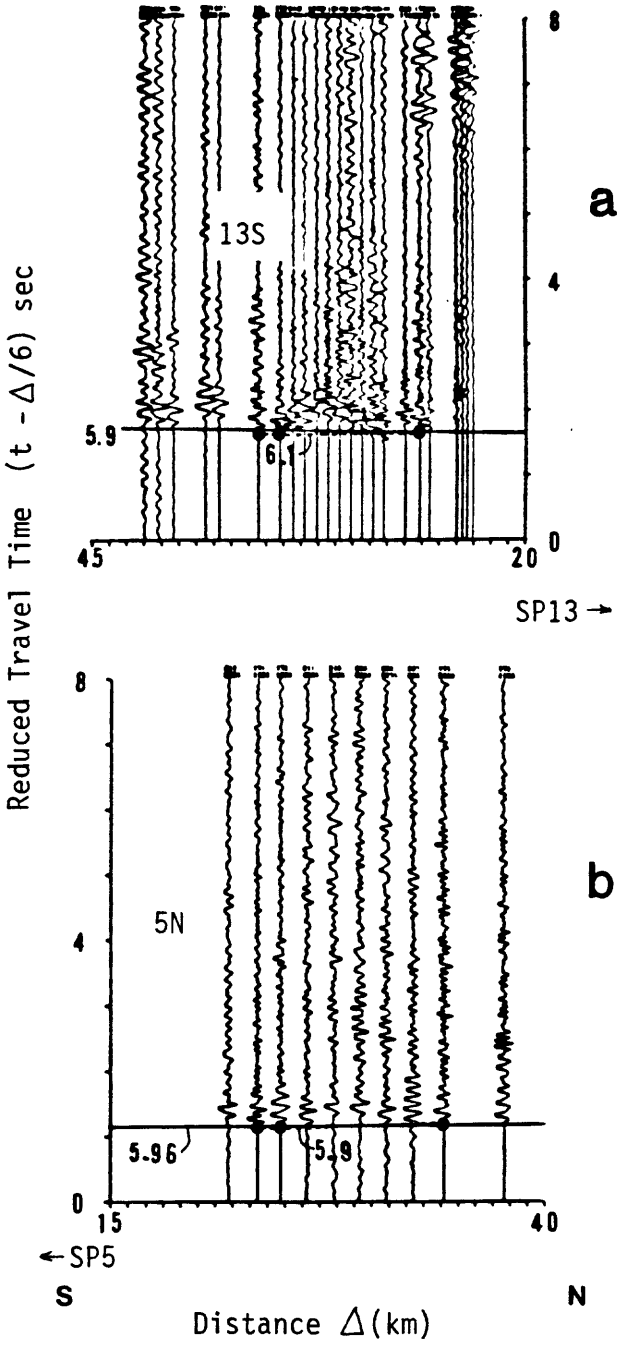
Reduced Travel Time (t - Δ/6) sec
13S
a
8
4
0
5.9
6.1
45
20
SP13 →
5N
b
8
4
0
5.96
5.9
15
40
← SP5
S
N
Distance Δ (km)

Figure 7

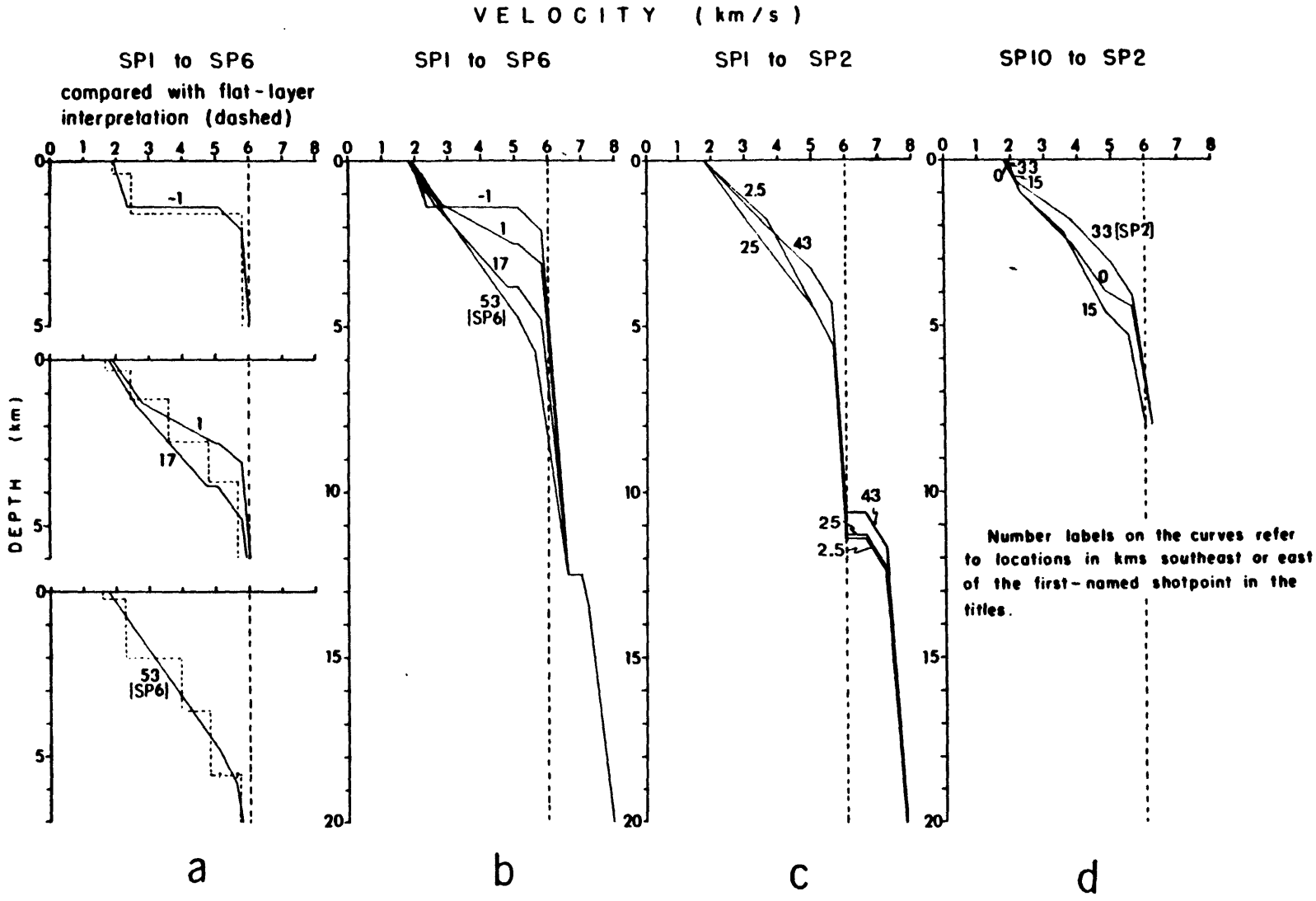
VELOCITY (km/s)
SP1 to SP6
compared with flat-layer interpretation (dashed)
SP1 to SP6
SP1 to SP2
SP10 to SP2
DEPTH (km)
-1
1
17
53 [SP6]
2.5
25
43
0
15
33 [SP2]
Number labels on the curves refer to locations in kms southeast or east of the first-named shotpoint in the titles.
a
b
c
d

Figure 8

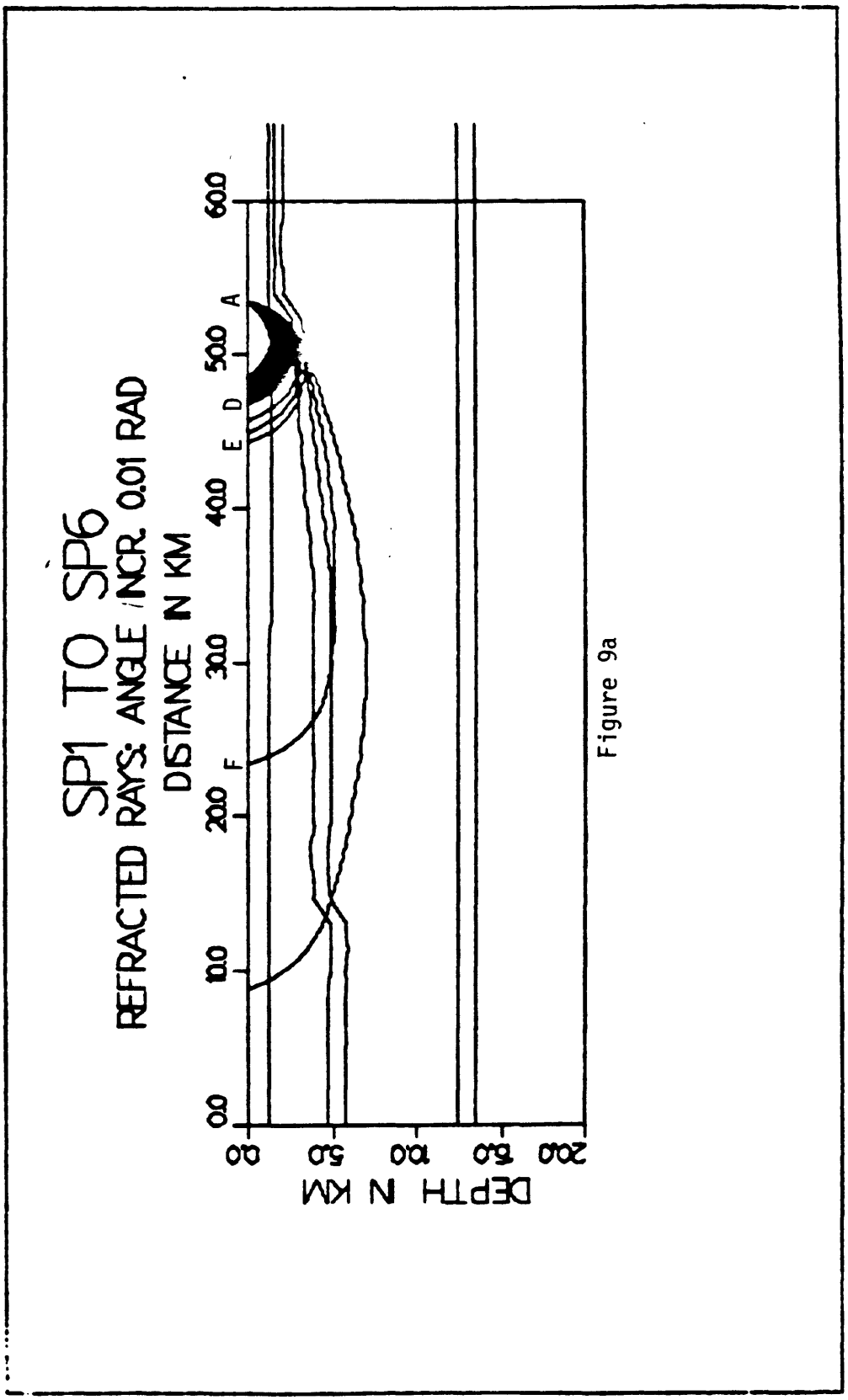
SP1 TO SP6
REFRACTED RAYS: ANGLE INCR. 0.01 RAD
DISTANCE IN KM
DEPTH IN KM
0.0
10.0
20.0
30.0
40.0
50.0
60.0
A
D
E
F
0.0
50
100
150
200

Figure 9a

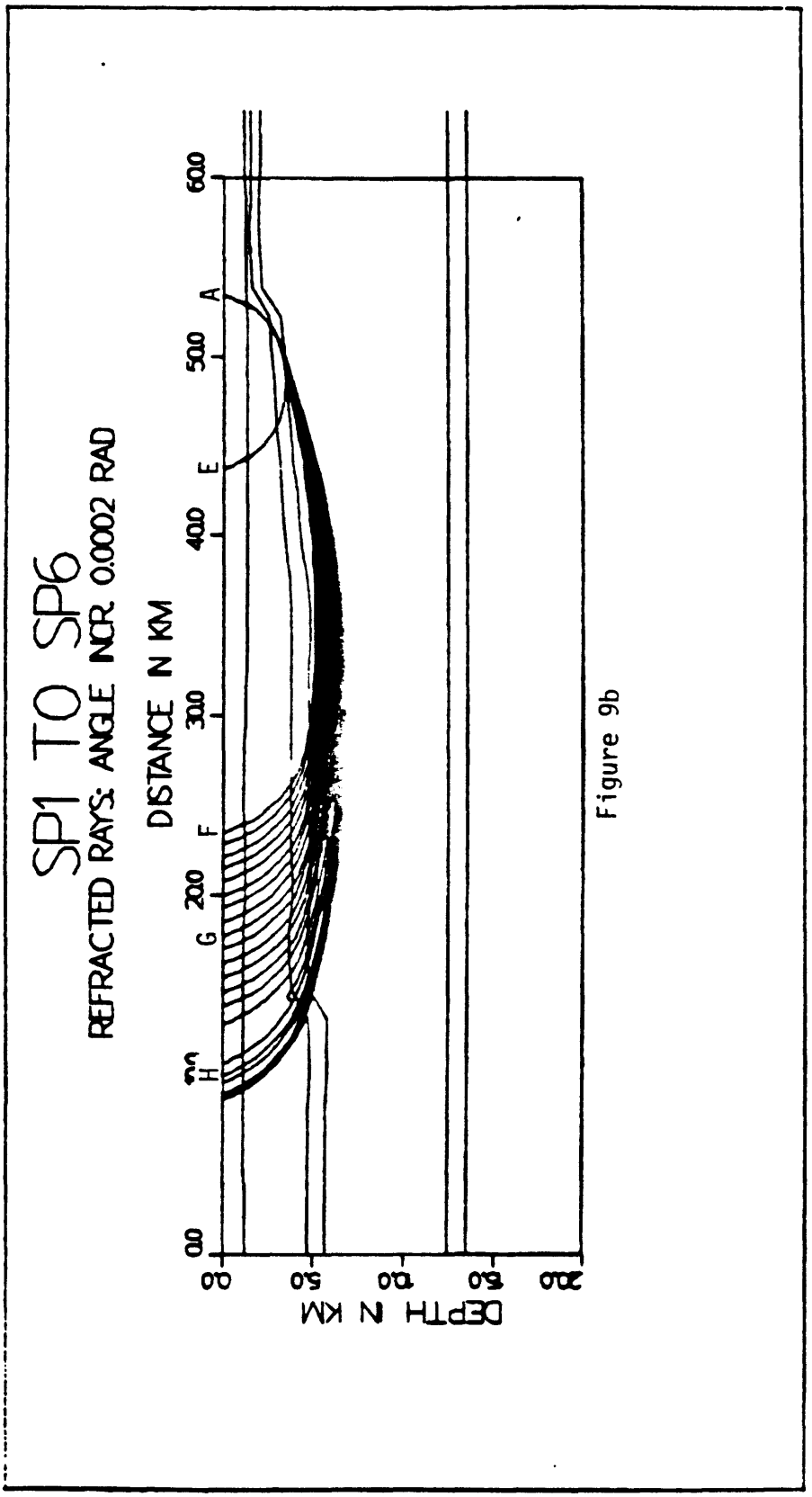
SP1 TO SP6
REFRACTED RAYS: ANGLE INCR 0.0002 RAD
DISTANCE IN KM
DEPTH IN KM
A
E
F
G
H
0.0
5.0
10.0
15.0
20.0
0.0
100.0
200.0
300.0
400.0
500.0
600.0

Figure 9b

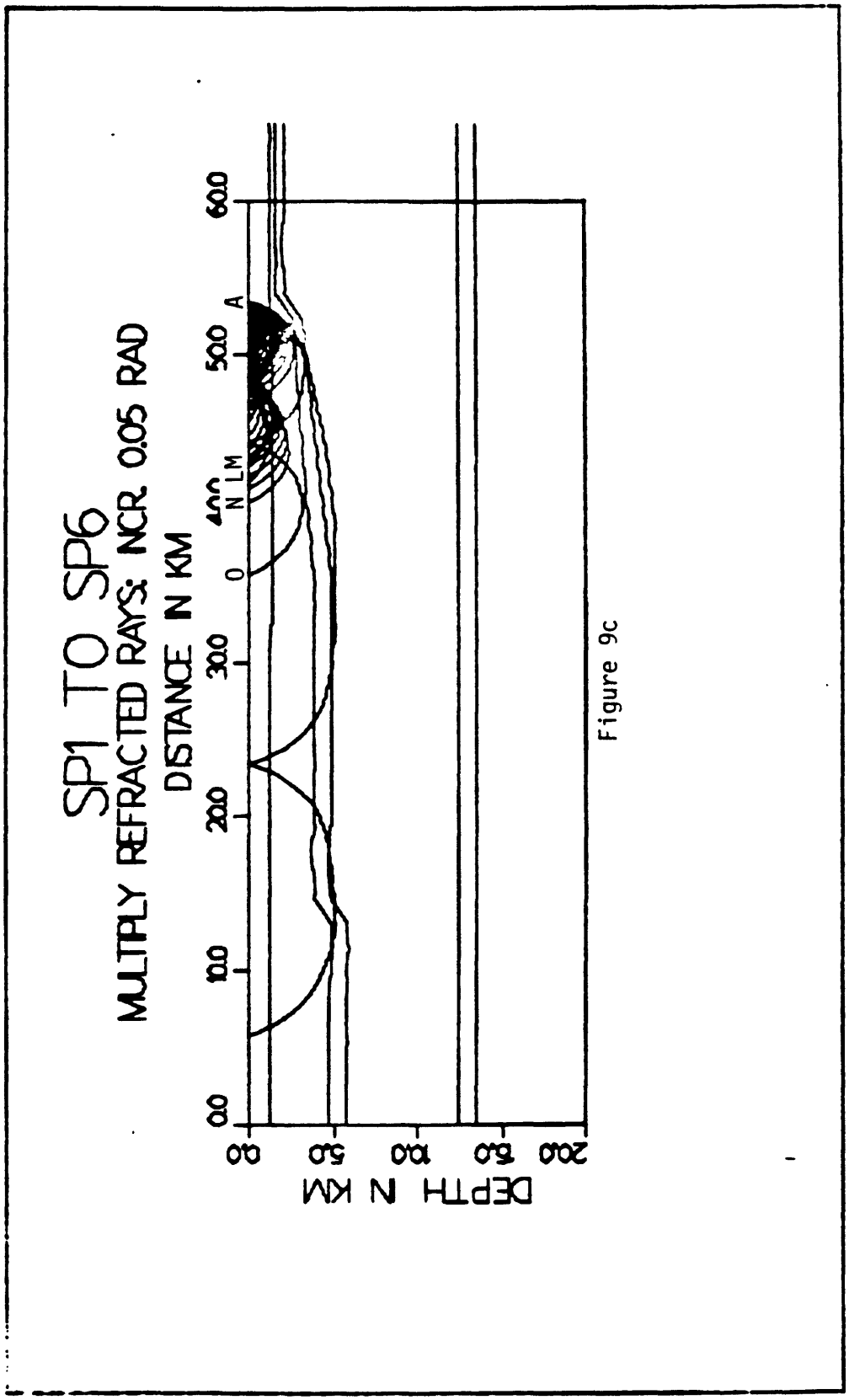
SP1 TO SP6
MULTIPLY REFRACTED RAYS: NCR 0.05 RAD
DISTANCE IN KM
DEPTH IN KM
0.0
10.0
20.0
30.0
0
50.0
60.0
A
N LM
0.0
50
100
150
200

Figure 9c

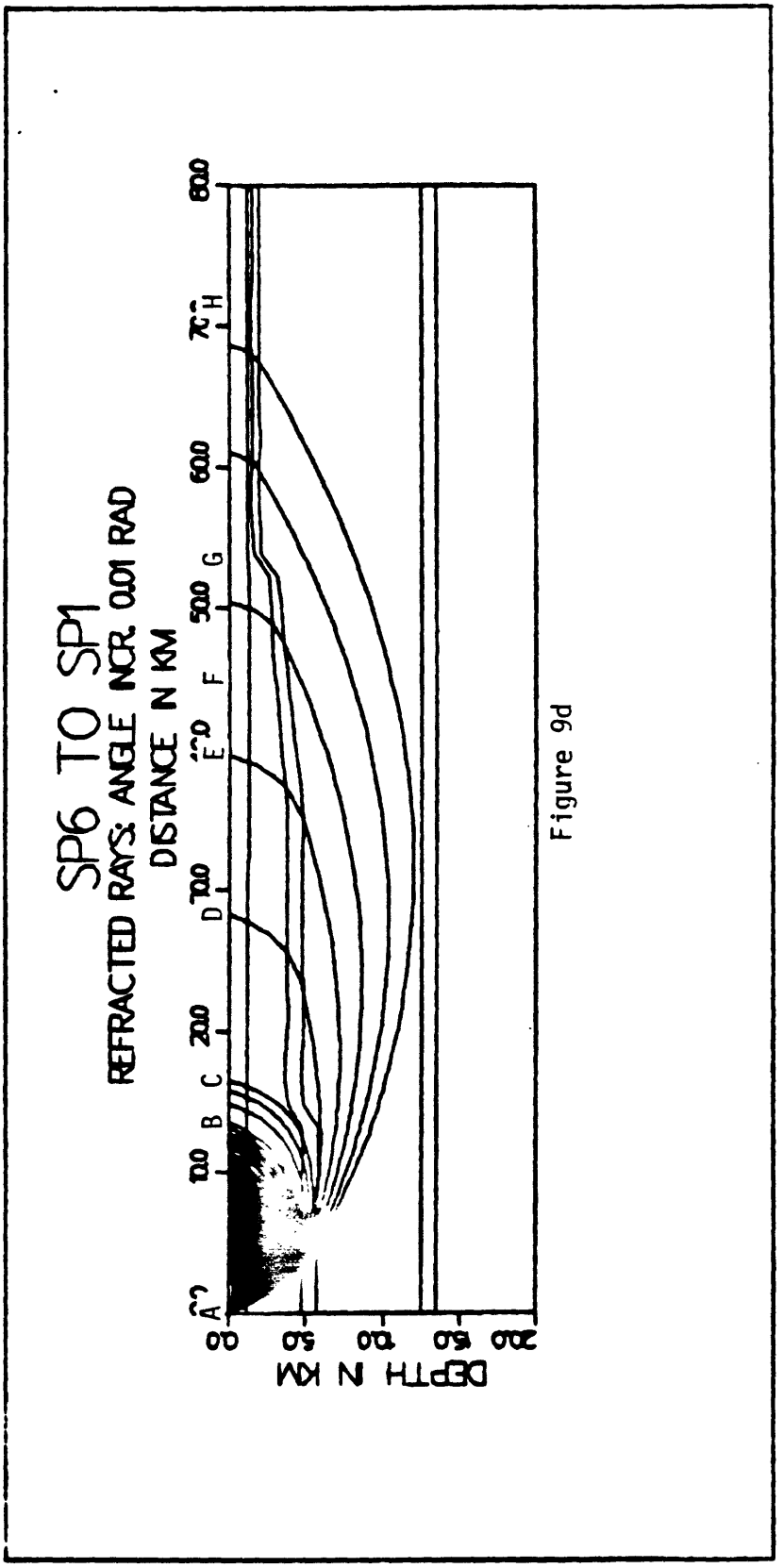
SP6 TO SP1
REFRACTED RAYS: ANGLE INCR. 0.01 RAD
DISTANCE IN KM
DEPTH IN KM
A
B
C
D
E
F
G
H

Figure 9d

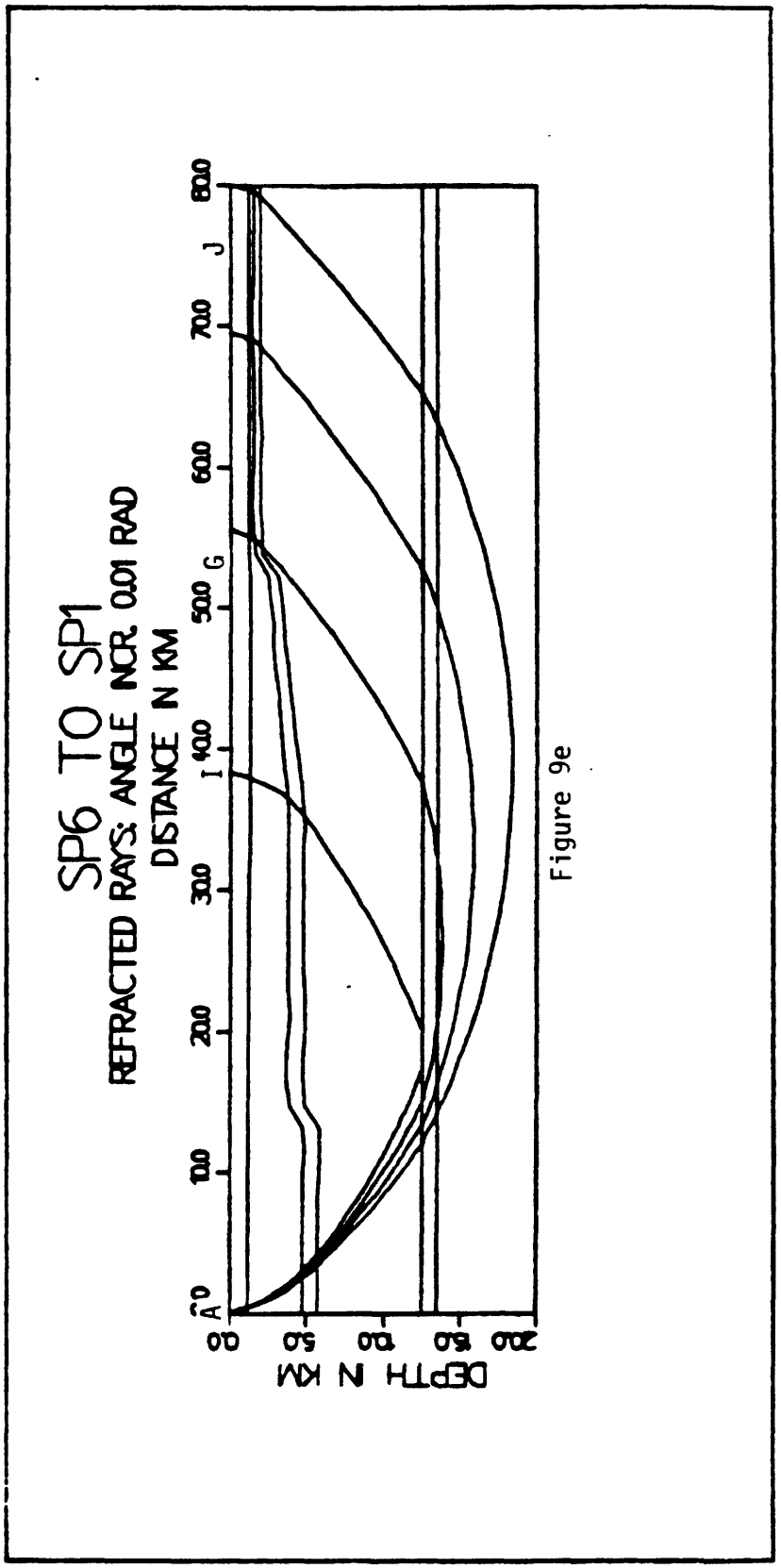
SP6 TO SP1
REFRACTED RAYS: ANGLE INCR. 0.01 RAD
DISTANCE IN KM
DEPTH IN KM
A
G
I
J

Figure 9e

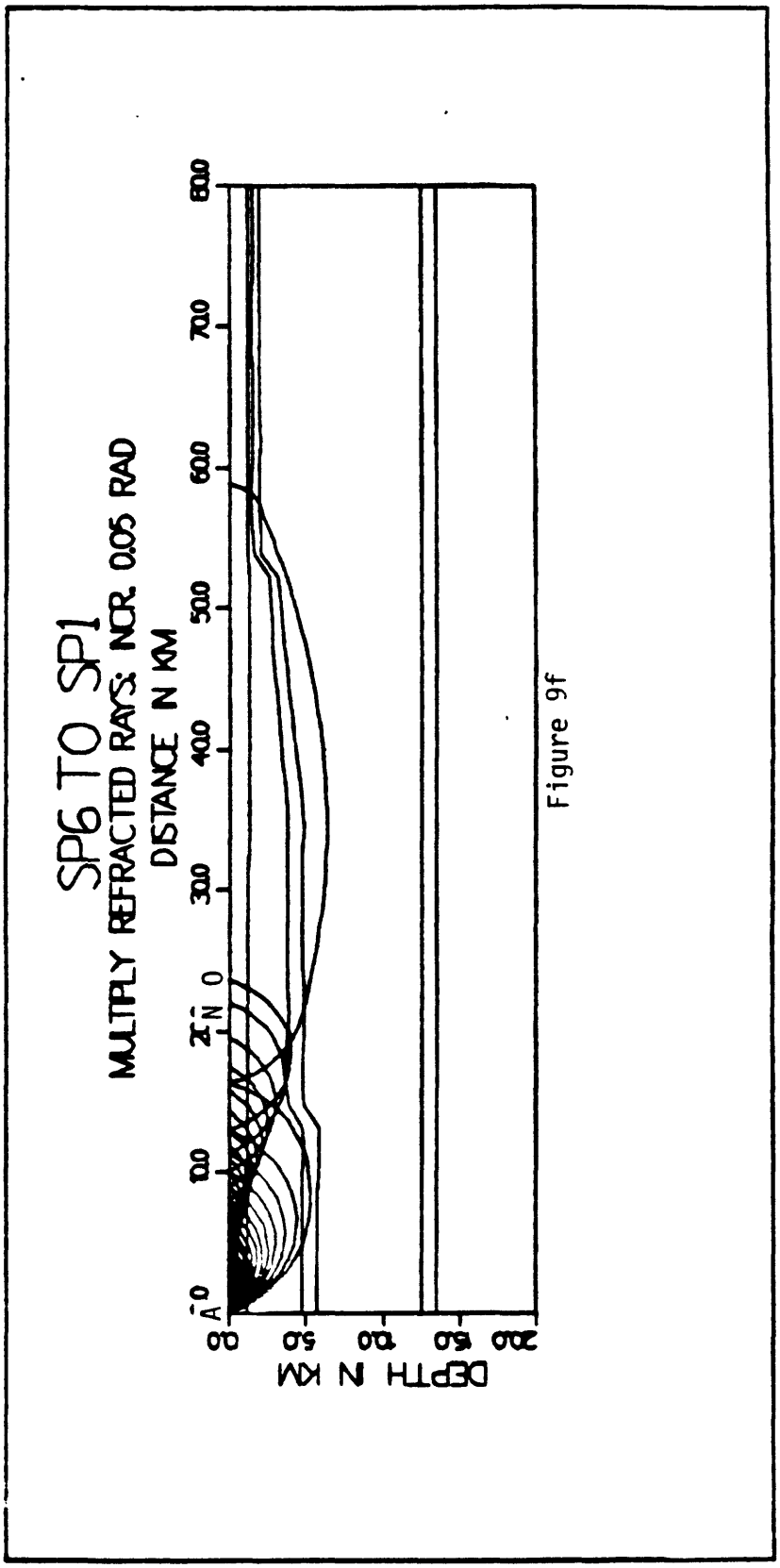
SP6 TO SP1
MULTIPLY REFRACTED RAYS: NOR. 0.05 RAD
DISTANCE N KM
DEPTH IN KM
0.0
50.0
100.0
150.0
200.0
0.0
100.0
200.0
300.0
400.0
500.0
600.0
700.0
800.0

Figure 9f

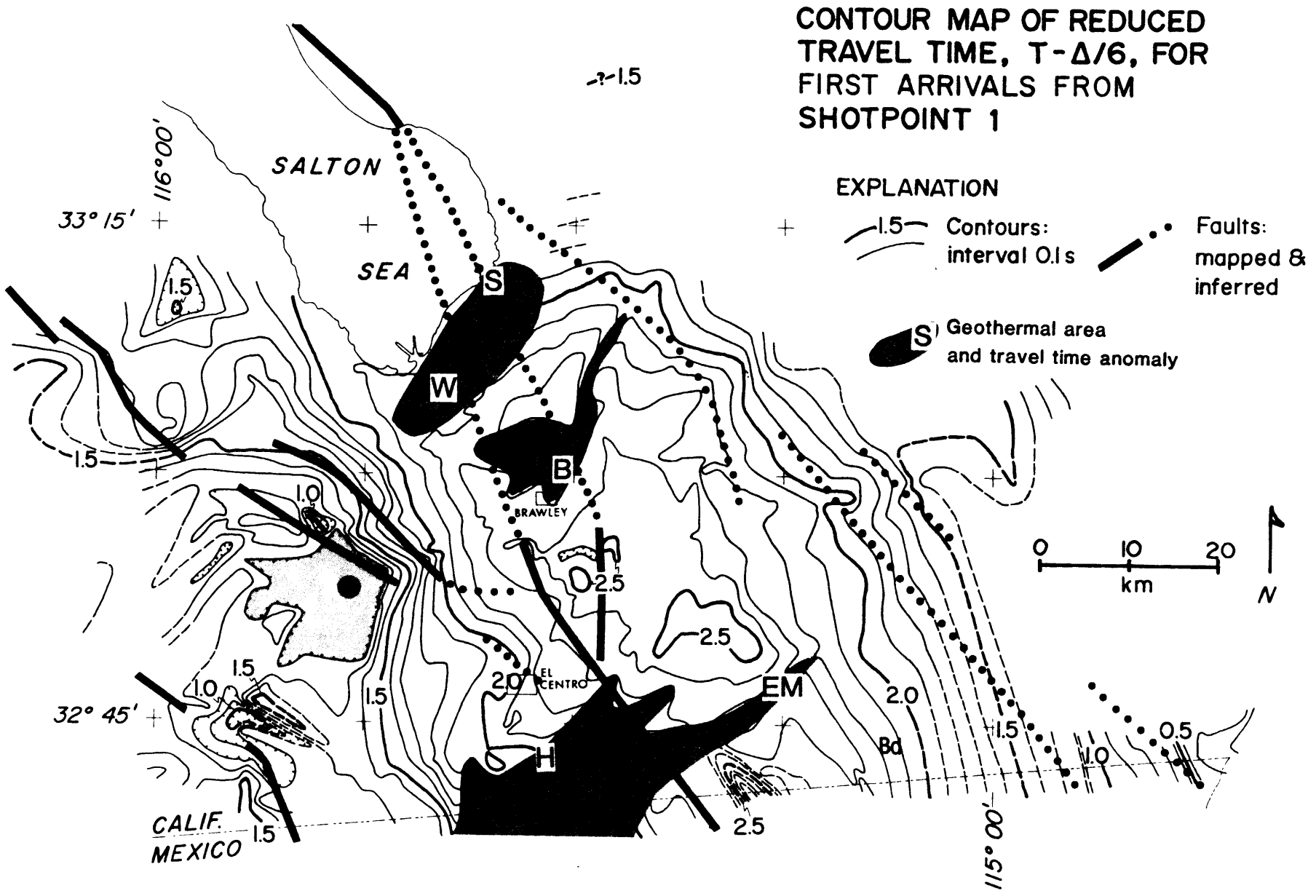
CONTOUR MAP OF REDUCED TRAVEL TIME, T-Δ/6, FOR FIRST ARRIVALS FROM SHOTPOINT 1
EXPLANATION
1.5 Contours: interval 0.1s
Faults: mapped & inferred
S Geothermal area and travel time anomaly
SALTON SEA
S
W
B
H
EM
BRAWLEY
EL CENTRO
33° 15'
32° 45'
116° 00'
115° 00'
CALIF.
MEXICO
0 10 20
km
N

Figure 10

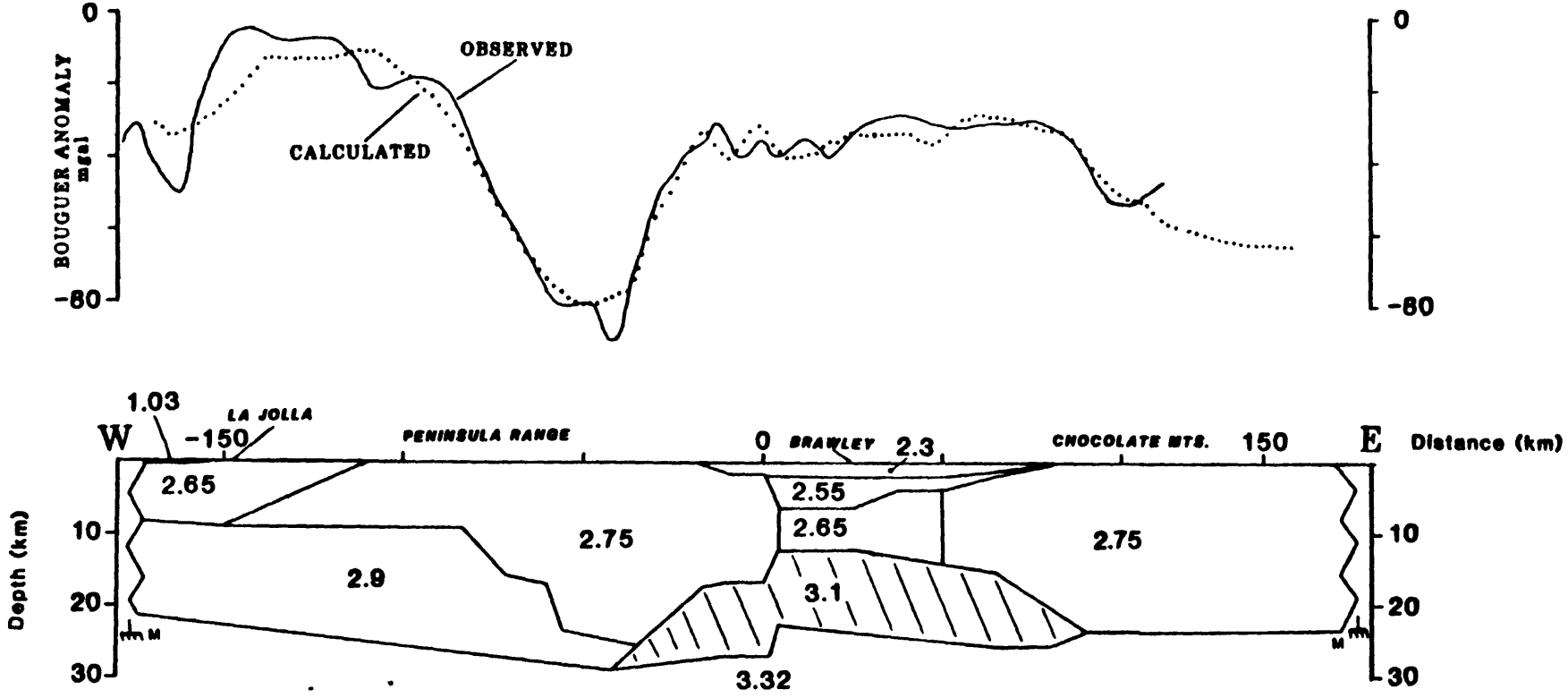
0
BOUGUER ANOMALY
mgal
-80
OBSERVED
CALCULATED
0
-80
1.03
LA JOLLA
W
-150
PENINSULA RANGE
0
BRAWLEY
2.3
CHOCOLATE MTS.
150
E
Distance (km)
Depth (km)
2.65
2.55
2.65
2.75
2.75
2.9
3.1
10
20
30
3.32

Figure 11